Check for updates

ADVANCED MATERIALS
www.advmat.de

Recent Advances in Electrocatalytic Hydrogenation Reactions on Copper-Based Catalysts

Min Zheng, Junyu Zhang, Pengtang Wang, Huanyu Jin, Yao Zheng, and Shi-Zhang Qiao**

Hydrogenation reactions play a critical role in the synthesis of value-added products within the chemical industry. Electrocatalytic hydrogenation (ECH) using water as the hydrogen source has emerged as an alternative to conventional thermocatalytic processes for sustainable and decentralized chemical synthesis under mild conditions. Among the various ECH catalysts, copper-based (Cu-based) nanomaterials are promising candidates due to their earth-abundance, unique electronic structure, versatility, and high activity/selectivity. Herein, recent advances in the application of Cu-based catalysts in ECH reactions for the upgrading of valuable chemicals are systematically analyzed. The unique properties of Cu-based catalysts in ECH are initially introduced, followed by design strategies to enhance their activity and selectivity. Then, typical ECH reactions on Cu-based catalysts are presented in detail, including carbon dioxide reduction for multicarbon generation, alkyne-to-alkene conversion, selective aldehyde conversion, ammonia production from nitrogen-containing substances, and amine production from organic nitrogen compounds. In these catalysts, the role of catalyst composition and nanostructures toward different products is focused. The co-hydrogenation of two substrates (e.g., CO_2 and NO_x^n, SO_3^{2-}, etc.) via C—N, C—S, and C—C cross-coupling reactions are also highlighted. Finally, the critical issues and future perspectives of Cu-catalyzed ECH are proposed to accelerate the rational development of next-generation catalysts.

1. Introduction

Hydrogenation is regarded as an important category of catalytic reactions for producing fine chemicals, petrochemicals, fertilizers, and pharmaceuticals.[1–4] Remarkably, ≈25% of chemical transformations involve at least one hydrogenation step, highlighting its pivotal role in the catalysis field.[5] The current industrial-scale hydrogenation reactions are commonly operated through thermocatalytic hydrogenation (TCH), where the gaseous hydrogen (H_2) is catalytically dissociated for subsequent reduction of substrates.[6–7] For example, the hydrogenation of carbon dioxide (CO_2) is applied worldwide for industrial production of carbon monoxide (CO) through reverse water gas shift and various downstream hydrocarbons and oxygenates (e.g., methanol, dimethyl ether) through modified Fischer–Tropsch or methanol-mediated synthesis routes.[8] While TCH processes exhibit high conversion efficiency and favorable kinetics, their H_2 source is dominated by the fossil fuel-based steam reforming process that inevitably releases huge amounts of CO_2. Moreover, the handling of highly explosive H_2 in large quantities would incur additional costs due to special precautions required in the storage and transportation. To circumvent the problems associated with pure H_2, transfer hydrogenation (TH) using organic hydrogen donors (e.g., alcohols, formic acid, hydrazine, alkanes, benzothiazoles, and ammonia-boranes) as a sacrificial hydrogen source has been proposed as a powerful method to obtain hydrogenated organic compounds.[9–10] While TH offers facile experimental setups with greater control over hydrogen donors, it is still plagued by the significant generation of toxic organic waste.[11] Therefore, it is highly desirable to develop safe, energy-saving, and eco-friendly processes for efficient hydrogenation.

Recently, with the increasing availability of renewable electricity, electrocatalytic refinery has been identified as a sustainable route to upgrade earth-abundant feedstocks into valuable fuels and chemicals.[12] In particular, electrocatalytic hydrogenation (ECH) enables oxidized reactants to gain electrons from external circuits by directly tuning the cathodic potential and current, allowing fine control of product selectivity.[13] Compared with the traditional TCH, ECH under ambient conditions is suitable for the on-demand production of chemicals that are not economically viable for transportation.[14–15] Importantly, in aqueous electrolytes, water is utilized as a sustainable hydrogen source to electrochemically generate active chemisorbed hydrogen (*H)

M. Zheng, J. Zhang, P. Wang, H. Jin, Y. Zheng, S.-Z. Qiao
School of Chemical Engineering
The University of Adelaide
Adelaide, SA 5005, Australia
E-mail: yao.zheng01@adelaide.edu.au; s.qiao@adelaide.edu.au

The ORCID identification number(s) for the author(s) of this article can be found under https://doi.org/10.1002/adma.202307913

© 2024 The Authors. Advanced Materials published by Wiley-VCH GmbH. This is an open access article under the terms of the Creative Commons Attribution License, which permits use, distribution and reproduction in any medium, provided the original work is properly cited.

DOI: 10.1002/adma.202307913

15214095, 2024, 14, Downloaded from https://advanced.onlinelibrary.wiley.com/doi/10.1002/adma.202307913 by Cochrane Chile, Wiley Online Library on [30/09/2026]. See the Terms and Conditions (https://onlinelibrary.wiley.com/terms-and-conditions) on Wiley Online Library for rules of use; OA articles are governed by the applicable Creative Commons License

on catalyst surfaces, avoiding the safety issues of H_2 gas. The *H species are then combined with organic or inorganic substrates, including CO_2, alkynes, aldehydes, inorganic nitrogen compounds (e.g., N_2, nitrates, nitrites), and organic nitrogen compounds, which contain unsaturated bonds such as C≡C, C═O, C≡N, N≡N, and N═O, to form a range of hydrogenation products. Given the above advantages, ECH has become an attractive option for clean and mild synthesis of high-value hydrogenated chemicals.

For efficient ECH reactions to occur, the development of electrocatalysts with high activity, selectivity, and durability is a prerequisite. Till now, noble-metal-based materials (e.g., Pt, Pd, Ag, Ru, Rh) have been widely exploited as high-efficiency catalysts for hydrogenation transformations. For example, the easy adsorption of reactants and rich active sites have led to exceptional activity in the ECH of aldehydes on Pd-based catalysts and phenolic compounds on Pt- and Rh-based catalysts.[16–17] However, their scarcity and prohibitive cost impede their large-scale application. Furthermore, the favorable binding energies of noble metals with *H also suggest their high activity in the HER side reaction, which hampers the selectivity and FE of value-added products in ECH. Recent research efforts have led to a surge in finding non-noble transition metal electrocatalysts. In particular, Cu-based nanomaterials have garnered extensive attention for electrocatalysis owing to their abundant presence, low cost, and outstanding catalytic activity.[18–20] From a structural viewpoint, the filled electronic configuration of Cu ($3d^{10}4s^1$) with high availability of 3d electrons suggests its intrinsic suitability for hydrogenation by donating electrons to the ECH substrates. Meanwhile, on the basis of Sabatier principle, the moderate binding energies of reactive intermediates on catalysts are most favorable for electrocatalytic activity and kinetics. Compared with noble metals, Cu has near-ideal binding affinity toward various ECH substrates, such as CO_2 and aldehydes, to activate the molecules. This property offers Cu comparable or even superior activities than noble-metal materials in hydrogenation reactions, especially for the ECH of biomass-derived organics.[21] As such, Cu-based materials with different sizes, structures, morphologies, and compositions have been extensively applied in both TCH and ECH.

It is noteworthy that ECH reactions generally face a severe selectivity challenge, given the inherent competition between ECH to obtain complex products and hydrogen evolution reaction (HER) when the applied potential is in the HER zone. The relatively weak binding affinity with *H on Cu catalysts results in its moderate *H surface coverage, which inhibits the dimerization of H atoms in the Tafel or Heyrovsky step and ensures the effective transfer of *H to the ECH substrate.[22] To date, the significant progress of ECH has been reviewed by several articles. Li et al. reviewed the synthesis of high-value products from small-molecule electrocatalytic reduction reactions, including HER, CO_2 reduction reaction (CRR), nitrogen reduction reaction (NRR), and NO_x^n species (e.g., NO, NO_2^-, NO_3^-) reduction reaction (NO_x^nRR).[23] Despite the progress, there is still a need for systematic discussion of ECH reactions that encompass both the production of valuable inorganic and organic molecules. For example, selective hydrogenation of alkynes and aldehydes is widely recognized as crucial thermocatalytic reactions in industrial organic synthesis. However, there has been limited review and comprehensive investigation of the significant potential of ECH for these organic compounds in obtaining high-order valuable products, particularly in the context of Cu-catalyzed processes. Additionally, there is a lack of review papers specifically focusing on the design of Cu-based nanomaterials in various ECH reactions, which hinders a comprehensive understanding of the structure–activity relationship.

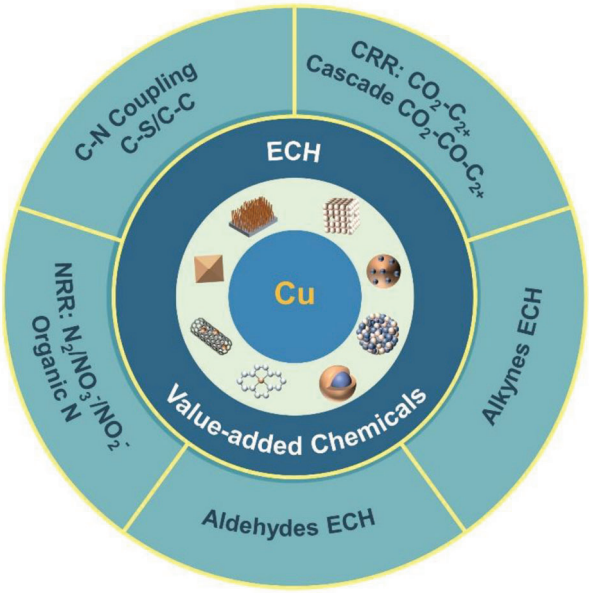

Figure 1. The production of complex value-added chemicals through electrocatalytic hydrogenation reactions on Cu-based nanomaterials.

Herein, we analyze the recent representative works on the development of Cu-based nanomaterials and their applications in the sustainable valorization of chemicals through ECH reactions (**Figure 1**). We highlight the unique physicochemical properties of Cu for favorable ECH catalysis and the major modulation strategies of Cu-based catalysts for enhanced performance. Then, we provide an up-to-date summary of Cu-based nanomaterials for ECH of CO_2 (direct and tandem reactions), alkynes, aldehydes, inorganic nitrogen compounds (e.g., N_2, nitrates, nitrites), and organic nitrogen compounds (e.g., nitrobenzene, nitriles), with a specific focus on the relationship among catalyst structure, physicochemical properties, reaction pathways, and electrochemical performance. Notably, the emerging co-hydrogenation reactions for coupling formation of C—N coupling products (amides, urea, and amines), cross-coupled C—C products, and C—S organic products are discussed in detail. Finally, we present the current challenges and future perspectives in the rational design of Cu-based ECH catalysts.

2. Unique Properties and Design Principles of Cu-Based ECH Electrocatalysts

The performance of ECH reactions is significantly influenced by catalyst properties. Cu-based materials, with their unique physical and electronic properties, are particularly well-suited for hydrogenation reactions and can be tailored to form diverse nanostructures with improved activity and selectivity. This section

© 2024 The Authors. Advanced Materials published by Wiley-VCH GmbH

Table 1. The characteristics of design strategies for Cu-based catalysts.

Design strategies	Characteristics
Nanostructuring	(a) Constructing porous structures and nanowire/nanosheet sites
	(b) Different sizes and morphologies
	(c) Large surface area-to-volume ratios
	(d) Maximizing exposure of active sites
Facet engineering	(a) Regulating the packing of atoms and exposed crystal facets
	(b) Optimizing the exposure of catalytically active surfaces
Support effect	(a) Avoiding the aggregation of Cu nanoparticles
	(b) Enhancing the stability and active site exposure
	(c) Facilitating the charge and mass transport kinetics by metal-support interaction
Creating single-atom sites	(a) Downsizing catalyst particles to the atomic scale
	(b) Near 100% atom utilization efficiency
Defect engineering	(a) Non-perfect lattice structures such as anion vacancies, cation vacancies, grain boundaries, and lattice distortions
	(b) Modulating the electronic structure and charge distribution
Heteroatom doping	(a) Non-metal dopants with different atomic radius, electronegativity and lattice structure
	(b) Allowing fine-tuning of local electronic configuration
Alloying	(a) Creating new active phases and breaking the limitation of monometallic catalysts
	(b) Synergistic effects of multiple elements for complex reactions
	(c) Adjusting the electronic structure
Constructing heterojunctions	(a) Accelerating the electron transfer kinetics at the Schottky heterojunction
	(b) Adjusting the local electrophilic and nucleophilic regions

provides an overview of the unique properties and design strategies of Cu-based ECH electrocatalysts.

2.1. Unique Properties of Cu-Based Electrocatalysts

The unique physicochemical characteristics of Cu element make Cu-based catalysts highly appealing for various applications.[18] Firstly, metallic Cu is soft, malleable, non-toxic, and easily accessible with a concentration of about 60 g per ton in the earth's crust.[24] Secondly, as a first-row transition metal, copper has a valence electronic configuration of $3d^{10}4s^{1}$. Such electronic structure enables its highest occupied molecular orbital and lowest unoccupied molecular orbital to match with a variety of substrates, demonstrating its strong capabilities of electron donation and activation of hydrogenation steps.[22,25] Thirdly, the high electrical conductivity and versatile redox properties of Cu are conducive to electron transfer pathways and facilitate the facile transition of oxidation states during ECH, such as the conversion between Cu^{II} and Cu^{I}/Cu^{0}.[26] Fourthly, the hydrogen adsorption free energy on the Cu electrode is around 0.16 eV and the HER exchange current density is lower than many noble metals (e.g., Pt, Ir) by 3 orders of magnitude.[27] Therefore, the detrimental competition between ECH and HER can be minimized on Cu-based catalysts to achieve high Faradaic efficiency (FE) of target ECH products. Lastly, copper catalysts are suitable for catalyzing a diverse range of reactions.[28–29] The rich chemistry of Cu with different oxidation states (Cu^{0}, Cu^{I}, Cu^{II}, and Cu^{III}) and a broad range of nanostructured compounds (Cu_2O, CuO, Cu_3N, Cu_2S, Cu organic complexes, bimetallic and multimetallic compounds) is beneficial for exhibiting electrochemically active surface structures and electronic states. Such diversities in composition and structure allow Cu to associate well with various functional groups through Lewis acid interactions or π-coordination, enabling versatile ECH. Overall, the above advantages provide a vast opportunity for the development of Cu-based materials favorable for ECH reactions.

2.2. Design Principles of Cu-Based ECH Electrocatalysts

In recent years, various design strategies have been proposed to enhance the ECH performance of Cu-based catalysts, which include: 1) nanostructuring, 2) facet engineering, 3) support effect, 4) creating single-atom sites, 5) defect engineering, 6) heteroatom doping, 7) alloying, and 8) constructing heterojunctions (**Figure 2**). The corresponding characteristics of the eight design principles are shown in **Table 1**. These strategies are based on the principles of improving electrocatalytic activity by increasing the number of active sites or the intrinsic activity of individual active site, while also enhancing selectivity and FE by tuning the binding energy and adsorption configuration of ECH intermediates. Moreover, the above strategies are often combined to achieve synergistic effect.

2.2.1. Nanostructuring

Catalyst nanostructuring is effective in exposing a greater number of electrochemically active sites by creating porous structures, edge sites, and hollow structures. In particular, nanostructured Cu materials in different sizes and morphologies often exhibit

© 2024 The Authors. Advanced Materials published by Wiley-VCH GmbH

15214095, 2024, 14, Downloaded from https://advanced.onlinelibrary.wiley.com/doi/10.1002/adma.202307913 by Cochrane Chile, Wiley Online Library on [30/09/2026]. See the Terms and Conditions (https://onlinelibrary.wiley.com/terms-and-conditions) on Wiley Online Library for rules of use; OA articles are governed by the applicable Creative Commons License

15214095, 2024, 14, Downloaded from https://advanced.onlinelibrary.wiley.com/doi/10.1002/adma.202307913 by Cochrane Chile, Wiley Online Library on [30/09/2026]. See the Terms and Conditions (https://onlinelibrary.wiley.com/terms-and-conditions) on Wiley Online Library for rules of use; OA articles are governed by the applicable Creative Commons License

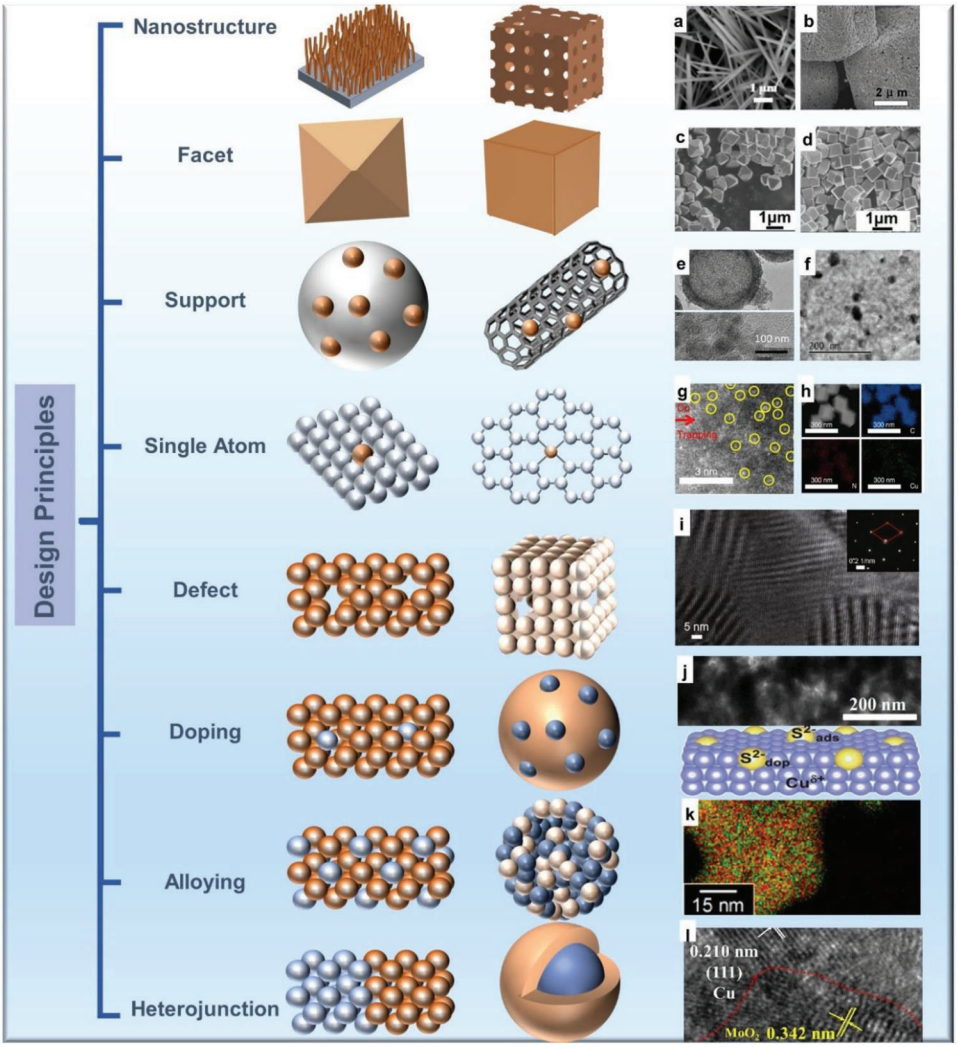

Figure 2. Schematic illustration of the design principles of Cu-based catalysts. a,b) Nanostructuring. a) Adapted with permission.[35] Copyright 2016, Wiley-VCH. b) Adapted with permission.[36] Copyright 2012, American Chemical Society. c,d) Facet engineering. c,d) Adapted under the terms of the CC-BY Creative Commons Attribution 4.0 International license (https://creativecommons.org/licenses/by/4.0).[37] Copyright 2020, The Authors, published by Wiley-VCH. e,f) Support effect. e) Adapted with permission.[38] Copyright 2019, The Authors, published by Springer Nature. f) Adapted under the terms of the CC-BY Creative Commons Attribution 4.0 International license (https://creativecommons.org/licenses/by/4.0).[39] Copyright 2022, The Authors, published by MDPI. g,h) Creating single-atom sites. g) Adapted under the terms of the CC-BY Creative Commons Attribution 4.0 International license (https://creativecommons.org/licenses/by/4.0).[40] Copyright 2019, The Authors, published by Springer Nature. h) Adapted under the terms of the CC-BY Creative Commons Attribution 4.0 International license (https://creativecommons.org/licenses/by/4.0).[40] Copyright 2019, The Authors, published by Springer Nature. i) Defect engineering. Reproduced with permission.[41] Copyright 2020, Elsevier. j) Heteroatom doping. Adapted under the terms of the CC-BY Creative Commons Attribution 4.0 International license (https://creativecommons.org/licenses/by/4.0).[42] Copyright 2021, The Authors, published by Springer Nature. k) Alloying. Adapted with permission.[43] Copyright 2017, American Chemical Society. l) Constructing heterojunctions. Adapted with permission.[44] Copyright 2023,Elsevier.

larger surface area-to-volume ratios for the mass transfer of active species, thereby achieving better electrocatalytic reactivity than bulk Cu catalysts in their pristine form. A typical example is the layered crystal structure of two-dimensional (2D) nanosheets with atomic thickness and abundant low-coordination edge sites. In a recent work, Cu_2Te nanosheet arrays were synthesized on commercial Cu foils via a two-step edge-oriented growth process of chemical etching and chemical vapor deposition.[30] The vertical planar structures of Cu_2Te nanosheets with highly exposed edge-active sites and step-sites enabled CO_2-to-CH_4 electroreduction at a low energy barrier.

2.2.2. Facet Engineering

Regulating the exposed crystal facets with specific packing of atoms can optimize the physical, chemical, and electronic properties of electrocatalysts.[31] While high-index facets are challenging to obtain due to the high surface energy, their abundant undersaturated sites and favorable surface atomic structures could effectively boost the catalytic kinetics and steer the product selectivity.[32] Luo et al. prepared Cu_2O nanoparticles with six different exposed facets by a reductant-controlled method for CRR. It was discovered that the star-shaped Cu_2O with exposed (332)

 © 2024 The Authors. Advanced Materials published by Wiley-VCH GmbH

facets achieved the highest C_2H_4 selectivity (FE 74.1%).[33] The unique geometry of Cu_2O (332) facets lowers the resistance at the electrode–electrolyte interface and the Gibbs free energy barrier during *CHO coupling toward C_2H_4 formation.

2.2.3. Support Effect

When dispersed down to the nanoscale, Cu-based nanoparticles are prone to aggregation and oxidation under atmospheric conditions, which undermines their activity and stability in catalysis.[18] Finding suitable catalyst supports (e.g., metal oxides) to disperse Cu-based catalysts could enable the support–metal interaction and facilitate charge and mass transport kinetics.[34] This synergistic interaction modulates the electronic structure of catalysts for favorable adsorption of ECH intermediates and could be directly involved in the multiple proton–electron transfer steps of ECH reactions. In addition, the porous structure, diverse morphologies, high electrical conductivity, and high specific surface area of carbon-based materials, such as carbon nanotubes, graphene, carbon black, and conjugated polymers, make them popular candidates to form composites with Cu nanoparticles.[45] Their activity can be further boosted by defects and heteroatom dopants in the carbon support to result in interfacial charge redistribution.

2.2.4. Creating Single-Atom Sites

Single-atom catalysts (SACs) are obtained when catalysts are downsized to reach the practical limitation at the atomic scale.[46–48] By definition, copper SACs consist only of isolated metal centers dispersed onto substrates without any Cu–Cu interaction, endowing the catalysts with low metal loading and 100% atom utilization efficiency.[49] This unique structure combines the advantages of homogeneous and heterogeneous catalysts and provides an ideal platform for delineating a well-defined structure–performance relationship. The tunable coordination environment of Cu SACs is important to trigger the strong interaction between single-atom sites and supports and adjust the adsorption behavior of ECH and hydrogen intermediates. As such, Cu SACs hold great promise in ECH applications to outperform their nanoparticle counterparts in terms of selectivity and intrinsic activity.

2.2.5. Defect Engineering

Defect engineering can disturb the periodic structures of lattice to induce the redistribution of catalyst electronic structure, which increases the intrinsic activity of the catalysts.[50] Typical nonperfect lattice structures such as anion vacancies, cation vacancies, grain boundaries, and lattice distortions are usually constructed in the defect engineering process. It is considered as an effective means to promote the catalytic performance through optimizing the intermediate adsorption on catalyst surfaces and interfacial charge transfer.[51] Gu et al. reported the defect-site-rich Cu surface for the regulation of CRR selectivity.[41] The preparation of the catalyst under CO-rich conditions resulted in enhanced *CO coverage and abundant defects. This approach yielded C_{2+} alcohols at an FE of ≈70% at 100 mA cm^{-2}, as compared with the selective C_2H_4 production on flat Cu surface.

2.2.6. Heteroatom Doping

Compositional engineering of Cu-based compounds by heteroatom doping is a facile and scalable functionalization strategy to reach high catalytic efficiency. The incorporation of non-metal dopants leads to a difference in atomic radius, electronegativity, and lattice structure, allowing fine-tuning of local electronic configuration. Such heteroatom-doped Cu catalysts can exhibit altered electrical conductivity, electronic band structure, and local charge distribution, with either the dopants or adjacent atoms acting as active sites.[52] Under operating ECH conditions, the heteroatom-doped Cu catalysts can be obtained by in situ structural reconstruction of Cu compounds, which is effective in exposing highly active zero-valence Cu or Cu^0/Cu^I phases and surface structures, such as morphologies, defects, and heterointerfaces.

2.2.7. Alloying

Alloying Cu with a second metal could create new active phases and form metal–metal bonds to break the limitation of monometallic catalysts.[53] The orbital hybridization in metal alloys could promote synergistic effects between metal sites, thereby influencing the activity and reaction kinetics. Rational alloy design can be achieved through the regulation of geometric and electronic effects, leading to various compositions and structures. Ma et al. reported bimetallic Cu–Pd catalysts with ordered, disordered, and phase-separated atomic arrangements for CRR toward C_1 or C_2 chemicals.[43] The production of C_2 products is favored in the phase-separated CCu–Pd configurations with neighboring Cu atoms, whereas the production of CH_4 is favored in the ordered alternating Cu–Pd arrangements. Additionally, the creation of Cu-based high-entropy alloys involving five or more elements can induce mixed metal states, harnessing the nearly continuous energy states of multiple elements for complex ECH reactions.

2.2.8. Constructing Heterojunctions

Inspired by semiconductor physics, the difference in Fermi-level energies could accelerate the electron transfer kinetics at the Schottky heterojunction and optimize the H* absorption behavior.[54] The rational design of Cu-based heterostructures with definitive local electrophilic and nucleophilic regions will enable the precise tuning of adsorption intermediates and electron distribution during ECH reactions. For example, the Cu/ZrO_2 heterostructure exhibited stabilized CO_2*/CO* adsorption and decreased C—C coupling barrier at its interfacial boundaries, which enhanced the CRR selectivity towards C_{2+} products.[55] Sun et al. created built-in electric field within the stacking layers of CuCl (111) and rutile TiO_2 (110), which resulted from their different work functions and Fermi levels.[56]

© 2024 The Authors. Advanced Materials published by Wiley-VCH GmbH

15214095, 2024, 14, Downloaded from https://advanced.onlinelibrary.wiley.com/doi/10.1002/adma.202307913 by Cochrane Chile, Wiley Online Library on [30/09/2026]. See the Terms and Conditions (https://onlinelibrary.wiley.com/terms-and-conditions) on Wiley Online Library for rules of use; OA articles are governed by the applicable Creative Commons License

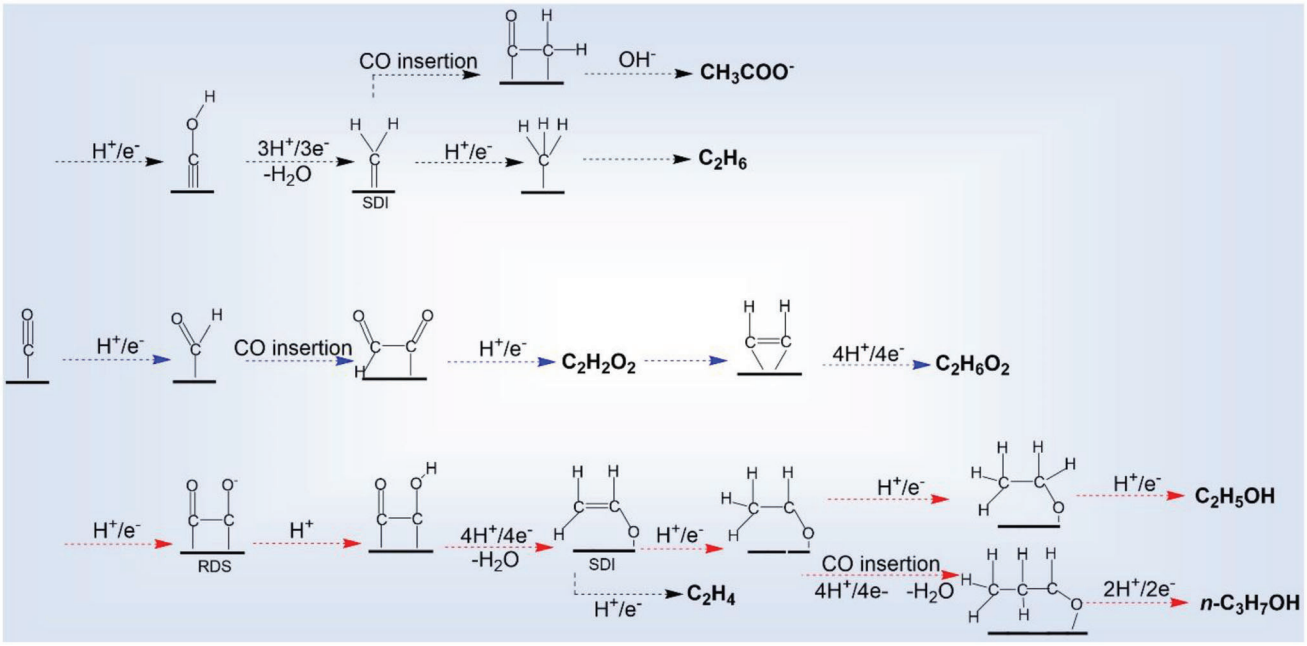

Figure 3. The most possible C_{2+} pathways starting from *CO on Cu surfaces.

The built-in electric field effectively accumulates nitrate ions at the electrode–electrolyte interface and raises the energy of the key *NO intermediate, thus achieving a lower energy barrier of the rate-determining step and NO_3^-RR at ultralow concentration.

3. CRR

Electrochemical CRR is a promising approach to addressing the growing concerns over climate change via mitigating CO_2 emissions and storing intermittent renewable energy in chemical bonds. Compared with simple C_1 products (e.g., carbon monoxide,[57] methane,[58] and formic acid[59–61]), high-order multicarbon-based products (e.g., C_2H_4,[62–63] CH_3COOH, C_2H_5OH,[64] C_3H_7OH, CH_3COCH_3, and $C_4H_4O_3$) possess higher economic value, higher energy density and greater market demand.[65] These versatile products can be further transformed into larger molecules with multiple carbon atoms and serve as building blocks for various products, including plastics, solvents, and pharmaceuticals. Many great reviews have been published regarding the CRR mechanism and C_{2+} products on Cu-based nanocatalysts.[66–68] However, the electrochemical production of C_{2+} products remains challenging due to issues such as complicated electrons transfer pathways, low selectivity, and substantial energy barriers for formation of C—C, C—H, and C—O/C═O bonds. Here, we review the direct CO_2 electrocatalysis, as well as the cascade catalyst and system design for tandem CO_2 electrocatalysis on Cu-based catalysts (**Table 2**).

3.1. Direct Electrocatalysis

Direct CO_2 electrocatalysis on Cu-based catalysts involves the straightforward conversion of CO_2 molecules into multicarbon products through multiple proton-electron transfer steps. Researchers are actively working to develop advanced catalysts and reactors to make the direct electrochemical CO_2-to-C_{2+} process more efficient and economically viable. Our research group has reported the most plausible C_{2+} pathways (**Figure 3**).[69] In these pathways, the routes to C_{2+} species are intricate, with the most challenging step being the CO–CO coupling. At present, copper is considered the only metal with irreplaceable superiority to produce value-added hydrocarbons and oxygenated products due to its optimized adsorption energy for H* and moderate adsorption energy for *CO intermediate, which can facilitate *CO dimerization and suppress the HER side reaction.[69–73]

3.1.1. Selectivity of C_{2+} Products on Cu-based Catalysts

The CRR process requires significant energy to activate CO_2 molecules and could lead to diverse reaction pathways, which poses a great challenge to the selective formation of C_{2+} products. The most important and common C_{2+} reduction products from CRR include ethylene (C_2H_4), acetate (CH_3COO^-), ethanol (C_2H_5OH), and *n*-propanol (C_3H_7OH).

Ethylene is an important chemical building block to produce polyethylene and can be produced with high FE from CRR. In one groundbreaking work, a sputtered Cu catalyst was synthesized on a porous PTFE membrane in a graphite/carbon NPs/Cu/PTFE cathode configuration. The alkaline-tolerating electrode achieved C_2H_4 production with a remarkable 70% FE for 150 h under highly alkaline media due to the lowered CO–CO coupling activation energy barriers by hydroxide ions (**Figure 4**).[74] Also, branched CuO nanoparticles prepared by a polyol process in aqueous ammonia demonstrated a high FE of ethylene (>70%), which is twice achieved by cubic CuO nanoparticles.[75]

© 2024 The Authors. Advanced Materials published by Wiley-VCH GmbH

15214095, 2024, 14, Downloaded from https://advanced.onlinelibrary.wiley.com/doi/10.1002/adma.202307913 by Cochrane Chile, Wiley Online Library on [30/09/2026]. See the Terms and Conditions (https://onlinelibrary.wiley.com/terms-and-conditions) on Wiley Online Library for rules of use; OA articles are governed by the applicable Creative Commons License

Table 2. Comparison of typical Cu-based electrocatalysts for CRR.

Cu-based electrocatalyst design for direct CRR							
Design principle	Catalyst	Product	FE [%]	Current density [mA cm^{-2}] or potential [V vs RHE]	Electrolyte	Electrolyzer	Refs.
Nanostructuring Cu/OD-Cu	Cu_2O superparticles	C_2H_4/C_{2+}	53.2/74.2	−1.15	0.1 M $KHCO_3$	H-type cell	[103]
Nanostructuring Cu/OD-Cu	Multihollow Cu_2O	C_{2+}	75.2 ± 2.7	Partial C_{2+} current of 267 ± 13	2 M KOH	Flow cell	[104]
Nanostructuring Cu/OD-Cu	Plasma-treated copper	C_2H_4	60	−0.9	0.1 M $KHCO_3$	H-type cell	[100]
Facet	Cu (100) facet	C_2H_4/C_{2+}	60/90	Partial C_{2+} current of 520	7 M KOH	Flow cell	[105]
Facet	(001)-oriented 2D-CuO	C_2H_4	33	Partial C_2H_4 current at 229	1 M $KHCO_3$	Flow cell	[106]
Facet	Dominant Cu (111) facet	C_{2+}	62	−0.67/current at 653	1 M KOH	Flow cell	[108]
Facet	High-index facets of copper oxide/hydroxide	C_{2+}	72.7	−1.09	0.1 M $KHCO_3$	H-type cell	[101]
Doping	N-Cu	C_{2+}	73.7	Partial C_{2+} current of 909	1 M KOH	Flow cell	[62]
Doping	Copper-on-nitride	C_{2+}	64	−0.95	0.1 M $KHCO_3$	H-type cell	[110]
Doping	B-doped Cu	C_{2+}	79	−1.1	0.1 M $KHCO_3$	H-type cell	[111]
Doping	Cu–CuI	C_{2+}	71	Partial C_{2+} current of 591	1 M KOH	Flow cell	[113]
Doping	F-Cu	C_{2+}	80	Current at 1600	2.5 M KOH	Flow cell	[114]
Surface alloys	Pd–Cu	C_{2+}	89 ± 4	Current at 500	0.5 M H-K_2SO_4 (pH 2.0)	Flow cell	[117]
Surface alloys	Cu/Pb core–shell	C_{2+}	73.5	Partial C_{2+} current of 294.4	1 M KOH	Flow cell	[118]
Surface alloys	Dealloyed nanoporous Cu–Al	C_2H_4	75	Current at 600	1 M KOH	Flow cell	[120]
Surface alloys	4H/fcc Au@Cu	C_2H_4	46.7	−1.17	0.1 M $KHCO_3$	H-type cell	[121]
Surface alloys	CuTi alloy	C_{2+}	49	−0.8	0.1 M $KHCO_3$	H-type cell	[122]
Modifying with amine	Cu-PANI	C_{2+}	Over 60/80	−1.1/−1.08	0.1 M $KHCO_3$	H-type cell	[124]
Other molecules or complexes	Tetrahydro-bipyridine coated Cu	C_2H_4	72/64	−0.83/current at 600	1 M $KHCO_3$/0.1 M $KHCO_3$	Flow cell/membrane-electrode assembly	[128]
Other molecules or complexes	Cu^0@PIL@Cu^I	C_{2+}	76.1	Partial C_{2+} current of 304.2	1 M KOH	Flow cell	[126]
Other molecules or complexes	Isolated Cu—S motif	C_2H_4	57.2	Current at 400	1 M KOH	Flow cell	[131]
Other molecules or complexes	*N,N'*-ethylene-phenanthrolinium dibromide–Cu	C_{2+}	64	−1.07	0.1 M $KHCO_3$	Flow cell	[132]
Tandem electrocatalysis							
Design principle	Catalyst	Product	FE [%]	Current density [mA cm^{-2}] or potential [V vs RHE]	Electrolyte	Electrolyzer	Ref.
Electrocatalyst design	Cu–Ag bimetallic design	C_{2+}	76	−1.05	0.1 M $KHCO_3$	H-type cell	[135]
System design	Modified Cu	C_2H_4	65	Current at 150	3 M KOH	Solid-oxide electrolysis cell + Membrane-electrode assembly	[136]
Reaction pathway design (CO_2-derived CO reduction)	Pd–Cu	Acetate	70 ± 5	Partial acetate current of 425	1 M KOH	Flow cell	[137]
Reaction pathway design (CO_2-derived CO reduction)	Cu electrode	*n*-propanol	20	−0.45	1 M KOH	Flow cell	[148]

© 2024 The Authors. Advanced Materials published by Wiley-VCH GmbH

15214095, 2024, 14, Downloaded from https://advanced.onlinelibrary.wiley.com/doi/10.1002/adma.202307913 by Cochrane Chile, Wiley Online Library on [30/09/2026]. See the Terms and Conditions (https://onlinelibrary.wiley.com/terms-and-conditions) on Wiley Online Library for rules of use; OA articles are governed by the applicable Creative Commons License

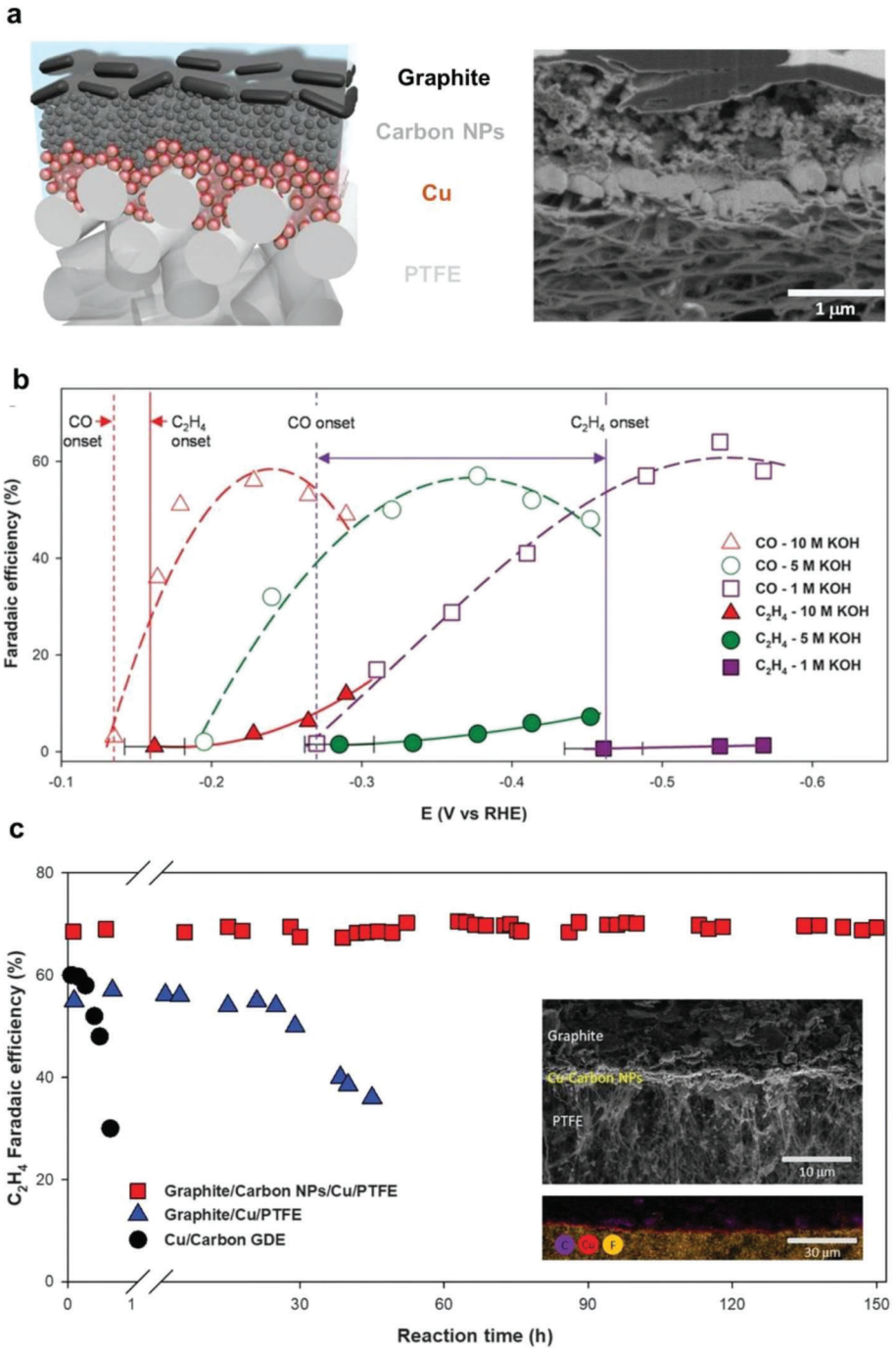

Figure 4. a) Schematic illustration and SEM image of a Cu gas diffusion electrode. b) FE of CO and C_2H_4 in KOH electrolytes with different pH. c) Long-term performance test using Cu electrode. a–c) Reproduced with permission.[74] Copyright 2018, The Authors, published by American Association for the Advancement of Science.

For the 8-electron CRR product, acetic acid is an important organic acid in chemical synthesis and a valuable carbon source for biological synthesis, which can be converted into glucose and other biological substances. Electrocatalytic CO_2-to-acetate was achieved using ultra-small monodispersed clusters of copper and silver ($(Cu)_n$,$(Ag)_m$) derived from electropolymerized poly-Fe(vbpy)$_3$(PF_6)$_2$ film surface, exhibiting a FE of 21.2% in 0.5 M $KHCO_3$.[76] Moreover, a 2D phthalocyanine-based conductive covalent organic framework demonstrated highly selective acetate formation with an FE reaching 90.3%.[77] The electron-dense Cu active sites facilitate the coupling of *CH_3 with another CO_2 to derive acetate, while preventing the conventional coupling of *CO with *CO or *CHO.

© 2024 The Authors. Advanced Materials published by Wiley-VCH GmbH

15214095, 2024, 14, Downloaded from https://advanced.onlinelibrary.wiley.com/doi/10.1002/adma.202307913 by Cochrane Chile, Wiley Online Library on [30/09/2026]. See the Terms and Conditions (https://onlinelibrary.wiley.com/terms-and-conditions) on Wiley Online Library for rules of use; OA articles are governed by the applicable Creative Commons License

15214095, 2024, 14, Downloaded from https://advanced.onlinelibrary.wiley.com/doi/10.1002/adma.202307913 by Cochrane Chile, Wiley Online Library on [30/09/2026]. See the Terms and Conditions (https://onlinelibrary.wiley.com/terms-and-conditions) on Wiley Online Library for rules of use; OA articles are governed by the applicable Creative Commons License

Compared with ethylene and acetate, ethanol[41,78–88] with higher energy density by volume (21 MJ L^{-1}) is regarded as one of the most important reduction products of CRR obtained through a 12-electron transfer pathway. The C_2 species are typically formed through the $*CH_2CHO$ as a common intermediate, in which a further hydrogenation process is required to obtain ethanol instead of proceeding with hydrogenolysis to form ethylene.[89] Recently, a novel mechanism for ethanol production was reported on a Ag-modified cubic Cu_2O from our group, which derived dCu_2O/Ag bimetallic alloy after activation under operating conditions.[64] The modification of *CO binding configuration created a mixed adsorption arrangement (atop and bridge sites), inducing asymmetric C—C coupling intermediates and resulting in increased ethanol production. Moreover, the co-modification of F anions and K cations on nanocrystal Cu (111) showed an outstanding CO_2-to-ethanol FE of 52.9 ± 3.7% with a partial current density of 423 ± 30 mA cm^{-2}.[90] The promoted ethanol selectivity was ascribed to the stabilized C—O bond and controllable hydrogenation of the C═C bond, which favored the formation of CH_2═CHO* intermediate. Derived from hollow Cu_2S, the Cu_2S_{1-x} hollow nanocubes with stabilized $Cu^{\delta+}$ sites achieved an excellent FE of 73.3% toward ethanol under a low overpotential of 0.19 V. The electron-donating property of the abundant $Cu^{\delta+}$ sites contributed to the lowered barrier for C—C coupling.[91]

Converting CO_2 into C_3 products is a critical process for multicarbon production. However, the complexity of the 18-electron process with C_2—C_1 coupling in CO_2-to-C_3 conversion hinders its industrial application. To improve the selectivity, a lithium-mediated strategy to construct double sulfur vacancies on hexagonal CuS (100) planes was proposed to stabilize both important OCCO* and CO* intermediates toward *n*-propanol with an FE of 15.4 ± 1%.[92] Copper foil electrodes have also been found to produce other C_3 products from CRR, such as acetone, hydroxyacetone, allyl alcohol, and propionaldehyde.[93] The acetone product of CRR was identified on single-atom Cu sites coordinated with four pyrrole-N atoms with a FE of 36.7%.[94] This high selectivity is attributed to the lower energy required for CO_2 activation and C—C coupling at these sites. Moreover, CuAg alloy achieved a remarkable FE of 56.7% toward 2-propanol instead of 1-propanol in a supersaturated carbonated electrolyte.[95] The performance was attributed to the key *CO intermediate for C_1—C_1 coupling and $*OCH_2CH_3$ intermediate for C_1—C_2 coupling, the increased local CO_2 concentration through CO_2-supersaturation strategy, and the weakened intermediate binding in the middle of the alkyl chain by the introduced Ag atoms. Very recently, metallic Cu nanocrystals derived from CuCl have been reported for propylene formation.[96] The designed Cu electrode mainly consists of Cu (100) and (111) facets, which preferentially absorb key $*C_1$ and $*C_2$ intermediates, respectively. Different from the *n*-propanol formation mechanism, the main pathway toward propylene involved the coupling of molecular/adsorbed CO_2 with the $*C_2$ intermediates, rather than *CO.

3.1.2. Cu-Based Electrocatalyst Design for Direct CRR

Engineering Cu-based catalysts is an effective strategy to boost their CO_2-to-C_{2+} performance. The construction of CO–CO intermediates can be induced by adjusting the intermediate adsorption and desorption on Cu-based catalysts by various methods, including morphology and structure control, facet engineering, doping p-block non-metallic elements, engineering with metals, and modification with amines, organic molecules, and complexes.

Firstly, metallic Cu and oxygen-derived Cu (OD-Cu) have widely been employed as CO_2-to-C_{2+} electrocatalysts.[75,97–102] Lum et al. provided evidence for the product-specific active sites of OD-Cu.[97] Isotope labeling experiments on oxide-derived Cu revealed three different types of active sites within Cu. One site is favorable for ethylene production, another site is responsible for ethanol/acetate, and the last one facilitates 1-propanol production. The morphology and structure of OD-Cu are highly tunable by rational catalyst design. A crystal facet engineering approach delivered selectively exposed Cu_2O (100) under in situ electrochemical CRR conditions.[98] Another work reported Cu_2O superparticles as a model precatalyst to investigate the important role of Cu^+ within the inside of Cu_2O, achieving an outstanding FE of 53.2% for C_2H_4 compared with geometrically simpler cubic Cu_2O.[103] By morphology control, Cu^+ species can be stabilized by carbon intermediates at cathodic potentials within multihollow Cu_2O, producing C_{2+} compounds with FE of up to 75.2 ± 2.7%, and C_2H_4 FE of 38.0 ± 1.4% (**Figure 5a–c**).[104] Moreover, nanoscaled defects were rationally constructed within Cu nanosheets to produce a high C_2H_4 FE of 83.2%.[99] Surface roughness is a determining factor of reactant adsorption and CRR selectivity. Plasma-treated copper with a rough surface was believed to induce high ethylene activity with key Cu^+.[100] The Cu^+ derived from copper oxychloride sol–gel was stabilized under a more negative reduction potential, exhibiting a high ratio of 200 for C_2:C_1 selectivity at −1.2 V versus reversible hydrogen electrode (RHE) with a partial ethylene current of 160 mA cm^{-2}.[102]

Secondly, most of the reported active facets for CRR are on the Cu (100) facet, but there are also other facets that exhibit decent activity. Cu-based catalysts are processed to form in situ electroreduced Cu, in which the preferentially exposed Cu (100) facets of Cu-CO_2 drive C_2H_4 FE of 60 ± 2% over 65 h under a relatively high current of 350 mA cm^{-2} (Figure 5d,e).[105] Meanwhile, the (001)-oriented 2D-CuO nanosheet catalyst was evaluated in neutral conditions to perform unprecedented C_2H_4 and C_{2+} activity.[106] Also, Cu (100) and stepped Cu

(211) are believed to favor C_{2+} formation.[107] Besides, a nonporous copper catalyst with a dominant Cu (111) facet primarily supports C_{2+} products, mainly C_2H_4.[108] Planar-square (two flat (111) planes with 60° lattice orientation) and convex-square (rotation and then splicing of two (111) planes) sites are predicted to produce C_2H_4, while step-square sites, i.e., $n(111) \times (100)$, are anticipated as catalytic activation sites for C_{2+} alcohols generation.[109] It should be noted that facet control can be achieved during in situ structural evolution of Cu-based catalysts. During the electroreduction pre-treatment, the copper oxide/hydroxide crystals underwent an in situ fragmentation process and created nanosized irregular grains with various high-index facets, which resulted in improved selectivity towards C_{2+} products.[101] These high-energy facets have tremendous potential to be preserved, especially under highly negative potentials and within a short time frame (−5.0 V vs Ag/AgCl for 10 s).

© 2024 The Authors. Advanced Materials published by Wiley-VCH GmbH

15214095, 2024, 14, Downloaded from https://advanced.onlinelibrary.wiley.com/doi/10.1002/adma.202307913 by Cochrane Chile, Wiley Online Library on [30/09/2026]. See the Terms and Conditions (https://onlinelibrary.wiley.com/terms-and-conditions) on Wiley Online Library for rules of use; OA articles are governed by the applicable Creative Commons License

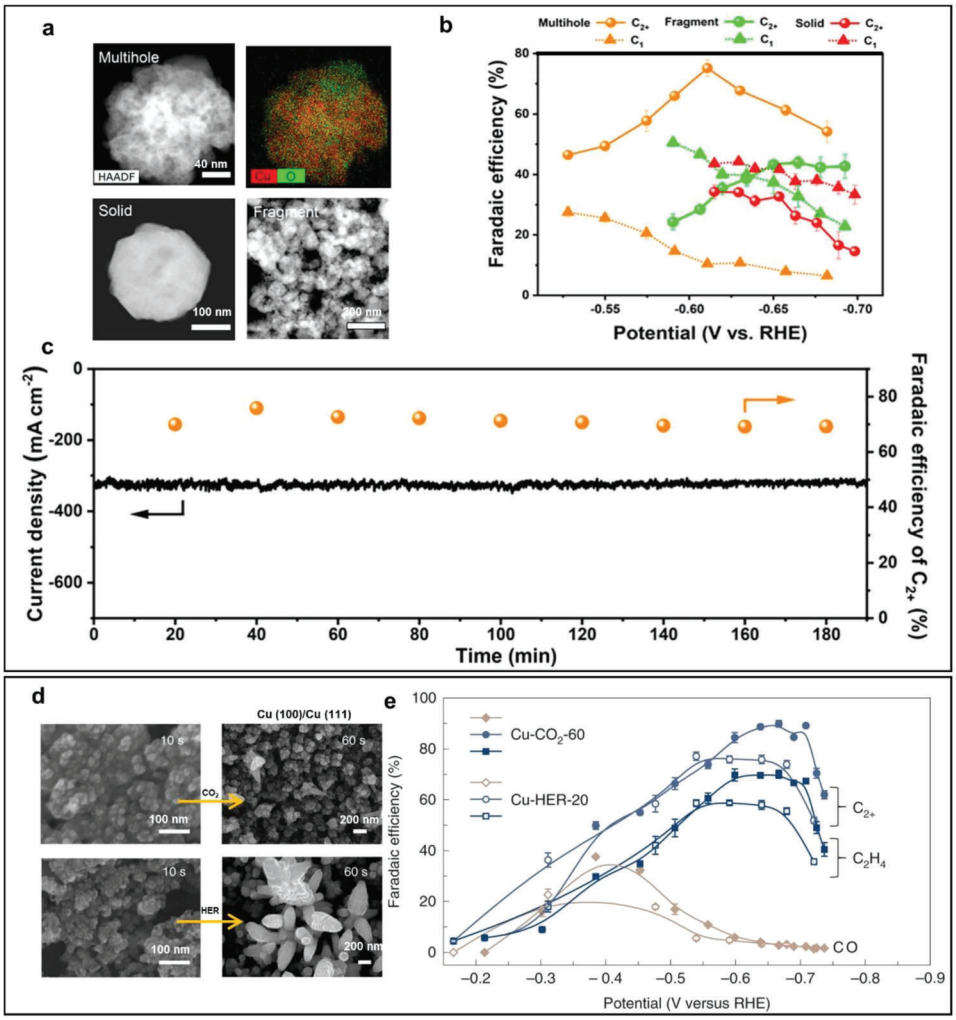

Figure 5. a) SEM images of multihollow, solid, and fragment Cu_2O catalyst. b) FE on Cu_2O. c) Long-term stability test for CRR. a–c) Reproduced with permission.[104] Copyright 2020, American Chemical Society. d) SEM images of Cu-CO_2 and Cu-HER. e) FE of Cu-CO_2 and Cu-HER. d) Adapted with permission.[105] Copyright 2020, The Authors, published by Springer Nature. e) Reproduced with permission.[105] Copyright 2020, The Authors, published by Springer Nature.

Thirdly, compositional engineering by p-block non-metallic elements in Cu-based catalysts can be applied to tune the electronic properties for CRR.[110–111] By systematically manipulating a series of heteroatoms of Cu-based compounds (N, P, S, O), our group reported the ampere-level current of CO_2-to-C_{2+} production achieved by tuning the *CO coverage (**Figure 6**a,b). Among the studied heteroatom-engineered Cu, nitrogen-engineered Cu showed the highest C_{2+} FE (73.7%) at 1100 mA cm^{-2}.[62] A Cu^+ support catalyst derived from Cu_3N was synthesized, showing an FE of 64 ± 2% for C_{2+} products.[110] In comparison to pure copper, a remarkable 40-fold increase in the ratio of C_{2+} to the competing CH_4 was achieved on copper-on-nitride. Meanwhile, the electron-deficient boron was found to effectively modify the electronic properties of Cu catalysts. Boron doping was used to adjust the ratio of $Cu^{\delta+}$ and Cu^0 and enhance the catalyst stability and C_{2+} selectivity.[111] The B-doped Cu ensures electron localization for maintaining high stability for over ≈40 h in CRR to multicarbon hydrocarbons (C_{2+} FE of 79 ± 2%). Moreover, the integration of N and B into the Cu/C platform adjusted the catalytic activity of reconstructed Cu to promote C_{2+} formation.[112] The introduction of B achieved a cathodic power conversion efficiency of 44% and a FE of 68.1% for C_2H_4 products, while N modification demonstrated an amplified FE of C_{2+} products of 82% with a partial current density exceeding 320 mA cm^{-2} and the increased stability over 180 h. Halogen elements have been incorporated into Cu-based materials to stabilize Cu species in CRR. For example, abundant Cu^0/Cu^+ interfaces with adsorbed iodine species were constructed after physical mixing of Cu–CuI composite.[113] The remaining Cu^+ and adsorbed iodine are crucial for the improved CO adsorption and C—C coupling, reaching a C_{2+} FE of 71% and C_{2+} partial current density of 591 mA cm^{-2}. In addition, the hydrogen-assisted C—C coupling mechanism was proposed over a fluorine-modified Cu catalyst.[114] The presence of fluorine is beneficial for water activation, CO adsorption, and *CHO formation, displaying an exceptionally high current density of 1.6 A cm^{-2} with a C_{2+} (mainly ethylene and ethanol) FE of 80%. Kim

 © 2024 The Authors. Advanced Materials published by Wiley-VCH GmbH

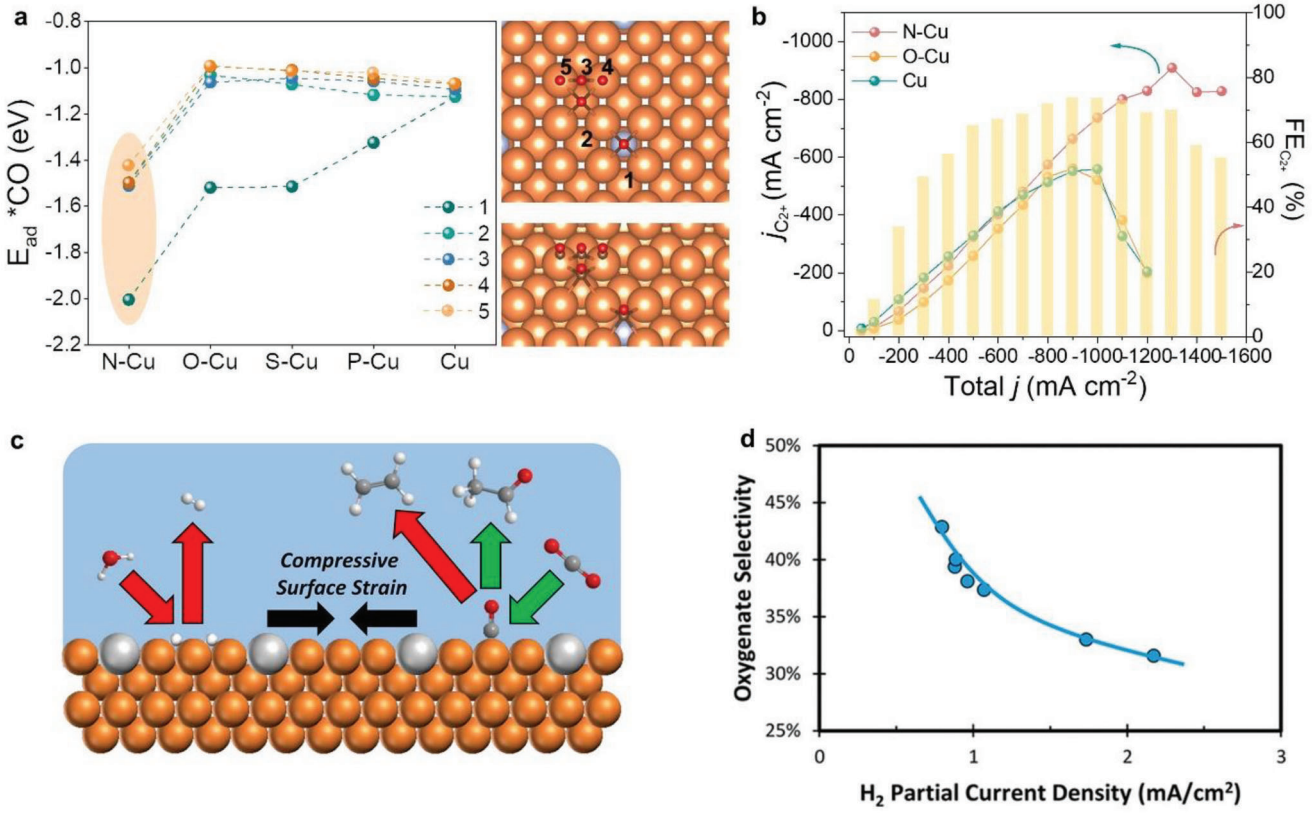

Figure 6. a,b) Adsorption energy of *CO intermediate at various adsorption sites on heteroatom-doped Cu surfaces for C_{2+} products. a,b) Reproduced with permission.[62] Copyright 2022, American Chemical Society. c,d) CRR on CuAg surface alloys with compressive strain for multicarbon oxygenate production. c,d) Reproduced with permission.[119] Copyright 2017, American Chemical Society.

et al. developed a scalable strategy to fabricate anodic halogenated Cu foil electrodes (CuCl, CuBr, and CuI) in brine solutions.[115] When applied under a cathodic potential, these catalysts were reconstructed with defective sites and low roughness, leading to the CO_2-to-C_2H_4 transformations with FE of 45.1% on Cl-Cu, 49.5% on Br-Cu, and 44.5% on I-Cu. Besides, by simply adjusting the counter anions from NO_3^-, Cl^-, to B^- on crystalline trinuclear copper clusters, the molecular model catalysts with pre-designed active sites showed the varied C_2H_4 FE range from 31.90% to 55.01%.[116] Such performance was attributed to the favorable C—C coupling of active *CHO intermediates on two adjacent Cu sites.

Fourthly, engineering Cu with metals also proves effective for boosting CRR activity and selectivity. For example, introducing Pd into Cu could improve *CO adsorption while simultaneously suppressing HER activity.[117] This modification allows the catalyst to operate efficiently in acidic solutions without CO_2 crossover. On the Pd–Cu electrode, the electrocatalytic conversion of CO_2 into C_{2+} products achieved a high FE of 89 ± 4% under a current density of 500 mA cm^{-2}, accompanied by a CO_2 utilization rate of 60 ± 2% toward C_{2+} products in acidic media (pH 2). Benefiting from the powerful synergy between the Cu core and ultrathin Pb shell, the nanocrystal Cu/Pb core–shell structure facilitated the conversion of CO_2 into C_{2+} products by lowering the formation energy of critical *COOH and *OCCOH intermediates.[118] Moreover, the formation of CuAg surface alloy induced compressive strain and reduced the oxophilicity of Cu atoms, resulting in weakened *H adsorption energy and improved multicarbon products derived from CO (Figure 6c,d).[119] Aided by active machine learning screening, the introduction of Al in the proximity of the Cu created a dealloyed nanoporous Cu–Al catalyst and produced C_2H_4 with a FE of 75 ± 4%, which was attributed to the enhanced C—C dimerization in the favorable Cu coordination environment.[120] In another study, the phase-dependent CRR behavior of Cu catalysts was analyzed on high-purity 4H Au@Cu, heterophase 4H/fcc Au@Cu core–shell nanostructures, and conventional fcc Cu.[121] The higher C_2H_4 selectivity was achieved over non-usual 4H and 4H/fcc Cu through crystal phase engineering. Hu et al. reported that introducing subsurface Ti atoms into Cu enriched the electron density of surface Cu, which led to coordinatively unsaturated Cu sites on amorphous CuTi alloy that tended to adjust *CO adsorption for dimerization.[122]

Fifthly, in addition to catalyst structure engineering, modifying the catalyst–electrolyte interface with amine offers a new degree of freedom to enhance the accumulation of CO_2 reactants, control product selectivity, and prevent the competing HER. Up to now, the modification of electrode surfaces with polyamine-related molecules has attracted significant interest in improving the electroreduction activity, but their exact mechanism remains controversial. Chemical absorption in a solution containing amine-based organic compounds has been proposed as the

© 2024 The Authors. Advanced Materials published by Wiley-VCH GmbH

15214095, 2024, 14, Downloaded from https://advanced.onlinelibrary.wiley.com/doi/10.1002/adma.202307913 by Cochrane Chile, Wiley Online Library on [30/09/2026]. See the Terms and Conditions (https://onlinelibrary.wiley.com/terms-and-conditions) on Wiley Online Library for rules of use; OA articles are governed by the applicable Creative Commons License

most efficient method for capturing CO_2 from factory exhaust, which could potentially explain their role in CRR.[123] Wei et al. reported a polycrystalline Cu electrode with a thick film of polyaniline of ≈50 nm covering its surface (**Figure 7**a,b).[124] The modified catalyst was applied in CRR, resulting in a substantial increase in FE from ≈15% to over 60% for the production of C_{2+} hydrocarbons in $KHCO_3$ solutions. Chen et al. presented a novel hybrid catalyst consisting of polyamine and copper.[125] This hybrid electrode was fabricated through co-electroplating, which led to significant improvements in the production of C_{2+} hydrocarbons, especially enhancing ethylene formation. Among the series of amine-containing additives (P1 to P5) modified on the copper electrodes, P1, i.e., poly-*N*-(6-aminohexyl)acrylamide, exhibited the most favorable CRR performance for ethylene with a high partial current density of 312 mA cm^{-2} and FE of 87%. The enhanced CO_2-to-C_2H_4 performance of Cu-P1 was attributed to the higher surface pH and the increased CO content due to the presence of the amine groups, which effectively stabilized the key intermediates and promoted the overall CRR efficiency.

Lastly, other organic molecules and complexes can be introduced on Cu to provide additional binding interactions and tune the intermediates in favor of CO_2-to-C_{2+} efficiency.[127] For example, the tetrahydro-bipyridine organic films coated on Cu effectively stabilized the "atop-bound" CO intermediate, converting CO_2 to ethylene with an FE of 72% and full-cell energy efficiency of 20% in neutral media.[128] By employing L-ascorbic acid as a chemical molecular scalpel, a Cu_2BDC–MOF-derived Cu catalyst demonstrated high FE for C_{2+} products owing to the formation of Cu^+ as a soft acid and BDC as a hard base ligand.[63] Furthermore, Zhu et al. reported a π–π stacking framework consisting of a trinuclear copper(I) compound, CuBtz, with pyrazolate-bridged dicopper(I) sites.[129] The exceptional CRR performance in terms of FE for C_{2+} products could be ascribed to the favorable C—C coupling of *CO intermediate on those uncoordinated N coordinated with the dicopper(I). The poly(ionic liquid) (PIL)-based Cu^0@PIL@Cu^I catalyst, with Cu^0 at the center and Cu^I on the outer layer, demonstrated excellent reaction selectivity for C_{2+} products (FE: 76.1%; Partial current density: 304.2 mA cm^{-2}).[126] The relatively weak intermolecular interactions between the key intermediates and the PIL layer contributed to the lower C—C coupling energy, thereby enhancing the CO_2-to-C_{2+} performance (Figure 7c). In another work, the presence of dual active Cu centers coordinated within a molecular scaffold of g-C_3N_4 contributed to the favorable generation of C_{2+} products when compared to the CH_4 production on single-site Cu–C_3N_4 catalyst.[130] By introducing local sulfur doping into a Cu-based MOF, an isolated Cu–S motif was achieved through reconstruction under reduction potential.[131] The stable $Cu^{\delta+}$ species within the Cu(S) matrix favor the *CO intermediate, leading to a high ethylene selectivity of 57.2% under a current density of 400 mA cm^{-2}. Additionally, using *N,N'*-ethylene-phenanthrolinium dibromide as a molecular additive, a nanostructured cube-like Cu was established on the copper electrode surface to reach CO_2-to-C_{2+} selectivity of 70% over 40 h.[132] This modification also suppressed the competing HER and CH_4 formation without any noticeable change in the surface morphology. Inspired by the plastron effect by aquatic arachnids, a hierarchically structured Cu dendrite was treated with 1-octadecanethiol to create a superhydrophobic surface.[133] The resulting hydrophobic electrode demonstrated a 56% FE for ethylene production. Besides, derived from an electrodeposited Cu complex film on a Cu substrate, a 3D dendritic Cu–Cu_2O composite achieved remarkable catalytic activity for the reduction of CO_2 to C_{2+} products with low overpotentials of 0.53 V (for acetic acid) and 0.48 V (for ethanol) in an aqueous KCl electrolyte.[134]

3.2. Tandem Electrocatalysis

The direct formation of C_{2+} products is challenging due to the extremely high energy barrier and the linear scaling relationship of CRR intermediates. To overcome the challenges of low activity, undesired side reactions, carbonate formation, and electrolyte degradation during direct electrocatalytic reduction of CO_2 to C_{2+} products, the multistep tandem process for CO_2 electroreduction presents a promising solution.[138] In this cascade process, the first step involves the conversion of CO_2 to CO in a non-alkaline solution. Subsequently, as CO is a crucial intermediate towards high-order C_{2+} products, the generated CO can be further reduced in the second step to achieve carbon–carbon coupling, thereby facilitating an efficient and economically viable CO_2-to-C_{2+} pathway.[139]

3.2.1. Electrocatalyst Design for Tandem Electrocatalysis

The design of tandem CRR electrocatalysts generally requires multiple active sites within a suitable distance to catalyze each elementary steps in the sequential reaction. Bimetallic electrocatalysts are typically employed in the tandem electrode design, where one metal, such as Ag or Au, promotes the reduction of CO_2 to CO, and then efficient C—C coupling is facilitated on the Cu surface. Through precise engineering of uniformly decorated Ag islands on Cu nanowires, an impressive FE of 76% for CRR toward high-order C_{2+} products was achieved (**Figure 8**a).[135] Operando spectroscopy confirmed the formation and high coverage of CO intermediate on dispersed Ag sites, leading to efficient C—C coupling owing to the nearly 95% spillover of CO transferred from Ag to Cu surface. A nanozyme structure comprising an Ag core and mesoporous Cu shell was designed for cascade CO_2-to-C_{2+} reaction, demonstrating high selectivity of CO_2-to-CO on the Ag core, followed by C_3 production (*n*-propanol and propionaldehyde) on the mesoporous Cu shell at a relatively low potential of −0.6 V vs RHE.[140] Moreover, Gurudayal et al. reported the temporal separation in the two steps of cascade CRR pathway by placing Ag upstream of Cu electrode.[141] The supersaturated CO concentration on the upstream Ag electrode promoted efficient carbon—carbon coupling on the downstream Cu electrode with a CO intermediate conversion rate of more than 80%. Apart from Ag, Au can also be selected as a CO-producing component owing to its ability to provide high coverage of CO intermediate. Morales-Guio et al. reported the deposition of gold nanoparticles onto polycrystalline copper electrodes by physical vapor deposition for highly active activity C_{2+} alcohol formation.[142] The formation of CO on Au provides a high local concentration of CO to the nearby Cu surface, which accelerates the C—C coupling at a relatively low overpotential.

© 2024 The Authors. Advanced Materials published by Wiley-VCH GmbH

15214095, 2024, 14, Downloaded from https://advanced.onlinelibrary.wiley.com/doi/10.1002/adma.202307913 by Cochrane Chile, Wiley Online Library on [30/09/2026]. See the Terms and Conditions (https://onlinelibrary.wiley.com/terms-and-conditions) on Wiley Online Library for rules of use; OA articles are governed by the applicable Creative Commons License

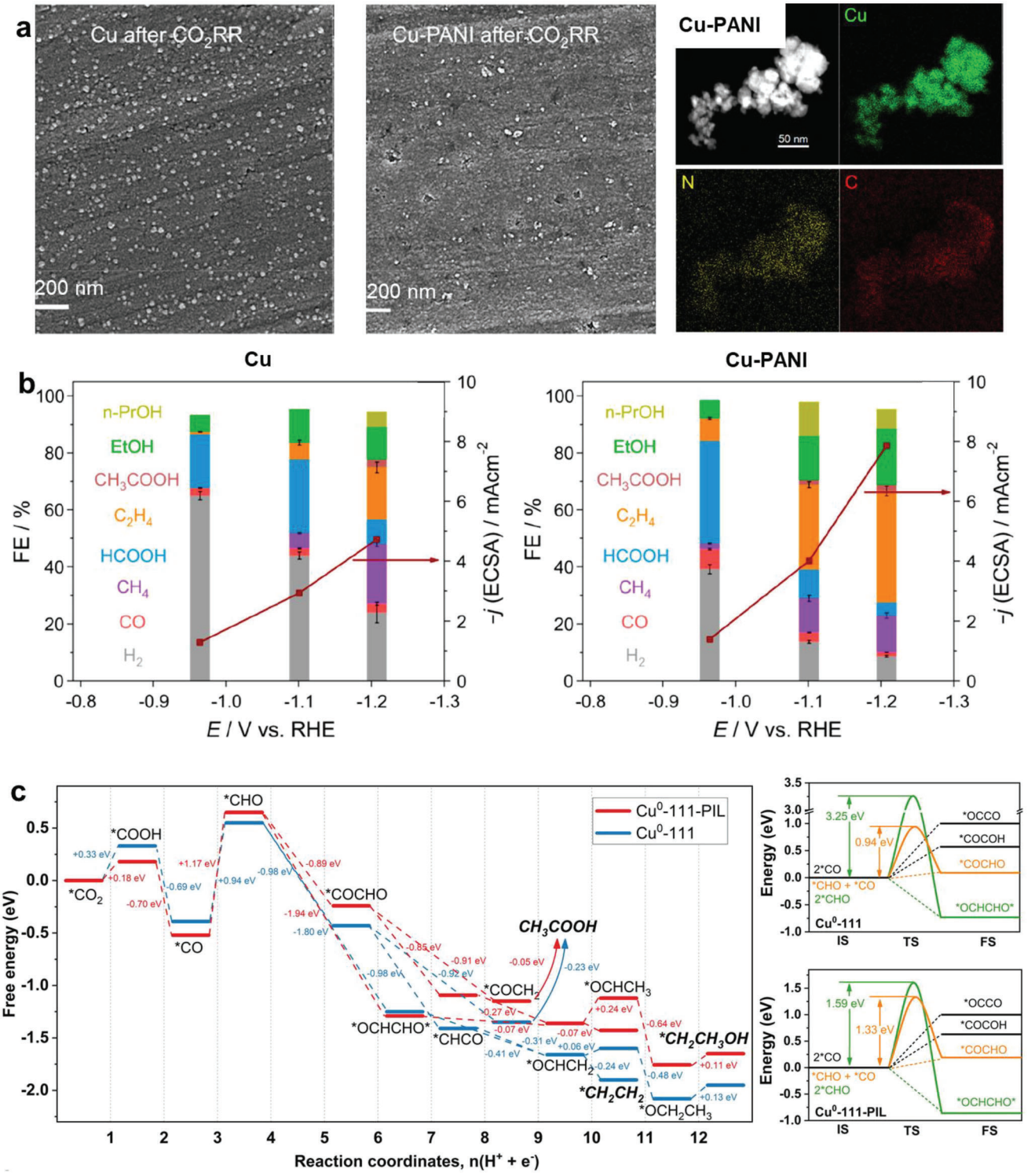

Figure 7. a) SEM images of Cu and Cu-PANI and elemental mapping images of Cu-PANI. b) The corresponding CRR performance for C_{2+} hydrocarbon production. a,b) Reproduced with permission.[124] Copyright 2020, American Chemical Society. c) The free-energy profile of CRR process of poly(ionic liquid)-based Cu^0@PIL@Cu^I electrocatalyst and energy diagrams of C–C coupling. Reproduced with permission.[126] Copyright 2021, Wiley-VCH.

© 2024 The Authors. Advanced Materials published by Wiley-VCH GmbH

15214095, 2024, 14, Downloaded from https://advanced.onlinelibrary.wiley.com/doi/10.1002/adma.202307913 by Cochrane Chile, Wiley Online Library on [30/09/2026]. See the Terms and Conditions (https://onlinelibrary.wiley.com/terms-and-conditions) on Wiley Online Library for rules of use; OA articles are governed by the applicable Creative Commons License

15214095, 2024, 14, Downloaded from https://advanced.onlinelibrary.wiley.com/doi/10.1002/adma.202307913 by Cochrane Chile, Wiley Online Library on [30/09/2026]. See the Terms and Conditions (https://onlinelibrary.wiley.com/terms-and-conditions) on Wiley Online Library for rules of use; OA articles are governed by the applicable Creative Commons License

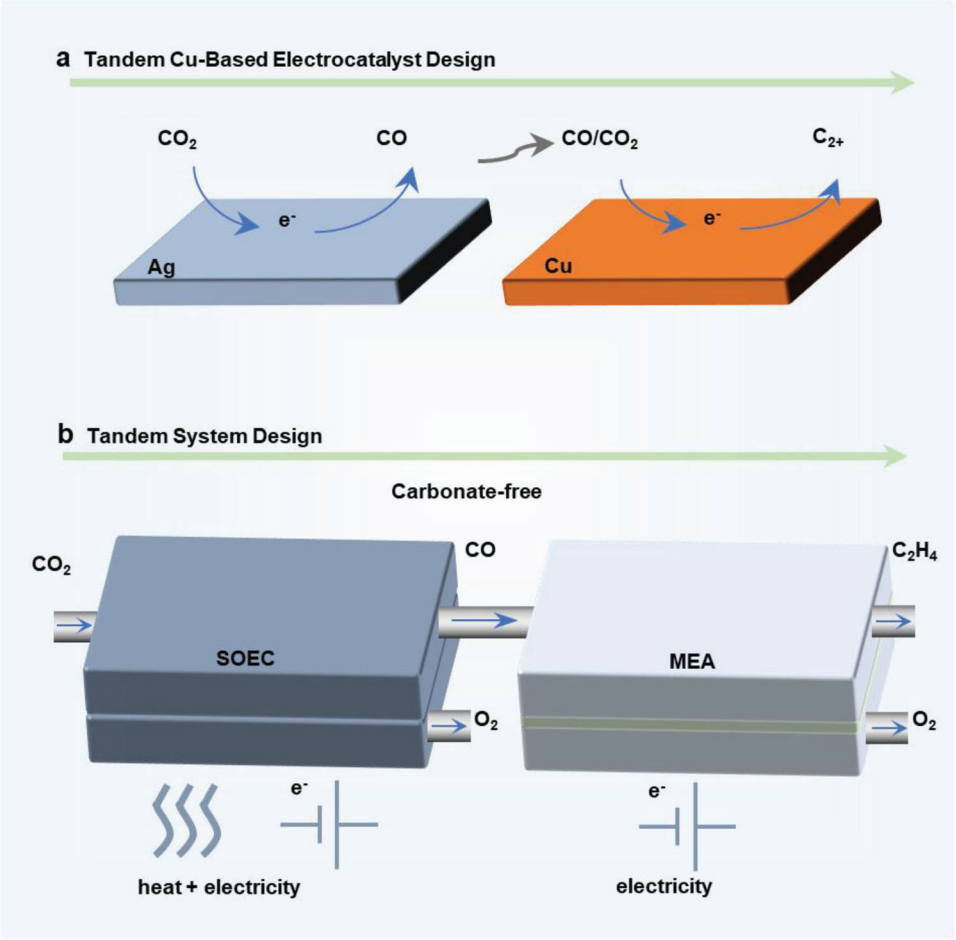

Figure 8. Tandem Cu-based electrode design for electrocatalytic CO_2 reduction. a) Tandem electrocatalyst design of Cu with Ag. b) The tandem CRR system features CO_2 reduction to CO in a solid-oxide electrolysis cell and CO reduction to multicarbon products in a membrane electrode assembly electrolyzer.

3.2.2. System Design for Tandem Electrocatalysis

Efficient CO_2 utilization and high C_{2+} selectivity can be achieved in cascade CO_2 electroreduction systems implemented with a two-reactor configuration. As a typical example, Ozden et al. reported a cascade approach involving CO formation derived from CO_2 reduction in a solid-oxide electrolysis cell, followed by a membrane electrode assembly electrolyzer to achieve efficient CO-to-C_2H_4 conversion (Figure 8b).[136] The system achieved a high FE of 65% and a full-cell energy efficiency of 28% on a layered Cu electrocatalyst modified with *N*-tolyl-tetrahydrobipyridine and SSC ionomer. In comparison to the direct CO_2-to-C_2H_4 pathway, the full cascade system requires an energy input of ≈138 GJ (ton C_2H_4)$^{-1}$, resulting in nearly 50% saving in the energy required. The technoeconomic analysis of the alkaline flow cell and neutral membrane electrode assembly for the cascade CO_2-CO-C_2H_4 process was also reported.[143] The main issues contributing to higher costs include the crossover in the neutral pH membrane electrode assembly cell, which results in CO_2 loss, and the generation of carbonate in the alkaline flow cell that leads to a non-ideal CO_2 utilization rate. To address these challenges, a proposed system includes electrolytic CO_2-to-CO via solid-oxide electrolysis with a high-temperature cell followed by electrocatalytic CO-to-C_2H_4 in an alkaline solution. This system effectively eliminates the carbonate problem and enables the production of C_2H_4 with a total energy efficiency of ≈52%. Romero Cuellar et al. presented an integrated system consisting of two flow cells for cascade CO_2-CO-C_{2+} conversion.[144] The first cell utilized Ag as the electrode for CO_2-to-CO conversion, while the second cell employed Cu as the electrode for CO-to-C_{2+} conversion, resulting in a higher FE of 62% compared to the direct pathway. Theaker et al. designed a tandem reactor for efficient CO_2-CO-C_2H_5OH conversion with an overall FE of 11.0%.[145] This high efficiency was maintained by excluding CO_2 as a reactant from the second-stage electrolyzer.

3.2.3. Reaction Pathway Design for Electrocatalysis

CO is the key intermediate in CRR and can also function as a reactant for subsequent multistep reduction processes. Electrocatalytic CO_2-derived CO reduction holds great potential for various high-order multicarbon products across the chemical production supply chain, especially for acetate or liquid alcohol

© 2024 The Authors. Advanced Materials published by Wiley-VCH GmbH

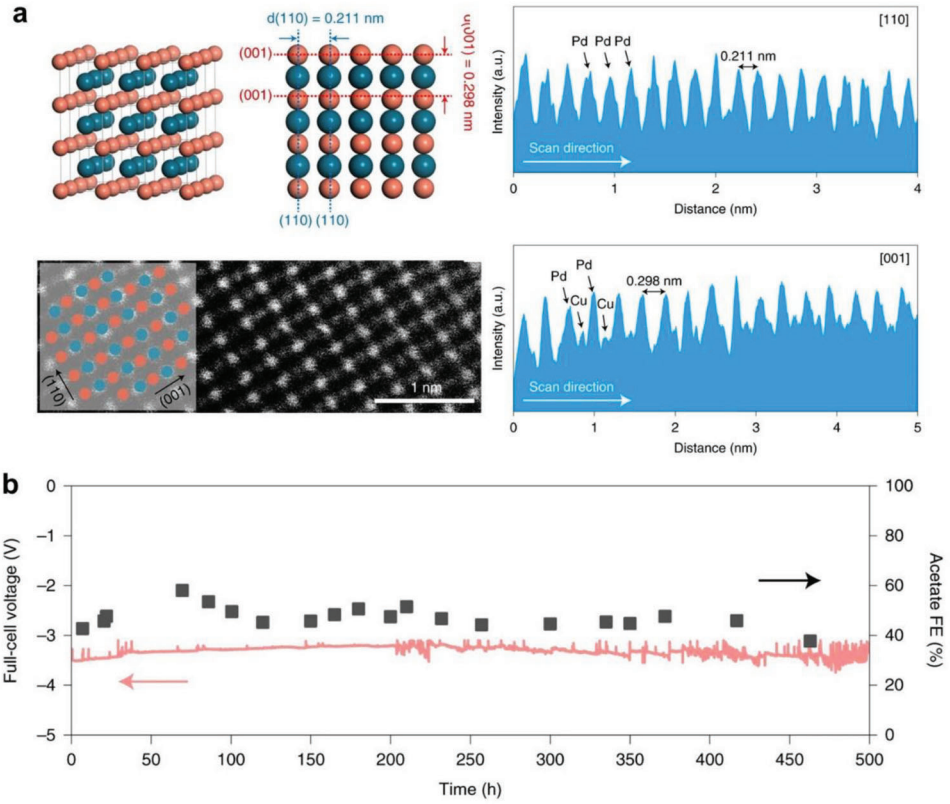

Figure 9. Electrocatalytic CO_2-derived CO reduction on PdCu. a) Crystal structure and high-angle annular dark-field scanning transmission electron microscopy (HAADF-STEM) images of PdCu. b) Long-term test for CO electroreduction. a,b) Reproduced with permission.[137] Copyright 2022, The Authors, published by Springer Nature.

formation.[146] Jouny et al. reported an electrocatalytic CO reduction cell with carefully controlled gas and ion transport, achieving a high rate of 850 µmol C_{2+} cm^{-2} h^{-1} on the Cu electrode, and a conversion of 68% under a low cell potential (2.5 V).[147] Also, an atomically ordered PdCu intermetallic compound was found to facilitate electrocatalytic CO-to-acetate conversion (**Figure 9**).[137] The abundant *CO coverage on the PdCu surface favors the stabilized key ethenone intermediate and suppresses the competing HER, thereby resulting in enhanced acetate production with an FE of 70 ± 5%. In a membrane electrode assembly, the PdCu catalyst exhibited a continuous acetate FE of ≈50% during long-term CO electroreduction for 500 h.

The formation of C_3 products from CO represents an effective route to further C—C coupling with the enhanced adsorption of CO on Cu electrode surfaces. Derived from highly fragmented Cu with a compact grain boundary structure, a Cu electrode achieved electrocatalytic FE of 20% toward *n*-propanol.[148] Density functional theory (DFT) calculation demonstrated that the crucial C_3 intermediate formation was induced at the interface between Cu (100) and Cu (111) facets. In addition, Wang et al. demonstrated that the incorporation of a second metal into Cu electrodes could lead to enhanced C_3 formation.[149] Among the catalysts studied, the Ag-doped Cu exhibited the highest FE of (33 ± 1)% for *n*-propanol as the primary C_3 product and a record-level half-cell energy efficiency of 21% during the electrocatalytic CO reduction process. The Ag dopants modified the electronic structure of Cu, resulting in distinct electronic configurations on the two neighboring Cu atoms. This asymmetry in electronic structure served as active sites for electrocatalytic carbon—carbon coupling, including the facilitated C_1—C_1 and C_1—C_2 coupling reactions.

In summary, copper and its derivatives have shown great potential in direct electrolysis or indirect tandem processes toward C_{2+} products. However, the economic efficiency of individual high-order products is still not satisfying, and breakthroughs in the design of electrochemical reactors are required for more efficient mass transfer and long-term stable CO_2 conversion at large current density and low overpotential. The capture and separation of ultralow concentration CO_2 in the atmosphere should also be deemed an essential aspect for the CRR technology to be practically operable.

4. ECH of Alkynes

Selective semi-hydrogenation of alkynes into alkenes (R—C≡C → R—C=C) is a key chemical process for the synthesis of value-added fine chemicals and represents a potential alternative to the industrial thermocatalytic transformation. Due to the high cost and limited availability of noble-metal materials (e.g., Pd), there has been growing interest in Cu-based catalysts for alkyne conversion. This section discusses the ECH of acetylene and other liquid alkynes on Cu-based catalysts (**Table 3**).

© 2024 The Authors. Advanced Materials published by Wiley-VCH GmbH

15214095, 2024, 14, Downloaded from https://advanced.onlinelibrary.wiley.com/doi/10.1002/adma.202307913 by Cochrane Chile, Wiley Online Library on [30/09/2026]. See the Terms and Conditions (https://onlinelibrary.wiley.com/terms-and-conditions) on Wiley Online Library for rules of use; OA articles are governed by the applicable Creative Commons License

Table 3. Comparison of typical Cu-based electrocatalysts for ECH of alkynes.

ECH of acetylene								
Design principle	Catalyst	Reactant	Product	FE [%]	Current density [mA cm^{-2}] or potential [V vs RHE]	Electrolyte	Electrolyzer	Refs.
Nanostructuring	Cu dendrites	Pure C_2H_2/1% C_2H_2	C_2H_4	97/61	−0.6	1 M KOH	Flow cell	[157]
Nanostructuring	LDH nanosheet-derived Cu	5% C_2H_2/0.5% C_2H_2	C_2H_4	≈80/selectivity over 90	−0.52	1 M KOH	Flow cell	[158]
Nanostructuring	ED-Cu NPs	C_2H_2	C_2H_4	97.7	Current at 500	1 M KOH	Flow cell	[161]
Nanostructuring	Cu microparticles	C_2H_2	C_2H_4	83.2	−0.6	1 M KOH	H-type cell	[159]
Complexes-derived Cu	NHC-Cu	Pure C_2H_2/1% C_2H_2	C_2H_4	≥98/ selectivity >99	−0.6 to −0.9	1 M KOH	Two-electrode flow cell	[162]
Complexes-derived Cu	$Cu_2Cl(OH)_3$-derived undercoordinated Cu nanodots	Pure C_2H_2/0.5% C_2H_2	C_2H_4	95.9/selectivity of 92.6	Current at 350	1 M KOH	Flow cell /two-electrode reactor	[160]
ECH of liquid alkynes								
Design principle	Catalyst	Reactant	Product	Performance [%]	Current density [mA cm^{-2}] or potential [V vs RHE]	Electrolyte	Electrolyzer	Ref.
Doping	Sulfur-derived Cu	4-Ethynylaniline	Alkenes	Selectivity up to 99	−1.25 to −1.5 V vs Hg/HgO	1 M KOH	Three-electrode system	[42]
Nanostructuring	Electrochemically derived Cu nanoarrays	2-Methyl-3-butyne-2-ol (MBY)	Methyl-3-butene-2-ol (MBE)	Selectivity up to 97	Partial current of 750	1 M KOH	Two-electrode electrolyzer	[163]
Alloy	Pd-engineered Cu	MBY	MBE	Selectivity up to 98.5	−0.3	V_{EtOH}/V_{KOH} = 2:1	H-type cell	[164]

© 2024 The Authors. Advanced Materials published by Wiley-VCH GmbH

15214095, 2024, 14, Downloaded from https://advanced.onlinelibrary.wiley.com/doi/10.1002/adma.202307913 by Cochrane Chile, Wiley Online Library on [30/09/2026]. See the Terms and Conditions (https://onlinelibrary.wiley.com/terms-and-conditions) on Wiley Online Library for rules of use; OA articles are governed by the applicable Creative Commons License

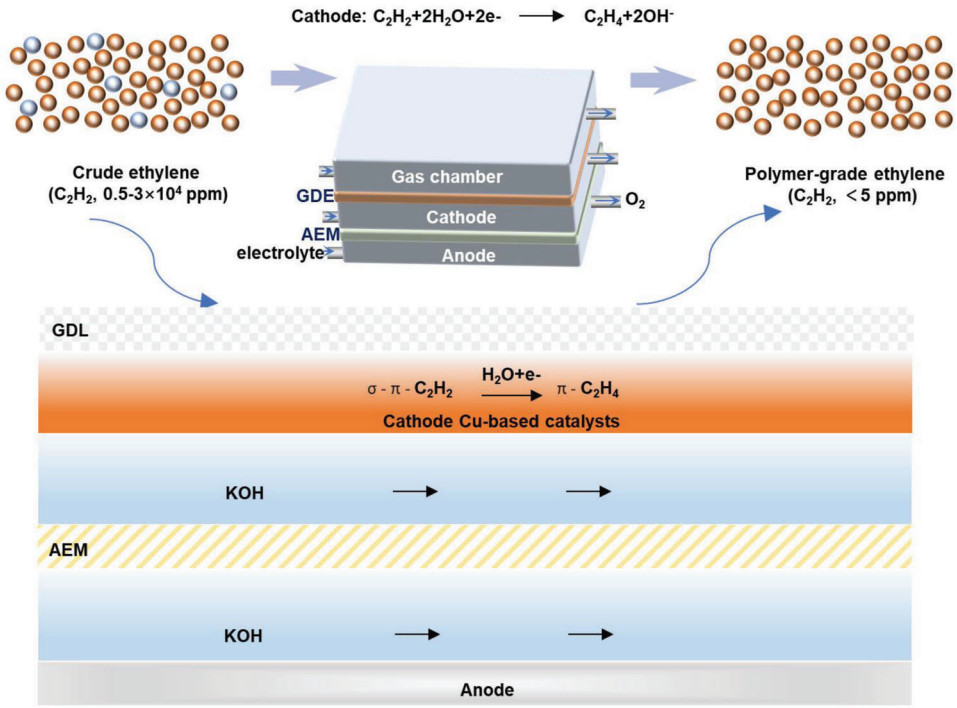

Figure 10. The proposed electrocatalytic selective C_2H_2-to-C_2H_4 process on Cu-based catalysts.

4.1. ECH of Acetylene

The semi-hydrogenation of acetylene (C_2H_2) to C_2H_4 is a key industrial process that provides useful commodity chemicals such as plastics (polyethylene) and other valuable fine chemicals such as ethylene oxide and ethylene dichloride.[5] Normally, the 0.5–3% acetylene impurity in the crude ethylene streams is poisonous for the Ziegler–Natta catalysts during the polymerization of light olefins such as ethylene. As such, to ensure the production of high-purity and polymer-grade ethylene, it is crucial to convert C_2H_2 impurities into C_2H_4 to achieve impurity levels below 5 parts per million. Solvent absorption of C_2H_2 impurities in C_2H_4 feedstock is a commercial physical method for purifying and separating C_2H_2 from C_2H_4-rich feeds, where C_2H_2 is dissolved in organic solvents such as ethyl acetate, *N,N*-dimethylformamide, or *N*-methylpyrrolidinone.[150] Another physical separation strategy is the use of adsorption-based or membrane-based methods to remove C_2H_2 from a gas mixture of C_2H_2 and C_2H_4 on porous structures with appropriate pore sizes, such as microporous metal–organic frameworks or covalent organic frameworks.[151–156] Besides, the TCH of C_2H_2 with H_2 via the Horiuti–Polanyi mechanism is widely employed. However, the H_2-hydrogenation process is associated with the use of hydrogen gas and noble-metal catalysts under harsh conditions. Common issues in this process include the presence of excess H_2, excessive hydrogenation to produce alkane impurities, and the occurrence of oligomerization (C—C) reactions resulting in the formation of higher hydrocarbon byproducts.

To overcome the above issues, there is a growing industrial need for advanced electrochemistry systems that can effectively minimize side reactions in the semi-hydrogenation of alkynes ($C_2H_2 + 2H_2O + 2e^- \rightarrow C_2H_4 + 2OH^-$; **Figure 10**). In the presence of water as a proton donor under ambient conditions, the C_2H_2 can be selectively hydrogenated to form C_2H_4 without introducing any additional impurities. In this context, copper is widely recognized as a primary electrocatalyst for effectively adsorbing C_2H_2, desorbing C_2H_4, inhibiting over-hydrogenation and C—C coupling reactions, and minimizing the competing HER.

4.1.1. Nanostructured Cu Electrocatalysts

In 2021, a pioneer work was conducted for polymer-grade production over Cu dendrites.[157] A series of metal electrocatalysts, including Pd, Au, Ag, Ni, and Cu, were screened using theoretical simulations and experimental investigations. It was revealed that Cu with (100) surface exhibited superior performance in the ECH of C_2H_2 due to favorable exothermal C_2H_2 adsorption, hydrogenation of CH_2CH* intermediate, and energetically favorable desorption of CH_2CH_2* to avoid over-hydrogenation. As a result, the in situ-generated Cu dendrites with aggregated nanoparticles exhibited 12-h durability with 97% FE under pure acetylene feedstock. Remarkably, under simulated industrial conditions with a low concentration of 1×10^4 ppm (1%) acetylene in an Ar stream supply, a remarkable FE of 61% and selectivity of 97% were achieved. In situ Raman demonstrated a semi-hydrogenation mechanism on the Cu dendrites, exhibiting the σ-configurational adsorption of acetylene reactants and weak π-configurational adsorption of ethylene products. To further improve the solubility and mass transport of C_2H_2 in water, a layered double hydroxide (LDH) nanosheet-derived copper with Cu^0/Cu^I

© 2024 The Authors. Advanced Materials published by Wiley-VCH GmbH

15214095, 2024, 14, Downloaded from https://advanced.onlinelibrary.wiley.com/doi/10.1002/adma.202307913 by Cochrane Chile, Wiley Online Library on [30/09/2026]. See the Terms and Conditions (https://onlinelibrary.wiley.com/terms-and-conditions) on Wiley Online Library for rules of use; OA articles are governed by the applicable Creative Commons License

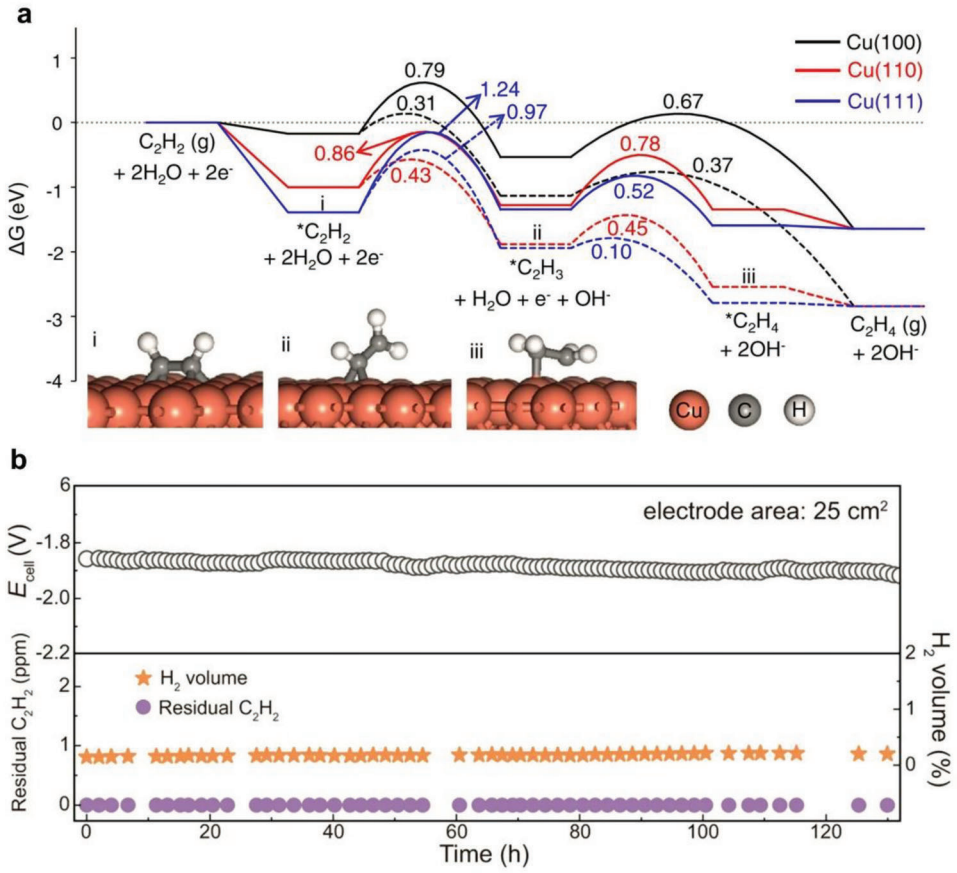

Figure 11. Selective ECH of alkynes on Cu-based catalysts. a) Free energy diagram for the C_2H_2-to-C_2H_4 conversion on Cu (100), Cu (110), and Cu (111) surfaces. Reproduced under the terms of the CC-BY Creative Commons Attribution 4.0 International license (https://creativecommons.org/licenses/by/4.0).[159] Copyright 2021, The Authors, published by Springer Nature. b) Long-term durability test for 130 h carried out in a two-electrode reactor at −50 mA with an area of 25 cm^2. Reproduced under the terms of the CC-BY Creative Commons Attribution 4.0 International license (https://creativecommons.org/licenses/by/4.0).[160] Copyright 2023, The Authors, published by Springer Nature.

heterostructure was used in a flow system. The system offered an onset potential of −0.39 V vs RHE for C_2H_4 production and achieved a C_2H_4 FE of up to ≈80% under 5% C_2H_2 balanced with Ar feedstock, along with a selectivity exceeding 90% under simulated C_2H_4-rich gas mixture (0.5% C_2H_2 and 20% C_2H_4 balanced with Ar).[158]

Cu nanoparticles are easy to prepare and can expose active facets and unsaturated sites, which could be useful to enhance the preferential C_2H_2 adsorption and hydrogenation while preventing H_2 formation. Zhao et al. synthesized electrochemically deposited Cu nanoparticles (ED-Cu NPs) with a size range of 3–5 nm and abundant low-coordination sites.[161] The higher energy barrier for *H coupling and weak adsorption of C_2H_4 led to an impressive FE of 97.7% toward C_2H_4 at a current density of 0.5 A cm^{-2}. In another work, more exposed active facets were constructed on Cu microparticles (MPs) with a porous gas diffusion layer, achieving an FE of 83.2% toward ethylene and an overall current density of 29 mA cm^{-2} at −0.6 V vs RHE.[159] The electronic interaction between Cu MPs and C_2H_2 molecules was investigated by in situ spectroscopic characterizations and first-principles calculations. The initial hydrogenation step, which involves the conversion of $*C_2H_2$ to $*C_2H_3$, is identified as the rate-limiting step (**Figure 11**a). Subsequently, there exists a comparatively lower energy barrier for the subsequent second hydrogenation. The easy desorption of C_2H_4 from the surfaces plays a crucial role in achieving efficient conversion of C_2H_2-to-C_2H_4, while preventing excessive hydrogenation to alkanes at potentials prior to −0.6 V vs RHE. The DFT-simulated Cu K-edge X-ray absorption near edge structure (XANES) coupled with in situ Raman confirmed that the oxidation state of surface Cu was increased, which is attributed to the electron transfer to the antibonding π orbital of the adsorbed $*C_2H_2$.

4.1.2. Complexes-Derived Cu Electrocatalysts

Apart from pure Cu metal, Cu complexes have also been reported for C_2H_2-to-C_2H_4 conversion. By employing σ-donation and chelation of N-heterocyclic carbene (NHC) ligand, NHC–metal-complexes-derived electrocatalysts containing Pd, Au, Ag, and Cu were screened for C_2H_2 semi-hydrogenation.[162] Among them, NHC-derived Cu achieved the highest FE of ≥98% when exposed to pure C_2H_2 flow, and a superior selectivity of >99% during a 100 h stability test even in the presence of a crude

© 2024 The Authors. Advanced Materials published by Wiley-VCH GmbH

15214095, 2024, 14, Downloaded from https://advanced.onlinelibrary.wiley.com/doi/10.1002/adma.202307913 by Cochrane Chile, Wiley Online Library on [30/09/2026]. See the Terms and Conditions (https://onlinelibrary.wiley.com/terms-and-conditions) on Wiley Online Library for rules of use; OA articles are governed by the applicable Creative Commons License

ethylene feed containing 1% C_2H_2. Besides, carbon-supported $Cu_2Cl(OH)_3$-derived undercoordinated Cu nanodots achieved a FE of 95.9% toward C_2H_4 with a current density −350 mA cm^{-2} under pure acetylene feedstock.[160] This process was scaled up in a two-electrode membrane electrode assembly reactor under simulated industrial ethylene flow (0.5% C_2H_2, 20% C_2H_4 balanced with Ar), where a space velocity of 1.35×10^5 mL g_{cat}^{-1} h^{-1} and continuous operation of 130 h was achieved with output C_2H_2 less than 1 ppm (Figure 11b).

4.2. ECH of Liquid Alkynes

The broad applicability of Cu-catalyzed alkyne hydrogenation enables the expansion of the substrate scope to encompass alkynes with more intricate structures, including those in liquid form. For example, ECH of 4-ethynylaniline with H_2O as the H source was studied to obtain corresponding alkenes over sulfur-derived Cu (Cu-S) with unsaturated coordination.[42] The presence of adsorbed sulfur on the catalyst surface facilitates its interaction with hydrated K^+ ions, resulting in the formation of a $S^{\delta-}$-$K^+(H_2O)_n$ network. This network aids in the dissociation of water and the moderation of active *H adsorption, achieving ultrahigh alkyne-to-alkene selectivity (up to 99%). In addition, Bu et al. proposed electrocatalytic selective hydrogenation of alkynols (2-methyl-3-butyne-2-ol) to alkenols (2-methyl-3-butene-2-ol) on electrochemically derived Cu nanoarrays.[163] A partial current density of 750 mA cm^{-2} and specific selectivity of up to 97% toward alkenol were achieved in alkaline electrolyte, and a high conversion of 93% was sustained when escalated to a two-electrode electrolyzer of 25 cm^2 surface area. The production of *H from water dissociation in ECH is dependent on the interfacial water structure. To this end, the tensile strained (111) facet over Pd-engineered Cu icosahedron was synthesized for electrocatalytic selective hydrogenation of alkyne into alkene.[164] The rational construction of an icosahedral twinned structure induces tensile strain, which promotes the formation of K^+ ion hydrated water ($K{\cdot}H_2O$) and 2-coordinated hydrogen-bonded water (2-$HB{\cdot}H_2O$). The $K{\cdot}H_2O$ enhanced the formation of *H from water splitting and escalated the conversion rate (96.5%) of alkynes, while the 2-$HB{\cdot}H_2O$ enhanced the selectivity (98.5%) toward alkenes.

In summary, copper is regarded as a promising metal in acetylene and liquid alkyne ECH to substitute noble metals (e.g., Pd) for alkene generation, but the development of highly active, selective, and durable Cu electrocatalysts is still a challenging task. The interaction between alkyne/alkene molecules and catalyst surfaces remains to be further investigated, which would shed light on the strategies to minimize the overpotential (onset potential ≈−0.3 V vs RHE; equilibrium potential +0.733 V vs RHE in 1 M KOH) and inhibit the side reactions, such as C—C coupling and overhydrogenation. From a practical viewpoint, the current alkyne electrolyzers can only be operated under alkaline environment for less than 200 h, meaning that more robust Cu structures that work under universal pH are highly needed for large-scale application.

5. ECH of Aldehydes

Carbon-rich biomass feedstock represents a naturally abundant source to produce valuable fuels and achieve efficient carbon utilization.[165–166] Aldehydes are common biomass-derived platform molecules with enormous potential for sustainable valorization to adhesives, lubricating oils, and resins. Typical aldehydes for ECH include furanic compounds, benzaldehyde, and glucose. **Table 4** summarizes typical ECH reactions of aldehydes on various Cu-based catalysts.

5.1. ECH of Furanic Compounds

Furanic compounds are commercially relevant platform molecules derived from the pyrolysis, hydrolysis, and dehydration processes of raw biomass.[167–168] As a representative example, furfural (F) is obtained from the acid-catalyzed dehydration of xyloses and other polysaccharides rich in pentose sugars, making it a prominent industrial C_5 chemical. The corresponding products, such as furfuryl alcohol (FA) and 2-methylfuran (2-MF), are important industrial intermediates for furan resins and alternative liquid fuels, respectively.[169–170] Moreover, the hydrolysis/dehydration of hexoses (predominantly fructose) and acid-catalyzed dehydration of cellulose present viable methods for the biorefinery production of 5-hydroxymethylfurfural (5-HMF) as renewable C_6 commodity chemicals.[15] The corresponding reduced products of 5-HMF include 2,5-dihydroxymethylfuran (DHMF) and 2,5-dimethylfuran (DMF), which act as key monomer precursors and potential high-energy-dense liquid fuels for industrial biorefinery, respectively.[2] The traditional TCH processes of F and 5-HMF use molecular H_2 and undergo numerous steps, including the hydrogenation of C═O or C═C, decarbonylation, and hydrogenolysis of C—O or C—C. In comparison, by utilizing the in situ H source from water, ECH under mild conditions can achieve selective hydrogenation of furanic compounds by tuning the electrocatalyst properties. The produced *H species generally attack the aldehyde groups in F or 5-HMF, resulting in the two-electron conversion into FA or DHMF, respectively, or alternatively follow a hydrogenolysis pathway leading to the production of 2-MF or DMF, respectively (**Figure 12**a).

5.1.1. Selectivity on Cu-based Catalysts

Electrode materials based on Cu are chosen for the electroreduction of furanics due to its exceptional capacity to produce hydrogenation and hydrogenolysis products with tunable selectivity. Chadderdon et al. explored the ECH mechanism of furfural on Cu electrodes in acid electrolytes, showing that the electroreduction processes resulted in the formation of FA, 2-MF, and dimer product hydrofuroin (Figure 12b,c).[171] Based on the electrochemical measurements of the copper electrode modified with organothiol self-assembled monolayers, the FA and 2-MF formation relied on direct chemical interaction with the electrode surface, while the hydrofuroin is relatively insensitive to the catalyst surface properties. The detected H/D isotope effects demonstrated that H_{ads} species are necessary for the hydrogenolysis and hydrogenation processes. Adjusting the electrolyte pH was found to sensitively steer the furfural conversion pathway. Under lower pH conditions, a preference for 2-MF was observed, while FA emerged as the primary product at relatively higher pH levels (up to 3.0).

© 2024 The Authors. Advanced Materials published by Wiley-VCH GmbH

15214095, 2024, 14, Downloaded from https://advanced.onlinelibrary.wiley.com/doi/10.1002/adma.202307913 by Cochrane Chile, Wiley Online Library on [30/09/2026]. See the Terms and Conditions (https://onlinelibrary.wiley.com/terms-and-conditions) on Wiley Online Library for rules of use; OA articles are governed by the applicable Creative Commons License

Table 4. Comparison of typical Cu-based electrocatalysts for ECH of aldehydes.

Design principle	Catalyst	Reactant	Product	Performance [%]	Potential [V vs RHE]	Electrolyte	Electrolyzer	Refs.
Nanostructuring	NP-Cu	F	FA	FE 95	−0.5	0.1 M PBS/MeOH = 5:1	H-type cell	[176]
Nanostructuring/Facet	R-Cu/Cu(110)	F	2-MF/FA	FE ≈80/≈40	−0.526	1 M H-K_2SO_4 (pH 3.0)	H-type cell	[177]
Nanostructuring	O_2-plasma engineered Cu	F	FA	FE 91	−0.56	0.25 M PBS (pH 6.8)	H-type cell	[178]
Alloy	Pd–Cu	F	2-MF	FE 75	−0.58	0.1 M acetic acid	H-type cell	[181]
Alloy	Ni–Cu	F	FA	Conversion ≈75.2	−0.45	0.5 M NaOH	H-type cell	[182]
Alloy	Ru_1Cu	5-HMF	DHMF	FE 85.6	−0.3	0.5 M PBS	H-type cell	[183]
Alloy	AgCu	5-HMF	DHMF	Selectivity>80	/	0.5 M borate buffer	Three-electrode cell	[185]
Alloy	AgCu	5-HMF	DHMF	Selectivity 85	50 mA cm^{-2}	0.5 M borate buffer	Three-electrode cell	[184]
Alloy	Ag–Cu nanowire	5-HMF/F	DHMF/FA	FE ≈92/selectivity≈95	/	0.5 M borate buffer	H-type cell	[186]

The furfural ECH to 2-MF involves the transfer of four H_{ads} and four electrons, which poses more challenging selectivity issues. In 2013, a pioneer work reported electrocatalytic conversion of furfural into 2-MF with 80% selectivity and the conversion of 5-HMF into DMF with 35.6% selectivity on a copper electrode under room temperature.[172] The electrolyte pH and reactant concentration are important factors in determining the reaction mechanism and directing the reaction toward 2-MF product. Under extremely acidic electrolytes with a pH lower than 1, Cu electrodes predominantly yield 2-MF as the major product, and the competing HER is effectively suppressed by increasing the concentration of furfural.[173]

Cu-based materials have also been found to be favorable for the selective formation of DHMF from 5-HMF electroreduction. The electrocatalytic activity and hydrogenation selectivity of 5-HMF were investigated on various metal electrodes. Among them, Fe, Ni, Cu, and Pb predominantly formed DHMF, while metals like Au, Ag, Cd, Sb, Co, and Bi supported the formation of DHMF and 2,5-dimethyl-2,3-dihydrofuran (DMDHF) depending on potentials, and metals such as Pd, Al, Pt, In, Zn, and Sb mainly produced DMDHF.[174] Oxygen-bearing Cu nanowires with abundant Cu/Cu_2O interfaces were reported to catalyze the electrochemical conversion of 5-HMF into DHMF, demonstrating a DHMF selectivity close to 100% and a FE of 90%. The Cu/Cu_2O

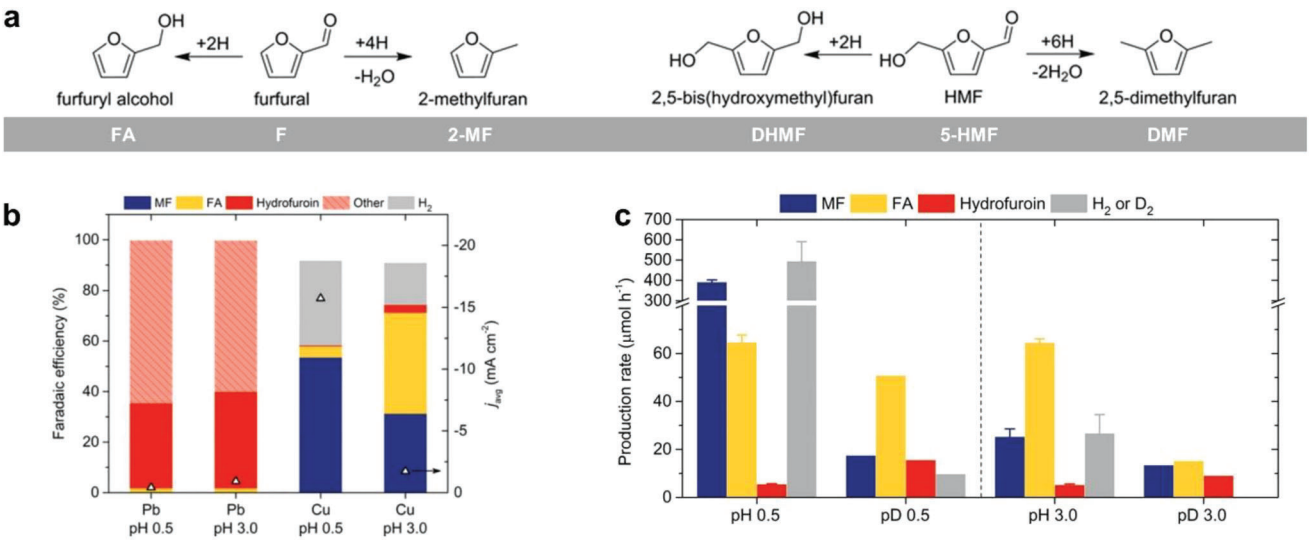

Figure 12. Selective ECH of aldehydes on Cu. a) The proposed electrocatalytic conversion pathways of biomass-derived furfural and 5-HMF. b,c) ECH activity and FE of furfural electrolysis on Cu and Pb electrodes with different pH values (b) and Cu electrodes in H- or D-electrolytes (c). a) Adapted with permission.[171] Copyright 2017, American Chemical Society. b,c) Reproduced with permission.[171] Copyright 2017, American Chemical Society.

© 2024 The Authors. Advanced Materials published by Wiley-VCH GmbH

15214095, 2024, 14, Downloaded from https://advanced.onlinelibrary.wiley.com/doi/10.1002/adma.202307913 by Cochrane Chile, Wiley Online Library on [30/09/2026]. See the Terms and Conditions (https://onlinelibrary.wiley.com/terms-and-conditions) on Wiley Online Library for rules of use; OA articles are governed by the applicable Creative Commons License

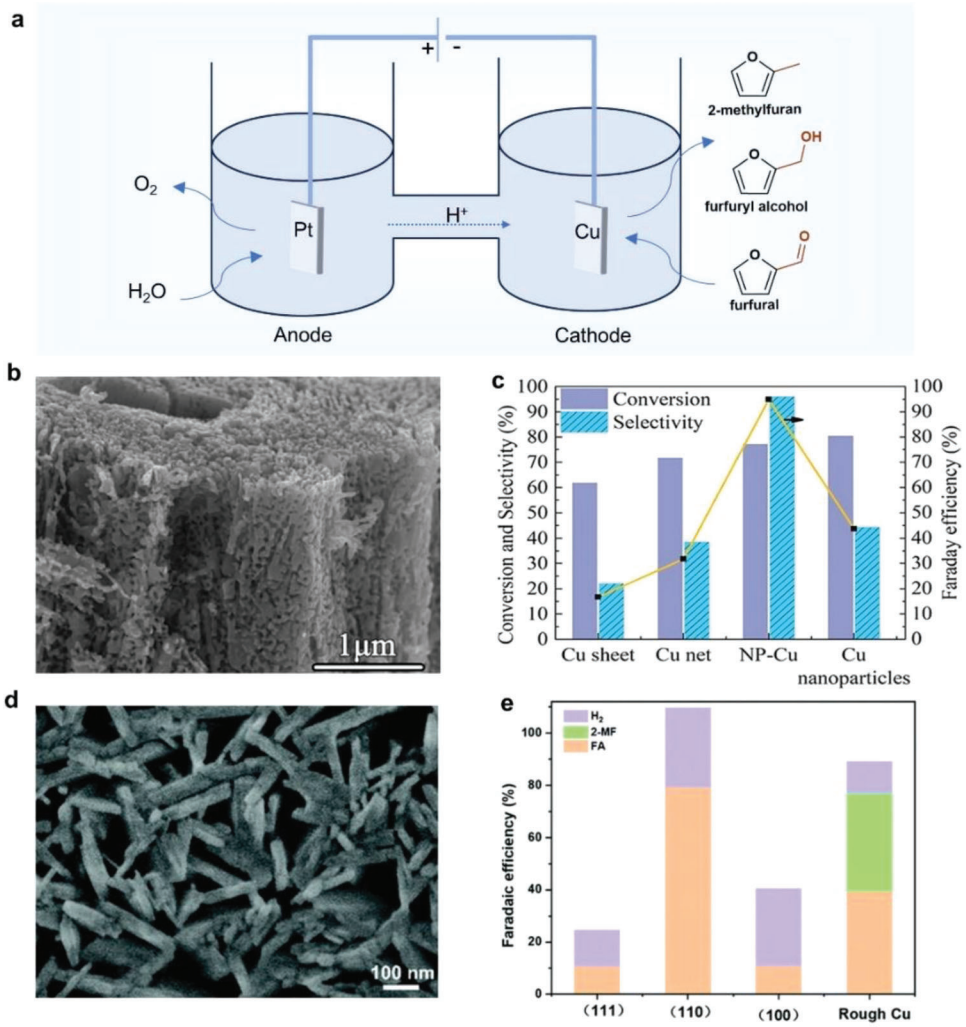

Figure 13. a) Selective ECH of aldehydes on nanostructured Cu in H-cell electrolyzer. b) SEM image and c) ECH activity of furfural on a nanoporous NP-Cu electrode. b,c) Reproduced with permission.[176] Copyright 2022, American Chemical Society. d) SEM image of R-Cu and e) FE of furfural hydrogenation products on different facets of Cu electrode. d,e) Reproduced with permission.[177] Copyright 2021, Royal Society of Chemistry.

interfacial structure was identified as catalytically active phase with the lowest energy barriers for 5-HMF-to-DHMF process, outperforming both pure Cu_2O and Cu structures.[175]

5.1.2. Nanostructured Cu Electrocatalysts

The ECH performance of furanic compounds strongly depends on the properties of nanoscale Cu-based catalysts and is usually tested in H-cell electrolyzer configuration (**Figure 13**a). Yang et al. obtained hierarchical nanoporous Cu (NP-Cu) with a large specific surface area from the chemical dealloying of CuAl alloy.[176] The NP-Cu could provide adequate H_{ads} for aldehyde hydrogenation and suppress the electrocondensation. When compared with commercial Cu sheets and Cu nanoparticles, the selectivity of F-to-FA conversion is significantly enhanced, reaching up to 96%, and the FE toward FA is elevated to 95% (Figure 13b,c). Using electrochemical measurements and operando Raman spectroscopy, Li et al. investigated the structural features determining the furfural reduction selectivity on electrochemically roughened Cu (R-Cu) and single crystal Cu with (100), (110), and (111) surfaces (Figure 13d,e).[177] In the initial stage of furfural reduction, the surface layer of oxidized copper is reduced to metallic copper and the protons are reduced to H_{ads} atoms, while F is adsorbed on the catalyst surface concurrently. Subsequently, the aldehyde group in furfural is hydrogenated by interacting with H_{ads}, leading to the formation of O—H bonds and FA as the final product, which is the predominant pathway on Cu (110). If the carbon within the aldehyde group undergoes further hydrogenation by H_{ads}, the alcohol C—O bond will break to form 2-MF. No 2-MF product was detected in the electrolysis of FA, providing strong evidence to rule out the continuous reduction of FA to 2-MF. Besides, the in situ catalyst reconstruction under ECH working conditions was found to be associated with electrochemically generated defects. Chen et al. introduced defects and roughness on Cu electrodes through plasma treatment to achieve efficient electrocatalytic F-to-FA hydrogenation.[178] The O_2-plasma-engineered catalyst produced CuO_x and then rapidly converted into

© 2024 The Authors. Advanced Materials published by Wiley-VCH GmbH

15214095, 2024, 14, Downloaded from https://advanced.onlinelibrary.wiley.com/doi/10.1002/adma.202307913 by Cochrane Chile, Wiley Online Library on [30/09/2026]. See the Terms and Conditions (https://onlinelibrary.wiley.com/terms-and-conditions) on Wiley Online Library for rules of use; OA articles are governed by the applicable Creative Commons License

ultrafine Cu with high roughness and rich defects, which accelerated the rate-determining steps involving H_{ads} and F_{ads}. Consequently, compared with electropolished or Ar-plasma-treated Cu, the O_2-plasma-engineered Cu delivered a superior FE of 91% and FA selectivity of 96%.

The active valence state of Cu-based catalysts is constantly changing during furfural ECH and therefore difficult to probe. Xia et al. demonstrated the synergistic effect of Cu^0 and Cu^+ and offered a profound comprehension of the electrochemical furfural hydrogenation mechanism by in situ characterizations and DFT calculation.[179] Cu^0 is believed to lower the energy barrier for FA desorption, while Cu^+ facilitates the second hydrogenation of F and acts as active sites for F-to-FA confirmed by SCN^--Cu^+ complexation experiment. The Cu^+/Cu^0 active sites were also observed on a highly dispersed Cu catalyst anchored on hierarchically porous N-doped carbon (Cu/NC_{900}) with a large surface area, achieving nearly 100% FA selectivity and above 95% FE in alkaline conditions.[180]

5.1.3. Engineering Cu with Other Metals as Electrocatalysts

Other metals such as Pd, Ni, Ru, and Ag can be incorporated into copper to form Cu-based bimetallic catalysts, boosting the electrochemical hydrogenation selectivity of furfural and 5-HMF. Zhou et al. reported the doping of Pd into Cu to achieve the highest FE of 75% toward 2-MF in 0.1 M acetic acid on Pd–Cu (**Figure 14**a,b).[181] In situ Raman spectroscopy revealed that the coverage of adsorbed *H was enhanced on the Pd–Cu electrode, leading to the changed adsorbed configuration of furfural from κ-(O) pattern on Cu to η^2-(C,O) pattern on Pd–Cu, which is beneficial for the F-to-2MF pathway. DFT calculations revealed that 2-MF formation pathway was favored on the Pd-engineered Cu catalyst due to the decreased energy barrier for the hydrogenation step of F-CH_2* to F-CH_3*. Besides, a non-noble bimetallic Ni–Cu electrode was obtained by co-electrodepositing of Cu and Ni onto porous Ni foam.[182] ECH of furfural on Ni–Cu yields high rates of FA products (118.7 ± 8 μmol h^{-1} cm^{-2}) in alkaline conditions. The adsorption ability of H_{ads} and furfural were optimized on Ni–Cu, resulting in nearly 100% conversion of F into FA even after 2 h electrolysis. Additionally, single-atom alloys (SAAs) combine the advantages of both SACs and alloys by creating a distinct bonding environment and synergistic effects among metals, making them highly attractive for ECH of furanics. In a recent work, the isolated single atom Ru was uniformly distributed on Cu nanowires via a facile galvanic replacement approach (Figure 14c,d).[183] The as-prepared Ru_1Cu SAA exhibited a decreased overpotential toward 5-HMF electroreduction conversion. Compared to pure Cu, Ru_1Cu achieved the enhanced DHMF yield (0.47 mmol cm^{-2} h^{-1}) and FE (85.6%), which is ascribed to the promoted water dissociation by the Ru single atoms. The enhanced H* coverage on electrode surface is conducive to subsequent hydrogenation of the carbonyl group in 5-HMF into DHMF. Notably, the FE of DHMF remained at an unprecedented level of 87.5% even at a high 5-HMF concentration of 100 mM.

Bimetallic CuAg nanostructured electrocatalysts have gained wide popularity in reduction of furanic compounds due to their enhanced activity and easy preparation. For example, bimetallic AgCu nanoparticles were coated on foam panels by electrodeposition for 5-HMF reduction.[184–185] Compared with the pure monometallic Ag and Cu foam, the relatively large electrochemical surface area and high electrical conductivity of bimetallic AgCu resulted in faster charge and mass transfer for 5-HMF-to-DHMF conversion. The nearly 100% conversion rate for 5-HMF, high selectivity toward DHMF (>80%) and DHMF productivity of 0.280 mmol cm^{-2} h^{-1} were obtained in basic solution, owing to the synergic effect of the uniformly distributed Ag and Cu active sites.[185] Despite the challenges in operating at high current densities, the AgCu catalyst demonstrated a balanced activation of 5-HMF and H_2O within the range of 40 to 50 mA cm^{-2}, resulting in a DHMF selectivity of 85% and a yield of 0.567 mmol cm^{-2} h^{-1}.[184] Furthermore, hierarchical Ag-decorated Cu nanowires were prepared with a robust structure to facilitate mass transport and prevent the aggregation of Ag particles, achieving selectivity above 95% for 5-HMF-to-DHMF and F-to-FA, and a FE above 92% for DHMF and FA.[186] Nanoalloy AgCu was supported on pyrolyzed sodium alginate and demonstrated a conversion rate of 93.2%, selectivity of 94%, and FE of 61.8% toward DHMF.[187] Besides, Roylance et al. synthesized Ag electrodes with high surface area (Ag_{gd}) and with flat morphology.[188] The conversion rate, selectivity, and FE of 5-HMF-to-DHMF were close to 100% on the Ag_{gd} electrode in a wide potential window of −1.3 to −1.8 V vs Ag/AgCl.

5.2. ECH of Other Aldehyde Compounds

Other aldehyde compounds, such as benzaldehyde and glucose, can also be hydrogenated on Cu-based electrodes, and the selectivity of hydrogenated products is significantly influenced by the chemical state of the catalysts. For example, Cu exhibits a distinctive capability to facilitate the C—C coupling during the electrochemical reduction of benzaldehyde, leading to the formation of hydrobenzoin.[189] In situ characterization revealed the strong ability of Cu to stabilize and accumulate of high concentrations of ketyl radical intermediates, thereby promoting the C—C coupling of benzaldehyde. Besides, the hydrogenation of glucose to sorbitol, a crucial reaction for organic synthesis and hydrogen storage, can be achieved on late transition metals such as Cu in neutral media.[190] This selectivity trend is obviously different from the trends observed for H_2 formation on early transition metals and platinum group metals, as well as 2-deoxysorbital formation on post-transition-metals, Zn, and Cd.

In summary, due to the diverse reaction pathways and potential products from aldehydes, achieving selective ECH is challenging and necessitates the design of Cu-based catalysts with tailored adsorption and desorption properties. In the ECH of furanic compounds, most reports focus on the production of alcohols and methylfurans as the main reduction products, while the further hydrogenation of furanic rings is seldom reported and may present new opportunities for exploring novel reaction pathways and applications. Additionally, it is essential to develop Cu-based structures with enhanced durability to avoid catalyst dissolution in acidic aldehyde ECH conditions.

6. ECH of N-Containing Substances

Nitrogen is a fundamental element in living organisms and plays an indispensable role in the global biogeochemical cycle.[191] A

© 2024 The Authors. Advanced Materials published by Wiley-VCH GmbH

15214095, 2024, 14, Downloaded from https://advanced.onlinelibrary.wiley.com/doi/10.1002/adma.202307913 by Cochrane Chile, Wiley Online Library on [30/09/2026]. See the Terms and Conditions (https://onlinelibrary.wiley.com/terms-and-conditions) on Wiley Online Library for rules of use; OA articles are governed by the applicable Creative Commons License

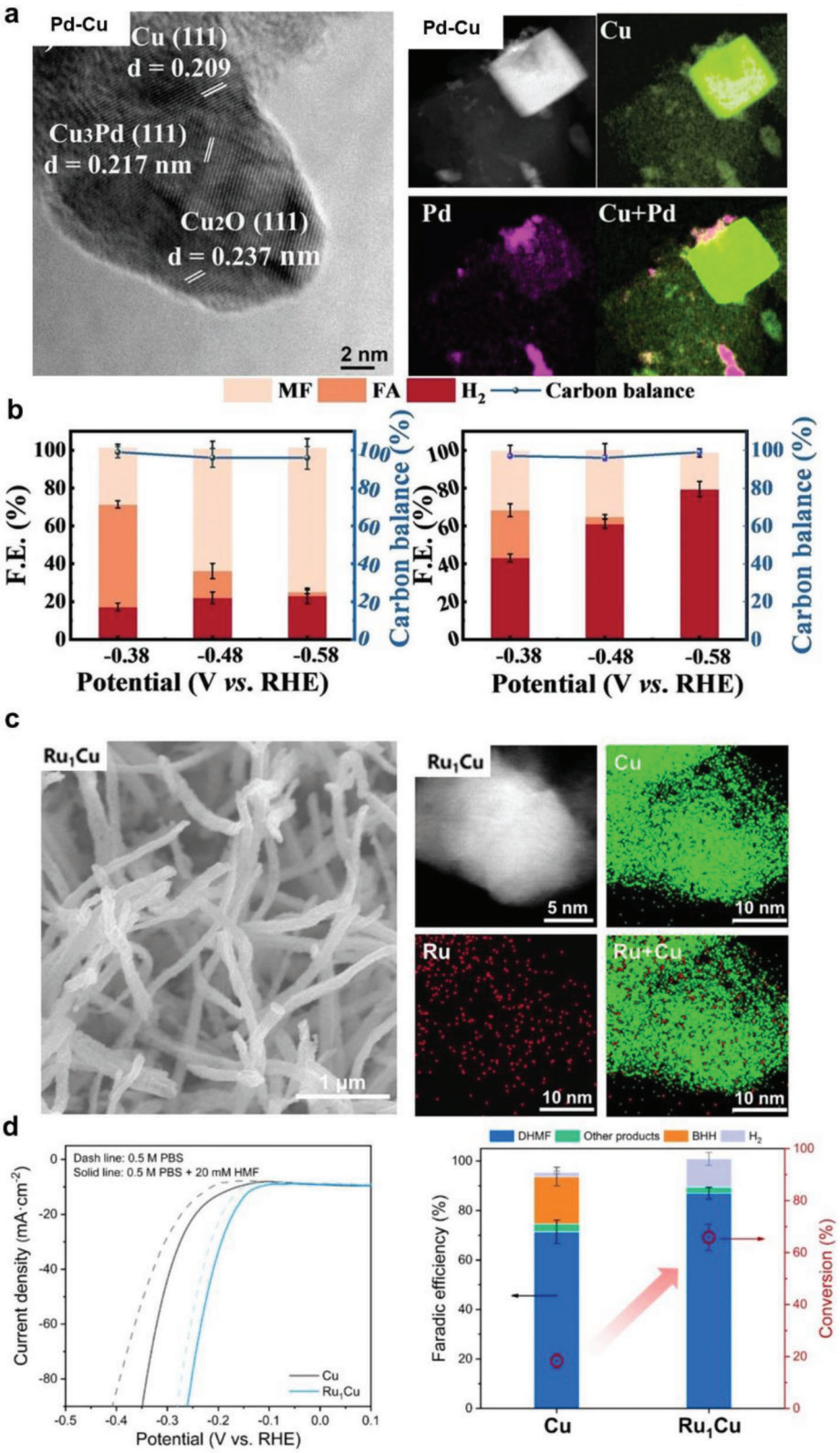

Figure 14. Selective ECH of aldehydes on Cu catalysts engineered with other metals. a) SEM and elemental mapping images of Pd–Cu catalysts. b) FE on Pd–Cu at pH 2.9 (0.1 M acetic acid) and pH 0.7 (0.1 M H_2SO_4). a,b) Reproduced with permission.[181] Copyright 2022, Wiley-VCH. c) SEM and elemental mapping images of Ru_1Cu single-atom alloy surfaces. d) Current density and FE on Cu and Ru_1Cu. c,d) Reproduced with permission.[183] Copyright 2022, Wiley-VCH.

© 2024 The Authors. Advanced Materials published by Wiley-VCH GmbH

15214095, 2024, 14, Downloaded from https://advanced.onlinelibrary.wiley.com/doi/10.1002/adma.202307913 by Cochrane Chile, Wiley Online Library on [30/09/2026]. See the Terms and Conditions (https://onlinelibrary.wiley.com/terms-and-conditions) on Wiley Online Library for rules of use; OA articles are governed by the applicable Creative Commons License

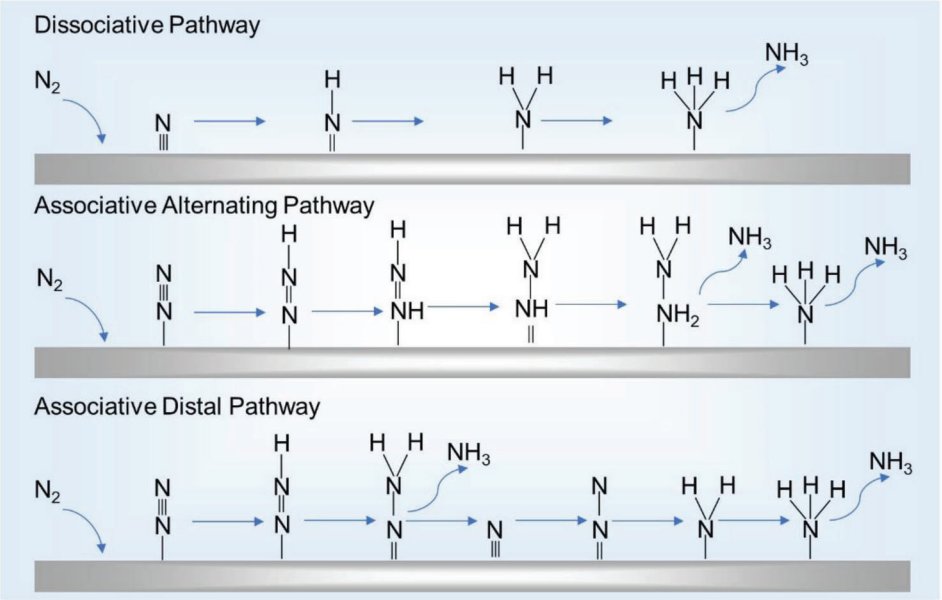

Figure 15. Schematic illustration of the mechanisms of NRR process.

significant process within this cycle is nitrogen fixation to produce ammonia (NH_3), one of the most versatile molecules in global agriculture, energy, and industrial processes.[192–194] Currently, the worldwide industrial-scale NH_3 production is dominated by the Haber–Bosch process. However, this process operates under harsh conditions (≈500 °C, 200–300 atm) with the H_2 reactant from natural gas steam reforming, resulting in 1–2% of global annual energy consumption and ≈1% of greenhouse gas emission.[195–197] Moreover, in recent decades, human activities have severely disturbed the natural nitrogen cycle by releasing an excessive amount of active nitrogen contaminants into the environment, such as nitrate (NO_3^-), nitrite (NO_2^-), nitric oxide (NO), nitrogen dioxide (NO_2), and nitrous oxide (N_2O). In this context, electroreduction of N_2 and nitrogen compounds powered by renewable electricity emerges as energy-efficient and eco-friendly approaches to NH_3 synthesis under ambient conditions.[198–199] Besides, the selective hydrogenation of organic nitrogen compounds, such as conversion of nitroarenes into anilines, is important for the production of commodity chemicals in the pharmaceutical, dye, and polymer industries.[200] In addition to their extensive use in CRR, Cu-based catalysts are also widely employed in the ECH of these N-containing substrates (**Table 5**).

6.1. NRR

Electrocatalytic N_2 reduction offers a sustainable and energy-efficient alternative to the traditional Haber–Bosch process for ambient NH_3 production. On heterogeneous catalysts, the dissociative mechanism and the associative mechanism have been identified for this multistep electron-proton transfer process (**Figure 15**).[201] The two mechanisms primarily differ in the stage at which the N≡N bond cleavage occurs. In the dissociative mechanism, the N≡N bond is broken prior to hydrogenation, while in the associative mechanism, the N≡N bond remains unbroken until one NH_3 molecule is released. The associative mechanism may follow either an alternating or distal pathway, depending on the sequence of hydrogenation steps. In the dissociative mechanism, the two adsorbed N atoms are alternately hydrogenated until two NH_3 molecules are formed. In contrast, for the associative distal pathway, the N atom further from the catalyst surface continuously performs three hydrogenation steps to release an NH_3 molecule, and the second NH_3 molecule is formed after the other N atom is hydrogenated.

The development of catalysts with high NRR activity and NH_3 selectivity is an important but challenging task due to the severe competitive HER in aqueous electrolytes, inherently low reactivity for N_2 adsorption and activation, and high overpotential (>500 mV).[202–204] Although noble-metal (such as Ru, Rh, Pd, Au) catalysts have shown the highest activity for NH_3 synthesis, their scarcity and high cost have triggered research in alternative earth-abundant transition metal catalysts.[205] Cu-based catalysts are among the promising non-noble-metal NRR candidates due to their full d-band electron configuration ($3d^{10}4s^1$) to facilitate the back donation process and thus N_2 activation.[206] Furthermore, their inherent low affinity for hydrogen ad-atoms plays a pivotal role in limiting their coverage and suppressing the undesired HER, thereby facilitating the NH_3 selectivity.[22]

Various strategies have been proposed to enhance the NH_3 production performance on Cu metal.[207–210] For example, Lin et al. reported the local electron depletion effect of Cu nanoparticles to improve the catalytic activity of NRR (**Figure 16**a).[207] The Cu/polyimide (PI) catalyst exhibited a high FE of 6.56% and an NH_3 yield rate of 12.4 μg h^{-1} cm^{-2} at −0.3 V vs RHE. DFT calculations confirmed that the NRR performance was attributed to the Mott−Schottky effect at the interface between Cu and PI support, facilitating the electron redistribution of Cu nanoparticles and suppressing the HER. Moreover, rational morphological control of Cu catalysts is an effective strategy to expose abundant active sites, which greatly impacts the catalytic performance.

© 2024 The Authors. Advanced Materials published by Wiley-VCH GmbH

15214095, 2024, 14, Downloaded from https://advanced.onlinelibrary.wiley.com/doi/10.1002/adma.202307913 by Cochrane Chile, Wiley Online Library on [30/09/2026]. See the Terms and Conditions (https://onlinelibrary.wiley.com/terms-and-conditions) on Wiley Online Library for rules of use; OA articles are governed by the applicable Creative Commons License

Table 5. Comparison of typical Cu-based electrocatalysts for ECH of nitrogen-containing substances.

NRR							
Design principle	Catalyst	FE [%]	NH_3 yield rate	Potential [V vs RHE]	Electrolyte	Electrolyzer	Refs.
Heterostructure	Cu/PI-300	6.56	12.4 μg h^{-1} cm^{-2}	−0.4	0.1 M KOH	Single chamber cell	[207]
Alloying	$Pd_{0.2}Cu_{0.8}$/rGO	≈0.6	2.80 μg h^{-1} mg_{cat}^{-1}	−0.2	0.1 M KOH	H-type cell	[213]
Alloying	Ru–Cu NPs	30.95	73.26 μg h^{-1} cm^{-2}	−0.1	0.1 M HCl	H-type cell	[214]
Facet engineering	bcc PdCu	11.5	35.7 μg h^{-1} mg_{cat}^{-1}	−0.1	0.5 M LiCl	H-type cell	[218]
Single-atom catalyst	NC-Cu SA	13.8	53.3 μg h^{-1} mg_{cat}^{-1}	−0.35	0.1 M KOH	H-type cell	[222]

NO_x^nRR							
Design principle	Catalyst	FE [%]	NH_3 yield rate	Potential [V vs RHE]	Electrolyte	Electrolyzer	Ref
Ligand effect	Cu–PTCDA	85.9	436 ± 85 μg h^{-1} cm^{-2}	−0.4	0.1 M PBS + 500 ppm KNO_3	H-type cell	[225]
Support effect	Cu@C	72.0	469.5 μg h^{-1} cm^{-2}	−0.3	1 M KOH + 1 mM KNO_3	H-type cell	[228]
Phase control	Metastable phase Cu	99.8	0.543 mmol h^{-1} cm^{-2}	−0.3	1 M KOH + 0.05 M $NaNO_3$	H-type cell	[229]
Facet and defect engineering	Cu-NBs-100	95.3	650 mmol g_{cat}^{-1} h^{-1}	−0.15	1 M KOH + 0.1 M KNO_3	H-type cell	[232]
Alloying	CuCo nanosheets	100 ± 1	4.8 mmol h^{-1} cm^{-2}	−0.2	1 M KOH + 0.1 M KNO_3	H-type cell	[234]
Alloying and support effect	CNTs@mesoC@CuPd	54.4 (N_2)	/	−0.65	0.1 M Na_2SO_4 + 100 mg L^{-1} $NaNO_3$	Single chamber cell	[239]
Singe-atom catalyst	Cu-*cis*-N_2O_2	≈81	27.84 mg h^{-1} cm^{-2}	−1.6	0.5 M Na_2SO_4 + 1000 mg mL^{-1} KNO_3	H-type cell	[242]
CO_2 assistance	Cu NWs	≈100	0.60 ± 0.015 mg mg_{cat}^{-1} h^{-1}	−1.3	Mixed NaH_2PO_4 + NaOH (pH 7) + 0.02 M $NaNO_2$	H-type cell	[233]

Organic nitrogen compounds							
Design principle	Catalyst	Reaction	Conversion [%]	Performance [%]	Potential [V vs RHE]	Electrolyte	Ref
Alloying	Cu_3Pt/C	Nitrobenzene to aminobenzene	≈100	Selectivity ≈99	−0.3	1 M KOH + 5 mM nitrobenzene	[246]
Ligand effect	PA-Cu foam	Nitrobenzene to aminobenzene	85	Selectivity 99	−0.53	0.3 M $HClO_4$ + 0.015 M nitrobenzene	[247]
Nanostructuring	Cu NPs	Acetonitrile to ethylamine	/	FE 96	−0.29	1 M NaOH + 8% acetonitrile	[248]
Nanostructuring	Cu Nas/Cu foil	Acetonitrile to ethylamine	/	Selectivity 99/FE 94	−0.7	0.5 M $KHCO_3$ + 0.5 M acetonitrile	[249]

© 2024 The Authors. Advanced Materials published by Wiley-VCH GmbH

15214095, 2024, 14, Downloaded from https://advanced.onlinelibrary.wiley.com/doi/10.1002/adma.202307913 by Cochrane Chile, Wiley Online Library on [30/09/2026]. See the Terms and Conditions (https://onlinelibrary.wiley.com/terms-and-conditions) on Wiley Online Library for rules of use; OA articles are governed by the applicable Creative Commons License

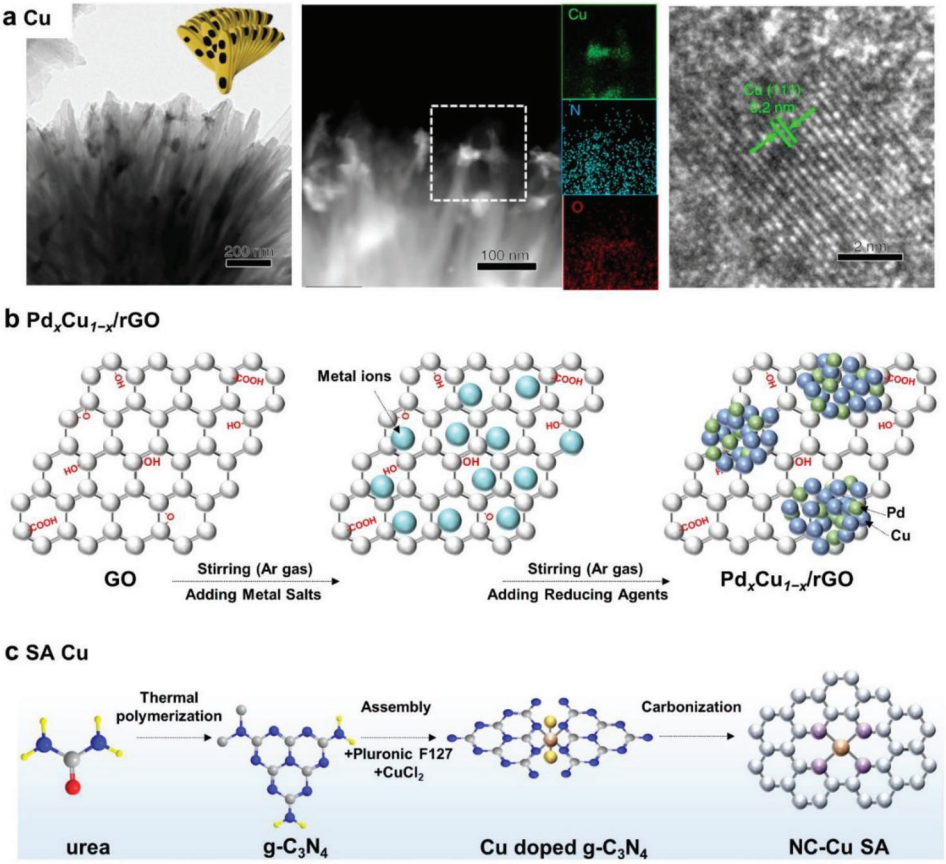

Figure 16. Electrocatalytic NRR on Cu-based catalysts. a) SEM and TEM images of Cu/PI electrodes for NRR. Reproduced under the terms of the CC-BY Creative Commons Attribution 4.0 International license (https://creativecommons.org/licenses/by/4.0).[207] Copyright 2019, The Authors, published by Springer Nature. b) The bimetallic Pd_xCu_{1-x}/rGO composites for NRR. c) Single-atom Cu within porous N-doped carbon network for NRR.

Considering that the spiky features on catalyst surfaces may amplify the local electric field and facilitate the interaction between catalysts and reactants, Li et al. prepared a dendritic Cu catalyst by a facile galvanic replacement method with rich oriented spikes and high surface area.[208] This unique Cu nanostructure resulted in outstanding activity (FE: 15.12%; NH_3 yield rate: 25.63 μg h^{-1} mg_{cat}^{-1}) and stability (24 h) in 0.1 M HCl electrolyte. Apart from metallic Cu, other nanostructured Cu-based compounds such as sulfide and phosphide also demonstrate NRR activity.[211–212]

Alloying or doping Cu with another metal is a powerful strategy to alter the electronic structure and surface properties, endowing the bimetallic system with favorable adsorption strength of NRR intermediates and enhanced NRR reactivity. Metals such as Pd, Ru, Fe, Ag, and Ti are widely chosen because of their high N_2 adsorption strength and intrinsic NRR activity.[213–217] As a proof-of-concept study, Shi et al. achieved effective tuning of NRR activity on PdCu amorphous nanoclusters dispersed on 2D graphene sheets (Pd_xCu_{1-x}/rGO).[213] The Pd_xCu_{1-x}/rGO composites were prepared by the co-reduction of graphene oxide, Cu, and Pd precursors (Figure 16b). The boundary within Pd_xCu_{1-x} and the embedded single atoms increased the accessible surface area for reactants adsorption, which contributed to a remarkable increase in the NH_3 yield (2.80 μg h^{-1} mg_{cat}^{-1}) compared to monometallic Cu and Pd. The optimal $Pd_{0.2}Cu_{0.8}$/rGO catalyst achieved an optimized balance to provide adequate NRR catalytic active sites while avoiding the hydrogen poisoning issue. For PdCu alloy, crystal facet engineering was found to efficiently boost the NRR activity and selectivity.[218] Compared with the conventional face-centered cubic (fcc) PdCu nanoparticles, the body-centered-cubic (bcc) counterparts showed superior NH_3 yield (35.7 μg h^{-1} mg_{cat}^{-1}) and FE (11.5%). The strong d–d orbital interactions between Pd and adjacent Cu sites enabled by crystal phase engineering were responsible for overcoming the coulomb barrier for N_2 electroreduction. Other strategies, such as stabilization on MOFs,[219] constructing ordered vacancies,[220] and developing bimodal nanoporous structure,[221] also proved effective in enhancing the catalytic performance of CuPd alloy structures. Furthermore, the construction of Cu-based alloys with immiscible elements (e.g., Ru) is limited by the difficulty in synthesis methods. Given this, Kim et al. developed a carbothermal shock method to prepare homogeneous Ru–Cu nanoparticles with immiscible property.[214] The non-equilibrium mixing of Ru and Cu atoms with a size of 20 nm was realized by applying a high electrical current of −1 A accompanied by a rapid high-temperature heating and cooling process. As a result, the catalyst delivered a higher NH_3 formation rate (73.26 μg h^{-1} cm^{-2}) than other Ru-based alloys at a low overpotential of 0.1 V vs RHE.

© 2024 The Authors. Advanced Materials published by Wiley-VCH GmbH

15214095, 2024, 14, Downloaded from https://advanced.onlinelibrary.wiley.com/doi/10.1002/adma.202307913 by Cochrane Chile, Wiley Online Library on [30/09/2026]. See the Terms and Conditions (https://onlinelibrary.wiley.com/terms-and-conditions) on Wiley Online Library for rules of use; OA articles are governed by the applicable Creative Commons License

Compared with their nanoparticle counterparts, single-atom catalysts have the advantages of maximized atomic utilization efficiency and well-defined structure–activity relationships. The activity and selectivity of SACs in electrocatalysis depend on central metal atoms, coordination environment, and supporting substrates. For NRR, regulating the electronic interaction between metal single atoms and the surrounding atoms is effective in activating N_2 molecules and promoting NH_3 selectivity. Zang et al. constructed atomically dispersed Cu catalytic sites supported on porous nitrogen-doped carbon by a facile surfactant-assisted approach (Figure 16c).[222] The Cu SAC exhibited pH-universal NRR performance in alkaline and acidic electrolytes (≈53.3 μg h^{-1} mg_{cat}^{-1} and FE 13.8% in 0.1 M KOH, ≈49.3 μg h^{-1} mg_{cat}^{-1} and FE 11.7% in 0.1 M HCl), owing to the active Cu—N_2 coordination structure revealed by XAS and DFT analyses. Although the Cu—N_2 configuration only accounted for 20% of the Cu single atoms, it enabled strong interaction between the highly dispersed Cu single atoms and N_2, which resulted in maximized exposure of active sites and reduced the energy required for the alternating reaction pathway. Very recently, the NH_3 yield on Cu SAC/TiO_2 was found to increase by a factor of 5 under a light irradiation field.[223] The accelerated electron transfer ability at the unique Cu–O–Ti interface and electron/hole mobility by the light field contributed to efficient N_2 activation and more electrons involved in NRR. In addition, the construction of a CuPd diatomic catalyst is promising for NRR because of its potential to alter the electronic interaction between single-atom Cu and Pd sites.[224] The incorporation of Cu moved the partial density of states of Pd toward the Fermi level and promoted the d–2π* coupling between Pd and adsorbed N_2, enabling efficient chemisorption and activation of N_2 molecules.

6.2. ECH of Inorganic Nitrogen Compounds

From an environmental perspective, inorganic nitrogen compounds such as nitrate, nitrite, and nitrogen oxides are common pollutants that pose a significant threat to ecosystem health. Nevertheless, the intrinsic lower dissociation energy of N—O and N═O bonds in these compounds has opened up tremendous potential for electrocatalytic NH_3 synthesis, which circumvents the difficult N≡N bond cleavage in traditional NRR. In this way, the upgrading of low-value oxidized nitrogen compounds and the removal of pollutants can be simultaneously achieved.

6.2.1. Pristine and Derived Cu Nanostructures

Electrocatalytic NO_3^-RR has garnered much interest owing to its advantage of converting the highly toxic water contaminant into value-added NH_3, thereby closing the anthropogenically disturbed N cycle. Cu-based materials are regarded as one of the most promising candidates for NO_3^-RR due to their favorable NO_3^- adsorption, low toxicity, and low cost. For example, Chen et al. reported a Cu-incorporated molecular solid (3,4,9,10-perylenetetracarboxylic dianhydride) catalyst for highly selective NH_3 electrosynthesis (FE of 85.9%).[225] Such performance was ascribed to the unique electronic properties of Cu, which induced the H—N combination and the transfer of protons and electrons to the Cu active centers. In addition, the reaction mechanism of NO_3^-RR on Cu (111), Cu (100), and Cu (110) surfaces was studied in detail.[226] Thermodynamic and kinetic analysis showed that the most favorable pathway in all pH ranges is NO_3^- → *NO_3 → *NO_2 → *NO → *NOH → *NHOH → *NH → *NH_2 → *NH_3 → NH_3(g). Furthermore, the competition between HER and NO_3^-RR is pH-dependent for different crystal facets; Cu (100) performs better in a strongly acidic environment, whereas Cu (111) is the best in near-neutral and alkaline environments. The obtained theoretical insights are conducive to guiding the further development of advanced Cu catalysts.

In practical applications, the NO_3^- concentrations in polluted groundwater (0.88–1.26 mM), industrial wastewater (41.6 mM), and textile wastewater (7.4 mM) are usually low.[227] To meet the requirements for treating NO_3^--containing sewage and achieving drinking water standards, the development of Cu catalysts to efficiently enrich and perform electroreduction of dilute NO_3^- at ultralow concentrations is a prerequisite. Song et al. encapsulated Cu nanoparticles into a porous carbon framework (Cu@C) and achieved NO_3^-RR with the NO_3^- concentration as low as 1 mM.[228] The superior activity of the Cu@C catalyst (NH_3 yield: 469.5 μg h^{-1} cm^{-2}; FE: 72.0%) than Cu nanoparticles was attributed to the enrichment effect of the unique porous carbon encapsulation that confined the localized NO_3^- and facilitated its mass transfer. To regulate the electronic properties of Cu for enhanced NH_3 production, metastable phase Cu was synthesized by a novel O_2/Ar plasma oxidation and subsequent electroreduction approach.[229] Owing to the upshifted d-band center to near Fermi level, the effective adsorption of reactive H* was greatly enhanced for boosted NO_3^- activity. The relatively strong H* adsorption then induced lower formation energy of NOOH*/NOH* for higher selectivity. Consequently, a remarkable NH_4^+ selectivity of 97.8% and FE of 99.8% were reached at a low potential of −0.3 V vs RHE, surpassing the performance observed with the conventional Cu phase.

During the NO_3^- electroreduction process, the catalysts typically undergo significant in situ structural evolution to expose the active phase.[230] Therefore, a fundamental understanding of active site behavior is needed for the rational design of efficient NO_3^-RR electrocatalysts. Wang et al. examined the activity origin of CuO nanowire arrays (NWAs) in NO_3^-RR.[231] Using in situ Raman spectroscopy and ex situ characterizations, it was revealed that the CuO NWAs catalyst was electrochemically reconstructed to form Cu/Cu_2O as the active phase. DFT calculations indicated that the electron transfer at the Cu/Cu_2O interface facilitates the formation of *NOH intermediate while inhibiting the undesired HER, resulting in a prominent FE of 95.8% and NH_3 selectivity of 81.2%. Meanwhile, a reaction intermediate-mediated synthesis approach under operating conditions has been shown to effectively regulate the facet of CuO nanobelts for boosted NO_3^-RR performance (**Figure 17**a).[232] During the reduction of CuO in the presence of NO_3^-, the generated *N species could act as capping agents to control the growth of Cu nanocrystals. This preferably exposed Cu (100) facet and abundant surface defects upshifted the d-band center of Cu, which was responsible for an NH_3 yield rate 2.3 times higher than that of the Haber–Bosch process.

Apart from NO_3^-, other nitrogen compounds (e.g., NO_2^-, NO_2, and NO) have also been used as reactants for environmentally

© 2024 The Authors. Advanced Materials published by Wiley-VCH GmbH

15214095, 2024, 14, Downloaded from https://advanced.onlinelibrary.wiley.com/doi/10.1002/adma.202307913 by Cochrane Chile, Wiley Online Library on [30/09/2026]. See the Terms and Conditions (https://onlinelibrary.wiley.com/terms-and-conditions) on Wiley Online Library for rules of use; OA articles are governed by the applicable Creative Commons License

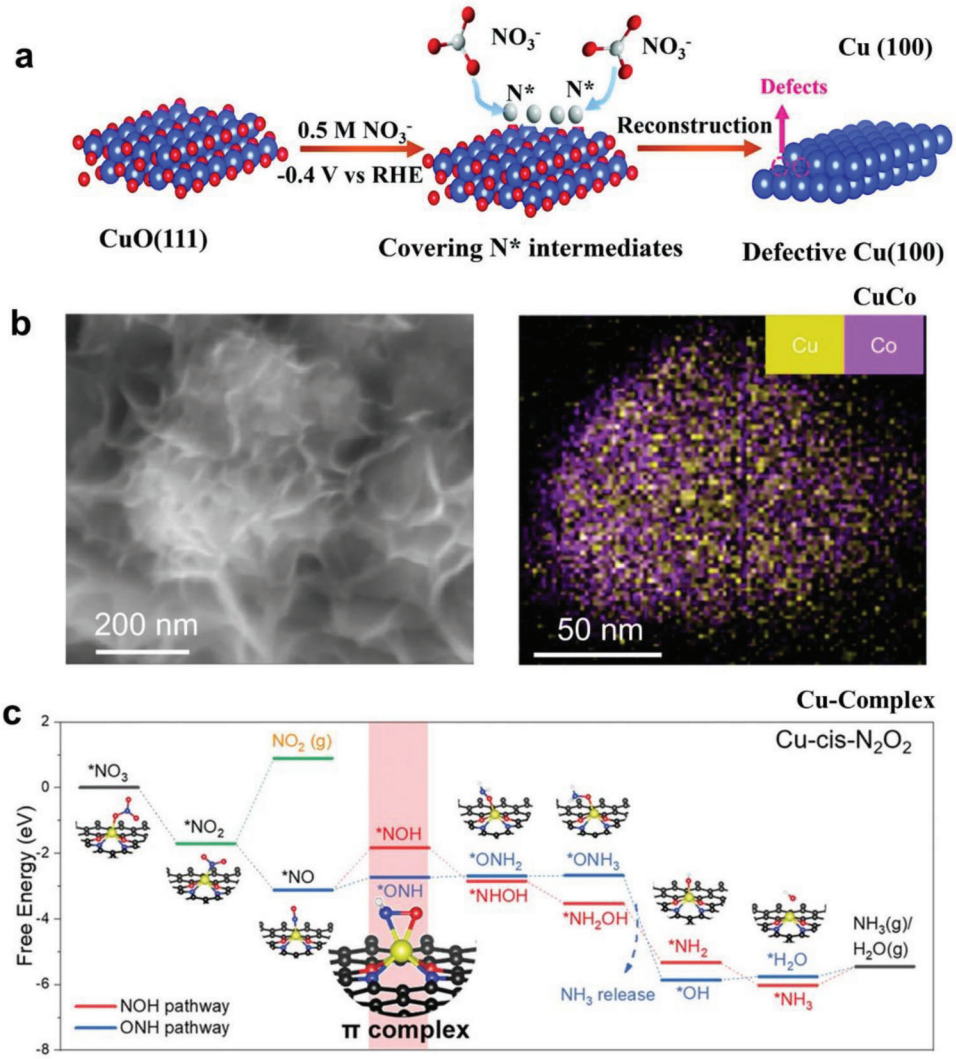

Figure 17. ECH of inorganic nitrogen compounds on Cu-based catalysts. a) Schematic illustration of the exposed defective Cu (100) facet manipulated by *N intermediates during NO_3^-RR. Reproduced with permission.[232] Copyright 2021, Royal Society of Chemistry. b) NO_3^-RR on CuCo catalyst. Reproduced under the terms of the CC-BY Creative Commons Attribution 4.0 International license (https://creativecommons.org/licenses/by/4.0).[234] Copyright 2022, The Authors, published by Springer Nature. c) Reaction pathway of NO_3^-RR on Cu-*cis*-N_2O_2 single-atom catalyst. Reproduced with permission.[242] Copyright 2022, Wiley-VCH.

friendly NH_3 production on Cu catalysts. On Cu nanowires, the NH_3 selectivity of NO_2^- electroreduction was increased to nearly 100% in a broad potential range of −0.7 to −1.3 V vs RHE upon the introduction of CO_2 molecules.[233] The CO_2 was reduced to *CO during the reaction, which reduced the energy barrier of *NO-to-*N conversion and catalyzed the hydrogenation of *NH_2 to release NH_3.

6.2.2. Engineering Cu with Other Metals

As NO_3^-RR is a multistep complex reaction with eight electron transfers, alloying Cu with a second metal could effectively tune the free energy of the reaction steps for higher activity. Inspired by the bifunctional nature of Cu-type nitrite reductase, Fang et al. proposed CuCo nanosheets by electrodeposition to endow the bimetallic catalyst with a strong synergetic effect between the two active centers (Figure 17b).[234] The Co sites generated the electrons and protons, whereas the Cu sites were favorable for NO_3^- adsorption and association. The Cu and Co sites balanced the coverage of adsorbed *H and *NO_3 species, reducing the free energy of the *NO_3 adsorption step on Cu sites and promoting the adsorption of *H on Co sites. Such synergy contributed to a NH_3 FE of 100% at an industrial ampere-level current density (1035 mA cm^{-2}). As an earth-abundant transition metal, Ni was also selected to form an alloy with Cu with enhanced catalytic activity. Wang et al. demonstrated a 0.12 V improvement in half-wave potential and 6-fold increase in NO_3^-RR activity on $Cu_{50}Ni_{50}$ alloy compared to that of pure Cu.[235] Although the pure Ni catalyst is inactive for NO_3^-RR, replacing Cu with 50% Ni atoms could tailor the d-band center of Cu and the adsorption energies of reaction intermediates, including *NO_3^-, *NO_2, and *NH_2.

© 2024 The Authors. Advanced Materials published by Wiley-VCH GmbH

15214095, 2024, 14, Downloaded from https://advanced.onlinelibrary.wiley.com/doi/10.1002/adma.202307913 by Cochrane Chile, Wiley Online Library on [30/09/2026]. See the Terms and Conditions (https://onlinelibrary.wiley.com/terms-and-conditions) on Wiley Online Library for rules of use; OA articles are governed by the applicable Creative Commons License

15214095, 2024, 14, Downloaded from https://advanced.onlinelibrary.wiley.com/doi/10.1002/adma.202307913 by Cochrane Chile, Wiley Online Library on [30/09/2026]. See the Terms and Conditions (https://onlinelibrary.wiley.com/terms-and-conditions) on Wiley Online Library for rules of use; OA articles are governed by the applicable Creative Commons License

Furthermore, noble metals (e.g., Pd, Ru) with superior activity can alloy with Cu to greatly improve the electronic properties and electrochemical performance.[236–237] As a representative work, Gao et al. synthesized intermetallic CuPd nanocubes based on the knowledge from machine learning to break the energy-scaling relationship limits of NO_3^-RR.[238] The Bayesian theory of chemisorption was applied to uncover the origin of the scaling relationship between $*NO_3$ and *N on metal surfaces, predicting that the potential non-scaling behavior is possible for the (100)-type sites of ordered B2 intermetallics due to Pauli repulsion interactions between the metal d-states and adsorbate frontier orbitals. Following this strategy, the ordered intermetallic B2 CuPd nanocubes were synthesized and displayed an NH_3 FE of 92.5% at −0.5 V vs RHE and a yield rate of 6.25 mol h^{-1} g^{-1} at −0.6 V vs RHE. Recently, ultrafine CuPd nanoparticles were in situ confined in the mesochannels of carbon nanotubes@mesoporous carbon substrates.[239] The CNTs@mesoC@CuPd catalyst exhibited 100% NO_3^- conversion efficiency while the selectivity was steered to N_2 (98%), showing its potential for NO_3^- removal in environmental remediation. In another example, reduced graphene oxide supported RuCu alloy catalysts (Ru_xCu_x/rGO) were prepared to combine the relay catalytic function of NO_3^--to-NO_2^- transformation on Cu and NO_2^--to-NH_3 transformation on Ru.[237] The optimal Ru_1Cu_{10}/rGO catalyst showed an NH_3 formation rate of 0.38 mmol cm^{-2} h^{-1} and NH_3 FE of 98% under an ultralow potential of −0.05 V vs RHE, comparable to the Ru catalyst. Besides, Cu-based structures serve as excellent substrate platforms for anchoring other metal atoms, offering facile preparation methods and effective enhancements in catalytic activity. For example, Ru-dispersed Cu nanowires prepared by cation exchange were reported to provide an industrial-relevant NO_3^-RR current of 1 A cm^{-2} while maintaining an NH_3 FE of 93%.[240] DFT results suggested that the highly dispersed Ru sites were the active sites for NO_3^-RR, and the adjacent Cu sites were responsible for suppressing the HER. A Cu nanowire-supported Rh cluster and single-atom catalyst was also developed, where the adsorbed hydrogen on Rh atoms transfers to the nearby *NO intermediate on Cu atoms for subsequent hydrogenation and NH_3 production at a record level (1.27 mmol h^{-1} cm^{-2}).[241]

6.2.3. Single-Atom Cu

Single-atom catalysts featuring isolated metal active centers have the maximized atomic utilization efficiency and unique atomic-level coordination structure, thereby garnering increasing interest in NO_3^- electrocatalysis. The mechanism, synthesis, characterization, and application of transition metal SACs in electrocatalytic NO_3^-RR were summarized in a recent review.[243] For Cu SACs, engineering the coordination structure of Cu centers is effective in reducing the thermodynamic energy barriers in NO_3^-RR. Cheng et al. constructed Cu SACs bonding with two N and two O atoms to break the coordination symmetry and induce site polarity.[242] The polar active sites in the resultant Cu-*cis*-N_2O_2 catalyst are critical for NO_3^- accumulation near the catalyst surface and splitting of Cu 3d orbital, rendering a lower energy barrier for *ONH formation by an orbital-symmetry-matched π-complex (Figure 17c). Thus, the catalyst demonstrated an NH_3 production rate of 27.84 mg h^{-1} cm^{-2} at a current density of 366 mA cm^{-2} while maintaining stability for over 2000 h. In another study, the construction of Cu(I)-N_3C_1 moieties was found to effectively decrease the rate-limiting steps ($*HNO_3 \rightarrow *NO_2$, $*NH_2 \rightarrow *NH_3$) toward thermodynamically more favorable NH_3 production as compared with Cu(II)-N_4 structure, converting 94.8% of NO_3^- in wastewater at an NH_3 yield rate of 5466 mmol g_{Cu}^{-1} h^{-1}.[244] Moreover, elucidating the dynamic restructuring of single-atom sites during NO_3^-RR is of paramount importance to identify the real active sites and control selectivity. Yang et al. studied the structural evolution of Cu–N–C SAC by operando X-ray absorption spectroscopy and advanced electron microscopy.[245] When the applied potential was altered from 0 to −1 V vs RHE, the initially synthesized Cu–N_4 structure experienced a progressive transformation, evolving from Cu–N_3 units to nearly isolated Cu^0 single atoms, ultimately culminating in the formation of aggregated Cu^0 nanoparticles with a size of ≈5 nm. This potential-driven transformation resulted in an increased NH_3 production rate, reaching a maximum value of 4.5 mg cm^{-2} h^{-1} and a FE of 84.7%. The derived Cu nanoparticles were proved to be the genuine active sites for NO_3^-RR, and can be recycled to form the Cu—N_4 structure after being exposed to ambient conditions.

6.3. ECH of Organic Nitrogen Compounds

Selective electroreduction of organic nitrogen compounds holds a crucial role in the production of amine compounds, a group of important building blocks with diverse applications in agrichemicals, pharmaceuticals, and organic synthesis.[200] The electrification of amine manufacturing process by renewable electricity introduces a novel pathway that operates under mild conditions, reduces separation costs, and minimizes the reliance on toxic reagents. Recently, Cu-based materials have been fabricated for the hydrogenation of nitroorganic compounds with the —NO_2 functional group in aqueous electrolytes. Jin et al. reported a series of Cu_xPt_y alloying catalysts to produce azoxybenzene from selective ECH of nitrobenzene (Ph—NO_2).[246] The selectivity of hydrogenation products was found to be correlated with electrolyte pH and applied potential (**Figure 18**a). In acidic media, the production of aminobenzene is favored irrespective of the applied potential. On the other hand, in the alkaline media, the hydrogenation products are azoxybenzene at 0.3 V vs RHE and aminobenzene at –0.3 V vs RHE, respectively. By tuning the electronic structure with Pt, the Cu_3Pt/C catalyst achieved the optimal adsorption and activation of Ph—NO_2, resulting in ≈99% selectivity of azoxybenzene and aminobenzene in 1 M KOH. Moreover, it is critical to promote the proton adsorption and activation kinetics for the generation of *H species in nitrobenzene hydrogenation. To address this issue, Gao et al. designed a phytate-coordinated Cu foam and triggered the concerted proton-coupled electron transfer.[247] The phytate acts as a proton acceptor to overcome the kinetic limitations by upshifting the d-band center on Cu sites and proton enrichment effects, enhancing the nitrobenzene hydrogenation activity by a factor of 36.94.

The ECH of acetonitrile to form ethylamine product was also achieved on Cu. Xia et al. screened seven metal catalysts (Cu, Ni, Pd, Pt, Bi, In, and Sn) in a flow cell electrolyzer and found that Cu exhibited the optimal acetonitrile-to-ethylamine performance (Figure 18b).[248] The Cu nanoparticles achieved the highest FE

© 2024 The Authors. Advanced Materials published by Wiley-VCH GmbH

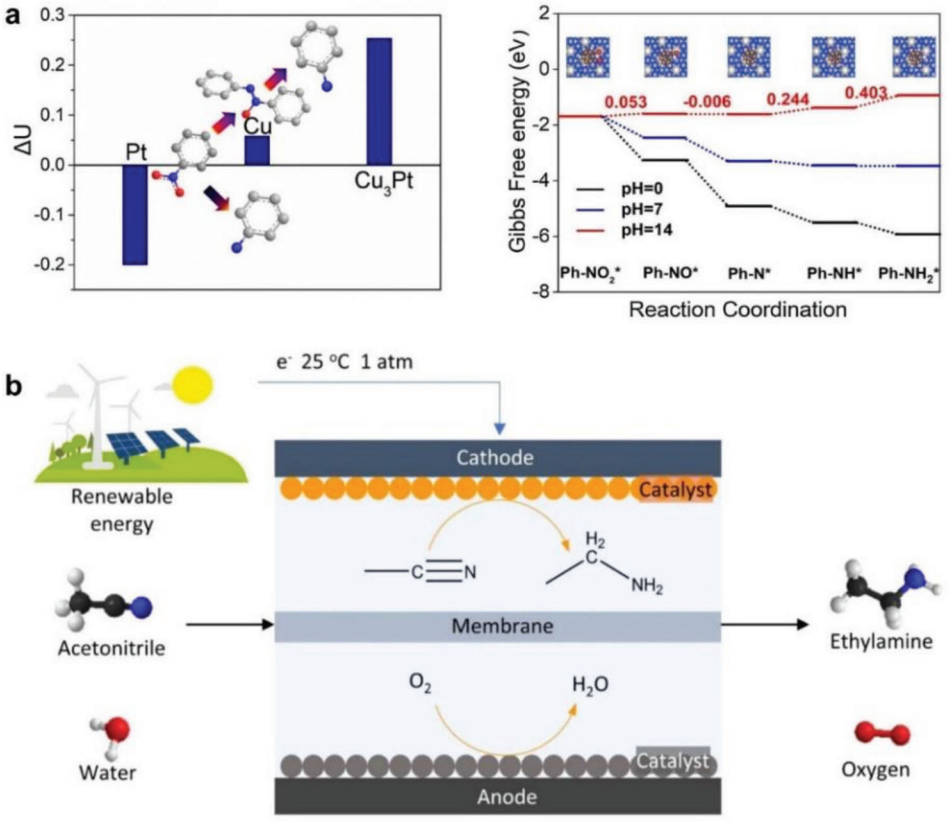

Figure 18. ECH of organic nitrogen compounds on Cu-based catalysts. a) The selectivity of the Cu (111), Pt (111), and Cu_3Pt (111) in nitrobenzene reduction, and the Gibbs free energy on Cu_3Pt (111) under different pH values. Reproduced with permission.[246] Copyright 2021, Elsevier. b) Schematic illustration of ECH of acetonitrile for primary amine production on Cu nanoparticles. Reproduced under the terms of the CC-BY Creative Commons Attribution 4.0 International license (https://creativecommons.org/licenses/by/4.0).[248] Copyright 2021, The Authors, published by Springer Nature.

of ethylamine (96%) at –0.29 V vs RHE as a result of the suppressed HER in alkaline conditions. DFT calculations suggest that the moderate binding affinity of the Cu (111) facet for the $*CH_3C_xN_y$ intermediate contributes to the thermodynamically favorable nitrile reduction. To increase the ethylamine selectivity and prevent the condensation reaction between the intermediates that lead to the formation of dimers and trimers, Zhang et al. introduced CO_2 into the electrolyte to protect the initially formed primary amine.[249] On a Cu nanostructured catalyst, the adsorption of acetonitrile is favored through the terminal C≡N group. Meanwhile, the CO_2 reacts with the NH_2 group to form $CH_3CH_2NHCOOH*$ and prevents the condensation side reactions. The synergistic effect between Cu and dissolved CO_2 contributes to the outstanding FE (94%) and ethylamine selectivity (99%).

In summary, Cu-based nanostructures have shown significant advantages for efficient ECH of N-containing substances. The direct N_2 conversion into NH_3 was achieved on current Cu catalysts, while the inorganic nitrogen compounds (e.g., NO_3^-, NO_2^-, NO_2, and NO) have also been used as reactants for environmentally friendly NH_3 production on Cu catalysts. Besides, selective electroreduction of organic nitrogen compounds was used to produce amine compounds. As ECH of N-containing substances is a multistep process with multiple N-containing intermediates, the electroreduction of N-containing substances could offer mechanistic insights into N-based conversion pathways and uncover the inner relations of Cu catalysts in these reactions. Future research should prioritize the design of advanced Cu nanostructures and explore novel processes and operational parameters in order to attain higher efficiency in ECH of N-containing substances.

7. ECH for Coupling Reactions

Electrocatalytic coupling reactions via co-hydrogenation of two reactants offer greater flexibility to construct more complex chemical structures containing C, N, and S atoms (Figure 19-22). In this section, we discuss the generation of amides, urea, and amines by C—N coupling as well as other emerging C—S and C—C cross-coupling reactions on Cu catalysts for expanding the product scope of ECH (**Table 6**).

7.1. C—N Coupling Reactions

The need for reducing CO_2 emissions and nitrogenous pollutants (e.g., NO_2^- and NO_3^-) has provided enormous opportunities for the co-reduction of the reactants to enable C—N bond formation, which can be extensively applied in drug synthesis, natural product formation, ligand design, and catalyst

© 2024 The Authors. Advanced Materials published by Wiley-VCH GmbH

15214095, 2024, 14, Downloaded from https://advanced.onlinelibrary.wiley.com/doi/10.1002/adma.202307913 by Cochrane Chile, Wiley Online Library on [30/09/2026]. See the Terms and Conditions (https://onlinelibrary.wiley.com/terms-and-conditions) on Wiley Online Library for rules of use; OA articles are governed by the applicable Creative Commons License

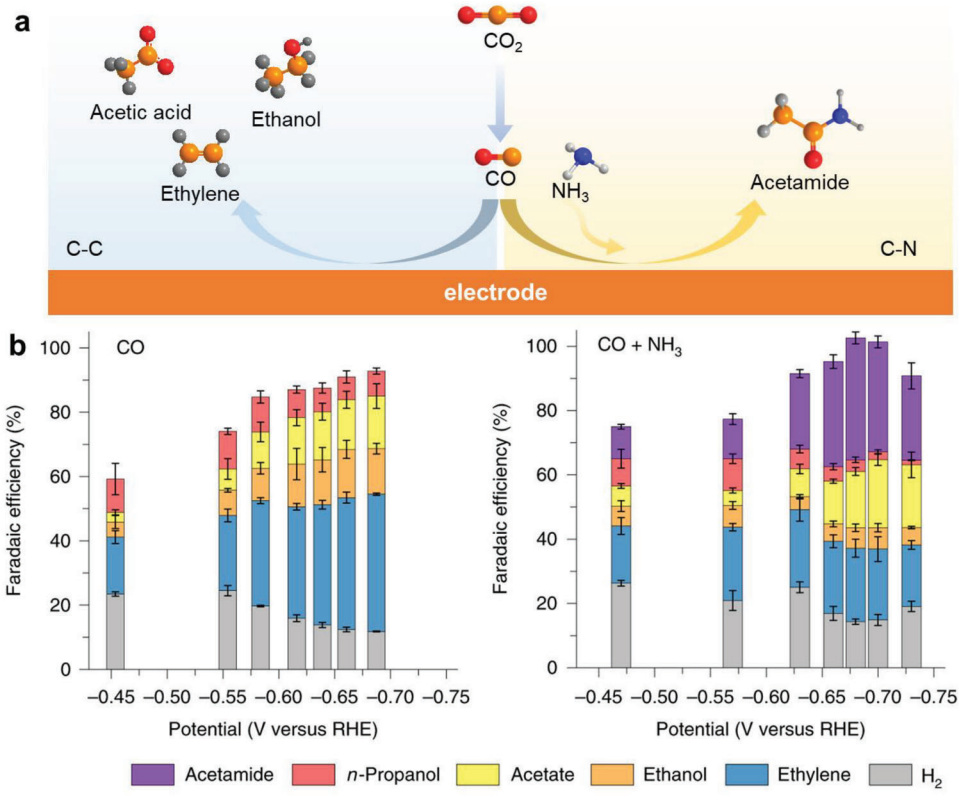

Figure 19. a) Schematic illustration of acetamide and other reduced products on Cu-catalyzed co-electrolysis of NH_3 and CO. b) The FE of CRR and C—N coupling. a) Adapted with permission.[251] Copyright 2019, The Authors, published by Springer Nature. b) Reproduced with permission.[251] Copyright 2019, The Authors, published by Springer Nature.

development.[250] Electrocatalytic C—N coupling reaction using clean renewable electricity under ambient conditions could save a considerable amount of energy than in traditional thermocatalytic processes for the construction of organonitrogen compounds. During the process, the carbon sources (e.g., CO_2 or CO_2-derived CO) and nitrogen sources (e.g., N_2, NO_3^-, NO_2^-, or NH_3) can be converted into amides (e.g., formamide ($HCONH_2$), acetamide (CH_3CONH_2)), urea ($CO(NH_2)_2$), and amines (e.g., methylamine (CH_3NH_2), ethylamine ($C_2H_5NH_2$)). Because Cu-based catalysts are critical in both CRR and NO_3^-RR, their inherent suitability toward C—N coupling reactions has aroused extensive attention.

7.1.1. Amides

Amides are widely applied in polymer and pharmaceutical industries. Jouny et al. reported the co-electroreduction of CO

Table 6. Comparison of typical Cu-based electrocatalysts for coupling reactions.

Reaction	Reactants	Catalyst	Performance [%]	Current density [mA cm^{-2}] or potential [V vs RHE]	Electrolyzer	Refs.
C—N coupling for amides	CO and NH_3	Cu nanoparticles	Selectivity 40	Current at 300	Flow cell	[251]
C—N coupling for amides	HCOOH and NO_2^-	Low-coordinated Cu	FE 29.7 /selectivity up to 90	−0.6	H-type cell	[252]
C—N coupling for urea	CO_2 and NO_3^-	Cu–N–C	FE 28	−0.9	H-type cell	[258]
C—N coupling for urea	N_2 and CO_2	PdCu alloy	FE 8.92	−0.4	H-type cell	[257]
C—N coupling for urea	NO_3^- and CO_2	Core–shell Cu@Zn	FE 9.28	−1.02	H-type cell	[260]
C—N coupling for amines	CO_2 and NO_3^-	O-derived copper	FE 0.36	−1	H-type cell	[262]
C—S coupling	CO_2 and SO_3^{2-}	Cu_2O	FE up to 6.8	/	Flow cell	[266]
C—C cross-coupling	Furfural and benzaldehyde	Cu-Pb	FE≈20	−0.5	H-type cell	[267]

© 2024 The Authors. Advanced Materials published by Wiley-VCH GmbH

15214095, 2024, 14, Downloaded from https://advanced.onlinelibrary.wiley.com/doi/10.1002/adma.202307913 by Cochrane Chile, Wiley Online Library on [30/09/2026]. See the Terms and Conditions (https://onlinelibrary.wiley.com/terms-and-conditions) on Wiley Online Library for rules of use; OA articles are governed by the applicable Creative Commons License

15214095, 2024, 14, Downloaded from https://advanced.onlinelibrary.wiley.com/doi/10.1002/adma.202307913 by Cochrane Chile, Wiley Online Library on [30/09/2026]. See the Terms and Conditions (https://onlinelibrary.wiley.com/terms-and-conditions) on Wiley Online Library for rules of use; OA articles are governed by the applicable Creative Commons License

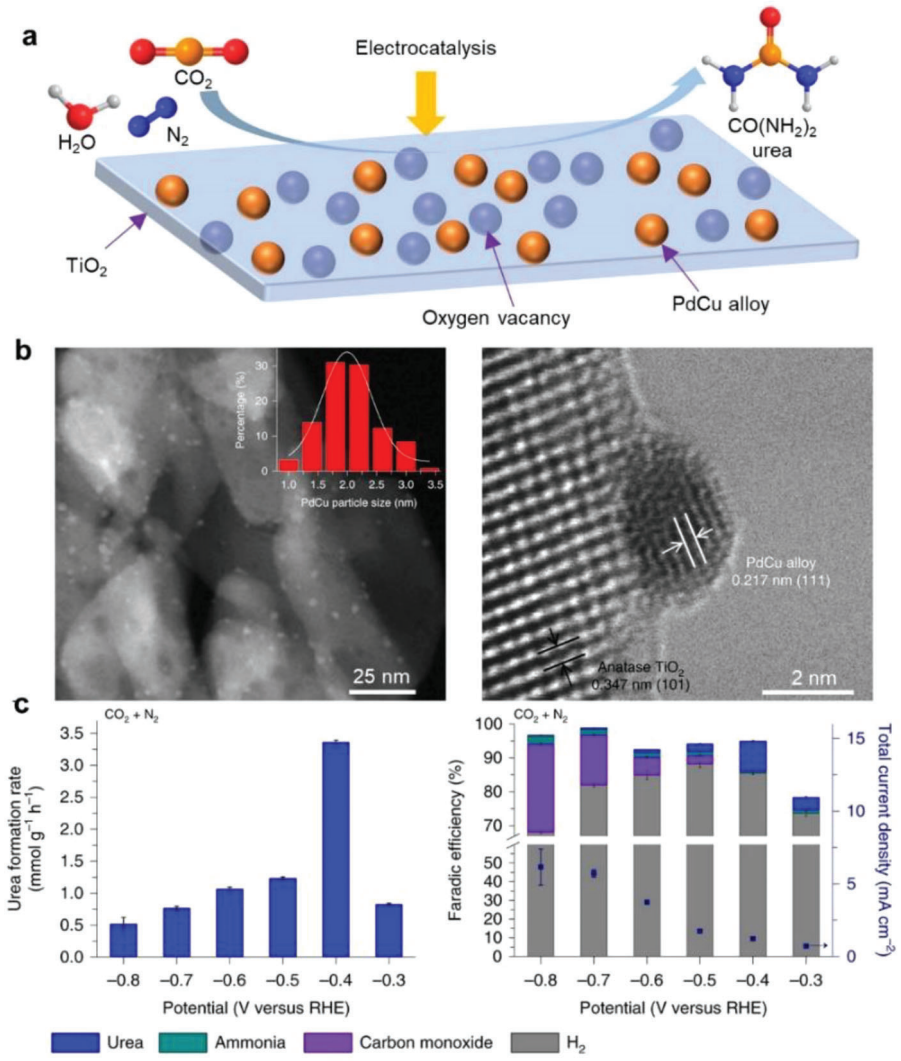

Figure 20. a) Schematic illustration of coupling N_2 with CO_2 to produce urea on PdCu alloy nanoparticles-decorated TiO_2 electrode. b) TEM images. c) Urea formation rate and FE. b,c) Reproduced with permission.[257] Copyright 2020, The Authors, published by Springer Nature.

derived from CO_2 and NH_3 with a ratio of 2:1 to obtain acetamide with a high selectivity of up to 40% (Figure 19).[251] The CH_3CONH_2 was formed via nucleophilic attack by adding NH_3 to the *C═C═O intermediate on the Cu surface. The mechanism of C—N coupling was successfully constructed to obtain various kinds of amide products via amine nucleophilic attack on the surface ketene intermediate, which selectively produces *N*-methylacetamide, *N*,*N*-dimethylacetamide, *N*-ethylacetamide, acetic monoethanolamide, and aceturic acid, instead of other C_{2+} products. Moreover, electrochemical C—N coupling toward $HCONH_2$ was achieved through the co-reduction of CO_2-derived formic acid (HCOOH) and nitrite (NO_2^-).[252] Derived from Cu_2O nanocubes, the low-coordinated Cu demonstrated an exceptional FE of 29.7% and selectivity of up to 90% toward $HCONH_2$ under ambient conditions, owing to the effective coupling of *CHO and $*NH_2$ intermediates during the reduction process. This coupling strategy is extendable to use CO_2-derived ethanoic acid (CH_3COOH) as the carbon source for CH_3CONH_2 formation and nitrate as N source. In another work, the gas–liquid–solid triple-phase boundary was constructed on a solid copper electrode to drive the electrocatalytic C—N coupling of CO_2 in the gas phase and NH_3 in the aqueous phase, resulting in FE of 0.4% and 10% toward $HCONH_2$ and CH_3CONH_2, respectively.[253] Through operando infrared spectroscopy, it was determined that the formate and formamide forming pathways share a common $*CO_2^-$ intermediate, while the acetate and acetamide formation follow a distinct reaction pathway involving key C_2 intermediates.

7.1.2. Urea

Apart from amides, urea can also be obtained by C—N coupling on Cu-based catalysts to circumvent the huge energy consumption and harsh conditions of the Haber–Bosch process.[254] In 1995, a pioneer work reported urea synthesis by the co-reduction of CO_2 and NO_3^- (current efficiency of 10%) or NO_2^- (current

© 2024 The Authors. Advanced Materials published by Wiley-VCH GmbH

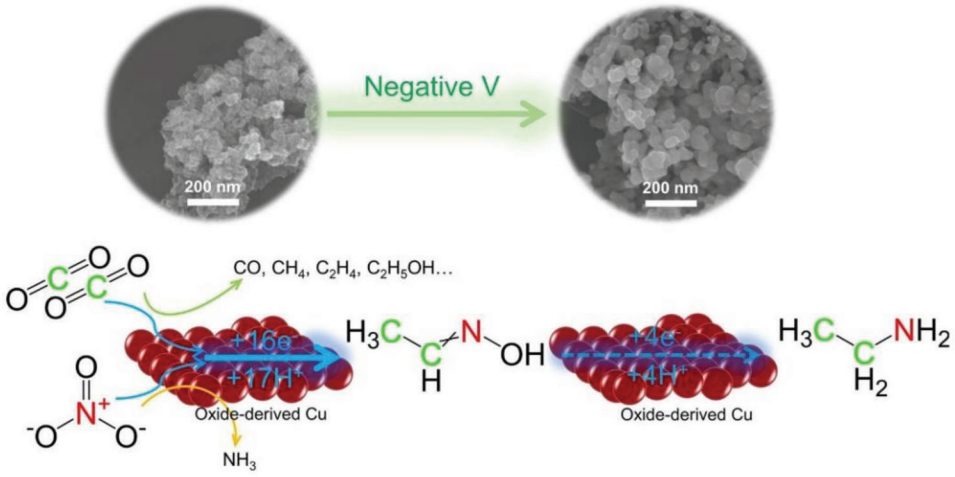

Figure 21. Schematic illustration of acetaldoxime and ethylamine formation by coupling NO_3^- with CO_2 on an oxide-derived Cu electrode. Reproduced with permission.[262] Copyright 2021, Science Press and Dalian Institute of Chemical Physics, Chinese Academy of Sciences, published by Elsevier.

efficiency of 37%) on a Cu-loaded gas diffusion electrode, with NH_3 being the key intermediate.[255] The urea formation was also achieved on Ag and Au catalysts and was believed to be formed by NH_3 and CO precursors.[256] In recent years, various Cu-based nanostructures have been developed in urea synthesis and their structure–activity relationship has been studied in detail. For example, single-atom Cu coordinated with a porous N-doped carbon framework (Cu–N–C) delivered a urea FE of 28%.[258] The catalytic activity was found to be significantly influenced by the coordination sphere, where Cu–N_4 sites displayed enhanced activity in CO_2 reduction, while Cu–N_{4-x}–C_x sites exhibited a higher NH_4^+ yield rate in NO_3RR. To facilitate the trapping and adsorption of reactants, Cao et al. reported the low-valence Cu-doped TiO_2 (Cu-TiO_2) for effective C—N coupling toward urea formation.[259] The rich oxygen vacancies in Cu-TiO_2 and the bi-Ti^{3+} defect sites favored the adsorption and activation of NO_2^- for forming NH_2* intermediates. At the same time, the Cu dopants acted as adsorption sites for CO_2 and donated electrons to form CO* intermediates, resulting in an outstanding urea yield of 20.8 μmol h^{-1} and an FE of up to 43.1%. Moreover, although it is difficult to activate the N≡N triple bond in N_2, efficient Cu structures have been synthesized for direct co-reduction of N_2 and CO_2. Chen et al. prepared PdCu alloy nanoparticles decorated on the TiO_2 nanosheets to catalyze the formation of C–N bonds under ambient conditions (Figure 20).[257] In the first step, the nitrogen was reduced to ammonia while the CO_2 was reduced to CO. Then, the thermodynamically spontaneous reaction between *N═N* and CO was responsible for urea formation, in which the generation of *NCON* intermediate from N_2 activation served as the key step. Besides, core–shell Cu@Zn nanowires were designed to couple NO_3^- and CO_2 to efficiently produce urea with a high FE of 9.28% and yield of 7.29 μmol cm^{-2} h^{-1}.[260] The *NH_2 and *CO intermediates were favorably generated by the electron transfer from the Zn shell to the Cu core, which promoted the coupling and decreased its energy barrier toward urea production. With 1D nanofiber structure and (111)-dominant facets, bimetallic AuCu achieved efficient urea formation with a FE of 24.7% and a yield of 3889.6 μg h^{-1} mg_{cat}^{-1} via co-reduction of CO_2 and NO_2^-.[261]

7.1.3. Amines

Amines are usually obtained by the thermocatalytic amination of alcohols using NH_3 at high temperature (100–250 °C) and high pressure (50–250 bar), which can alternatively be realized by electrocatalytic C—N coupling. As the simplest product, methylamine (CH_3NH_2) is predicted to be obtained by electrocatalytic coupling between CO (derived from CO_2) and NO.[263] Two Cu single atoms were coordinated within O-vacancy-rich MXenes of Mo_2NO_2 (denoted as Cu_2–ν-Mo_2NO_2), and then the carbene was modified on the surface to engineer the electronic configuration of copper pairs. In this case, the Cu—Cu distance was decreased and the electronic configuration between Cu pairs was perturbed, leading to optimized adsorption of the precursors and intermediates. Consequently, the functionalized copper achieved straightforward C—N coupling with a reduced kinetic barrier (0.12 eV). As the conversion from CO_2 and NO_3^- into amines involves complex proton and electron transfer steps, discovering cascade reaction pathways is helpful to enhance the selectivity. Based on this, an O-derived copper electrode was developed to achieve electrocatalytic coupling of CO_2 and NO_3^- toward acetaldoxime (C_2H_5NO) and ethylamine ($C_2H_5NH_2$) in a nearly neutral aqueous electrolyte (Figure 21).[262] The coupling interaction between the acetaldehyde intermediate derived from CO_2 reduction and the NH_2OH intermediate generated from NO_3^- reduction undergoes spontaneous condensation to form the pivotal C_2H_5NO intermediate, which eventually produces $C_2H_5NH_2$.

Organic compounds can also become the C source in C—N coupling reactions, providing further opportunities for synthesizing complex organonitrogen products. On a Cu-Hg electrode, the oxalic acid derived from CO_2 served as the C source and coupled with NO_3^- to synthesize glycine with an FE of 43.1%.[264] Three significant electrocatalytic reduction steps take place under optimized reaction conditions with balanced kinetics, including the

© 2024 The Authors. Advanced Materials published by Wiley-VCH GmbH

15214095, 2024, 14, Downloaded from https://advanced.onlinelibrary.wiley.com/doi/10.1002/adma.202307913 by Cochrane Chile, Wiley Online Library on [30/09/2026]. See the Terms and Conditions (https://onlinelibrary.wiley.com/terms-and-conditions) on Wiley Online Library for rules of use; OA articles are governed by the applicable Creative Commons License

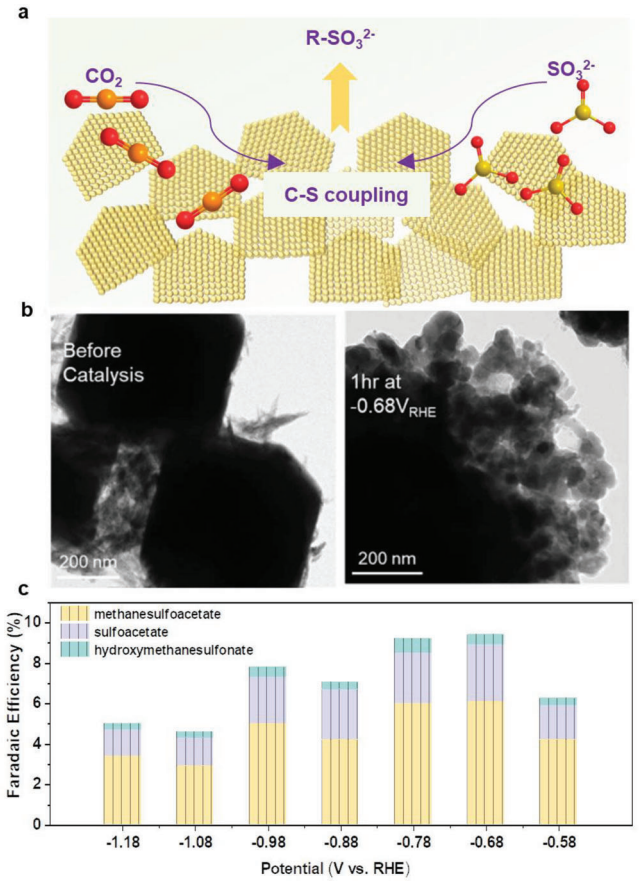

Figure 22. a) Schematic illustration of C—S bond formation by coupling SO_3^{2-} with CO_2 on Cu_2O. b) TEM images. c) FE for C—S coupling. b,c) Adapted with permission.[266] Copyright 2023, The Authors, published by Springer Nature.

oxalic acid reduction to electrophilic glyoxylic acid, NO_3^- reduction to nucleophilic hydroxylamine, and glyoxylic oxime reduction to glycine. Moreover, a low-cost Cu-S catalyst was demonstrated to electrochemically synthesize cyclohexanone oxime, a nylon-6 precursor, from cyclohexanone and NO_2^- with 92% yield and 99% selectivity. The introduction of S lowered the reductive capacity of Cu and led to the conversion of NO_2^- to the key intermediate species NH_2OH, instead of producing ammonia. The reaction follows a $NO_2^- \rightarrow NH_2OH \rightarrow$ oxime pathway and involves the spontaneous condensation between NH_2OH* and cyclohexanone occurring on the catalyst surface.[265]

7.2. C—S and C—C Coupling Reactions

Beyond C—N bond formation, other coupling reactions, such as C—S and C—C cross-coupling reactions, have the potential to enhance the value of inexpensive reactants by producing valuable organic compounds. In a typical example, electrochemical C—S coupling was demonstrated using CO_2 and SO_3^{2-} as cost-effective precursors on a Cu_2O electrocatalyst (Figure 22).[266] The main products were hydroxymethanesulfonate, sulfoacetate, and methanesulfonate, with FE of up to 6.8%. DFT calculations revealed that the *CHOH formed on the Cu metal surface serves as a key electrophilic intermediate and undergoes nucleophilic attack by SO_3^{2-}, ultimately leading to the efficient formation of C—S bonds. Furthermore, the C—C dimerization is a potent method to increase the molar mass of biomass derivatives toward multicarbon fuels and chemicals. The co-reduction of furfural and benzaldehyde led to electrocatalytic C—C coupling on Cu and Pb.[267] Reactivity studies demonstrate that both aldehydes exhibit self-coupling and cross-coupling reactions on the surfaces of the two metals. However, the selectivity varies between the two metals; a higher selectivity was achieved for the cross-coupling products of 1-(2-furyl)−2-phenyl-1,2-ethanediol on Cu, while the self-coupling dimerization of furfural was favorable on Pb. The cross-coupling of the two aldehydes follows a two-reactant Sabatier rule, indicating that the increased selectivity of Cu is attributed to its greater similarity in terms of the ketyl radical binding energies.

Overall, the co-hydrogenation of two reactants and coupling reactions pave the way for producing various high-value heteroatom-containing organic products. Despite significant advances in this emerging field, the performance of Cu-based catalysts for coupling reactions is not as efficient as the side reactions, and the underlying mechanisms remain controversial. To make further breakthroughs, novel catalyst design strategies need to be considered, such as creating dual active sites with suitable distance that can target the CO_2 and nitrogenous reactants and perform the coupling of reaction intermediates. Gaining a comprehensive understanding of model coupling reactions, such as urea synthesis, is also crucial for obtaining insights into more complex pathways and expanding the range of potential products.

8. Conclusions and Perspectives

Catalytic hydrogenation plays a pivotal role in the energy and chemistry fields. To address the issues of conventional TCH, ECH offers a sustainable strategy to convert substances in their oxidized form into value-added chemicals. Recent research has witnessed vast growth in the development of ECH catalysts, where Cu-based materials have attracted increasing attention as earth-abundant, low-cost, and active ECH candidates to replace noble-metal catalysts. In this review, we highlight the unique fundamental properties of Cu and recent progress in the development of advanced Cu-based materials for different ECH reactions. Various design principles of Cu-based electrocatalysts, including nanostructuring, facet engineering, support effect, creating single-atom sites, defect engineering, heteroatom doping, alloying, and constructing heterojunctions, have been proposed to enhance the ECH performance. In addition, we have provided an up-to-date summary of Cu-based nanomaterials for sustainable production of value-added chemicals through ECH of CO_2 (direct and tandem reactions), alkynes, aldehydes, N-containing inorganic compounds (e.g., N_2, nitrates, nitrites), and organic nitrogen compounds, with a specific focus on the catalyst structure–performance relationship. Notably, the emerging co-hydrogenation and coupling reactions for the formation of C—N, C—S, or C—C bonds have been discussed in detail. Despite significant advancements in Cu-based catalysts for ECH, several challenges still need to be addressed for the synthesis of novel complex value-added chemicals and potential scale-up applications.

© 2024 The Authors. Advanced Materials published by Wiley-VCH GmbH

15214095, 2024, 14, Downloaded from https://advanced.onlinelibrary.wiley.com/doi/10.1002/adma.202307913 by Cochrane Chile, Wiley Online Library on [30/09/2026]. See the Terms and Conditions (https://onlinelibrary.wiley.com/terms-and-conditions) on Wiley Online Library for rules of use; OA articles are governed by the applicable Creative Commons License

15214095, 2024, 14, Downloaded from https://advanced.onlinelibrary.wiley.com/doi/10.1002/adma.202307913 by Cochrane Chile, Wiley Online Library on [30/09/2026]. See the Terms and Conditions (https://onlinelibrary.wiley.com/terms-and-conditions) on Wiley Online Library for rules of use; OA articles are governed by the applicable Creative Commons License

Firstly, innovations in the rational design of Cu-based efficient structures are highly needed to further improve the activity, selectivity, and durability of catalysts. Currently, the most widely applied structures reported in the literature are metallic Cu, Cu compounds, Cu alloys, Cu SACs, doped Cu structures, and Cu-supported metal complexes. While these materials are versatile for ECH reactions, developing novel candidate materials that can target a specific category of substrates with unsaturated bonds is more helpful for elucidating the structure–activity relationship. An important starting point would be to consider the general ECH mechanism with the *H production from water dissociation, which supports the creation of dual active sites where the selective adsorption of the substrate and H_2O are separately targeted. The construction of dual-atom catalysts with appropriate interatomic distance is critical to achieve tunable adsorption energies especially in multistep ECH and tandem reactions. Moreover, catalyst design strategies that can break the scaling relationship in the reactant adsorption, intermediate evolution, and product desorption could offer another degree of freedom in ECH. Introducing strains, confinements, mechanochemical forces, and escalating the entropy toward high-entropy Cu-based materials are promising methods for boosting the inherent ECH activity via regulation of geometrical structure and electronic structure. Effective measures to enhance ECH selectivity should also encompass the regulation of catalyst electronic structure to induce specific adsorption configurations and energies of substrates, enabling improved product desorption and inhibited overhydrogenation.

Secondly, as Cu-based catalysts are prone to structural reconstruction under operating ECH conditions, advanced characterization techniques are required to investigate their real active species and dynamic evolution. Reconstruction is triggered by applied potential and involves ion and atom migration within catalysts or at the catalyst-electrolyte interface, often accompanied by the formation of new phases or surface local structures. The accurate tracking of catalyst reconstruction behavior is beneficial for elucidating the efficient structures and reaction mechanism. However, its instant occurrence and uncontrolled behavior pose significant challenges to gaining a clear understanding of real catalytic sites. Various in situ/operando spectroscopic, electrochemical, and microscopy imaging techniques are needed to probe the active site and phase of electrode materials with high resolution at the atomic scale.

Thirdly, as electrocatalytic reactions typically occur on the electrode–electrolyte interface, optimizing the local catalytic environment presents tremendous opportunities for cost-effective formation of ECH products. The modification of the catalyst surface at the electrochemical double layer can be achieved through the engineering of electrolytes, local pH, ions, organic additives, ionic liquids, and interfacial hydrophobicity. These strategies complement catalyst design and offer greater control over the reaction microenvironment to accelerate the reaction rate and suppress the unwanted HER. The understanding of the local environment can ultimately be integrated into reactor design with optimized device components, such as triple-phase boundary, to increase local concentration or facilitate mass transport toward improved conversion efficiency.

Lastly, expanding the range of ECH reactions and their catalytic pathways is essential as a further step toward practical application. Cu-based catalysts are effective in catalyzing simple ECH reactions, but the formation of more complex chemicals (e.g., long-chain aliphatic compounds, aromatic compounds, amino acids, and polymer intermediates) with higher value by electrocatalysis is challenging and may require insights from organic synthesis. The cathodic ECH can also be paired with another anodic oxidation reaction for simultaneous upgrading of two chemicals with a theoretical FE of 200%. Identifying the key intermediates involved in these transformation steps and establishing their adsorption energy relationships are helpful in uncovering the fundamental aspects of novel ECH reactions. Besides, most reports of ECH reactions till now remain at the stage of model chemicals, whereas the production in an integrated system under real conditions is less focused on. For example, while 5-HMF is commonly chosen as a biomass-derived platform molecule, there is limited knowledge regarding the high-quality ECH valorization of actual lignocellulose. Practical issues such as solubility, product separation, and reactor design remain challenging, which resulted in unsatisfactory conversion rate and FE. Thus, further research in the ECH reaction networks is necessary to overcome these obstacles in advanced electrolysis systems.

In summary, the combined understanding of rational catalyst design, structural reconstruction, electrode–electrolyte interfaces, and reaction pathways can unlock the full potential of Cu-catalyzed ECH, enabling the efficient and sustainable production of a wide range of valuable chemical compounds. The obtained insights are then possible to be integrated into escalated systems, such as membrane electrode assemblies, for industrial-level ECH application. It is also anticipated that the design principles established for Cu-based ECH catalysts are applicable to the development of next-generation transition-metal catalysts for other intricate electrocatalytic reactions. This progress will hold the potential to revolutionize energy and chemical industries, ultimately leading to carbon-neutral chemical production on a global scale.

Acknowledgements

M.Z. and J.Z. contributed equally to this work. This work was financially supported by the Australian Research Council (FL170100154, DP230102027, DP220102596, DP190103472, CE230100032, and FT200100062). The authors acknowledge Dr. Roy Lehmann, Yingjie Gao, Chaojie Chen, and Haifeng Shen for helpful discussions.

Open access publishing facilitated by The University of Adelaide, as part of the Wiley - The University of Adelaide agreement via the Council of Australian University Librarians.

Conflict of Interest

The authors declare no conflict of interest.

Keywords

copper, electrocatalysts, electrocatalytic hydrogenation, nanomaterials, value-added chemicals

Received: August 6, 2023
Revised: September 14, 2023
Published online: January 6, 2024

© 2024 The Authors. Advanced Materials published by Wiley-VCH GmbH

[1] F. Chang, W. Gao, J. Guo, P. Chen, *Adv. Mater.* **2021**, *33*, 2005721.
[2] Y. Kwon, K. J. P. Schouten, J. C. Van Der Waal, E. D. Jong, M. T. M. Koper, *ACS Catal.* **2016**, *6*, 6704.
[3] J. Zhang, H. Zhang, Y. Wu, C. Liu, Y. Huang, W. Zhou, B. Zhang, *J. Mater. Chem. A* **2022**, *10*, 5743.
[4] E. C. Ra, K. Y. Kim, E. H. Kim, H. Lee, K. An, J. S. Lee, *ACS Catal.* **2020**, *10*, 11318.
[5] L. Zhang, M. Zhou, A. Wang, T. Zhang, *Chem. Rev.* **2020**, *120*, 683.
[6] K. Liu, R. Qin, N. Zheng, *J. Am. Chem. Soc.* **2021**, *143*, 4483.
[7] P. A. Chase, G. C. Welch, T. Jurca, D. W. Stephan, *Angew. Chem., Int. Ed.* **2007**, *46*, 8050.
[8] S. Roy, A. Cherevotan, S. C. Peter, *ACS Energy Lett.* **2018**, *3*, 1938.
[9] D. Wang, D. Astruc, *Chem. Rev.* **2015**, *115*, 6621.
[10] S. Lau, D. Gasperini, R. L. Webster, *Angew. Chem., Int. Ed.* **2021**, *60*, 14272.
[11] C. Gunanathan, D. Milstein, *Science* **2013**, *341*, 1229712.
[12] C. Tang, Y. Zheng, M. Jaroniec, S.-Z. Qiao, *Angew. Chem., Int. Ed.* **2021**, *60*, 19572.
[13] A. Winiwarter, L. Silvioli, S. B. Scott, K. Enemark-Rasmussen, M. Sariç, D. B. Trimarco, P. C. K. Vesborg, P. G. Moses, I. E. L. Stephens, B. Seger, J. Rossmeisl, I. Chorkendorff, *Energy Environ. Sci.* **2019**, *12*, 1055.
[14] S. A. Akhade, N. Singh, O. Y. Gutiérrez, J. Lopez-Ruiz, H. Wang, J. D. Holladay, Y. Liu, A. Karkamkar, R. S. Weber, A. B. Padmaperuma, M.-S. Lee, G. A. Whyatt, M. Elliott, J. E. Holladay, J. L. Male, J. A. Lercher, R. Rousseau, V.-A. Glezakou, *Chem. Rev.* **2020**, *120*, 11370.
[15] C. Xu, E. Paone, D. Rodríguez-Padrón, R. Luque, F. Mauriello, *Chem. Soc. Rev.* **2020**, *49*, 4273.
[16] Y. Song, U. Sanyal, D. Pangotra, J. D. Holladay, D. M. Camaioni, O. Y. Gutiérrez, J. A. Lercher, *J. Catal.* **2018**, *359*, 68.
[17] Y. Song, O. Y. Gutiérrez, J. Herranz, J. A. Lercher, *Appl. Catal., B* **2016**, *182*, 236.
[18] M. B. Gawande, A. Goswami, F.-X. Felpin, T. Asefa, X. Huang, R. Silva, X. Zou, R. Zboril, R. S. Varma, *Chem. Rev.* **2016**, *116*, 3722.
[19] H. Zhou, B. Xiong, L. Chen, J. Shi, *J. Mater. Chem. A* **2020**, *8*, 20286.
[20] C. Panda, P. W. Menezes, M. Zheng, S. Orthmann, M. Driess, *ACS Energy Lett.* **2019**, *4*, 747.
[21] E. Andrews, J. A. Lopez-Ruiz, J. D. Egbert, K. Koh, U. Sanyal, M. Song, D. Li, A. J. Karkamkar, M. A. Derewinski, J. Holladay, O. Y. Gutiérrez, J. D. Holladay, *ACS Sustainable Chem. Eng.* **2020**, *8*, 4407.
[22] Y. Xiong, Y. Wang, J. Zhou, F. Liu, F. Hao, Z. Fan, *Adv. Mater.* **2023**, 2304021.
[23] R. Li, K. Xiang, Z. Liu, Z. Peng, Y. Zou, S. Wang, *Adv. Funct. Mater.* **2022**, *32*, 2208212.
[24] N. K. Ojha, G. V. Zyryanov, A. Majee, V. N. Charushin, O. N. Chupakhin, S. Santra, *Coord. Chem. Rev.* **2017**, *353*, 1.
[25] W. Zhang, C. Huang, Q. Xiao, L. Yu, L. Shuai, P. An, J. Zhang, M. Qiu, Z. Ren, Y. Yu, *J. Am. Chem. Soc.* **2020**, *142*, 11417.
[26] X. Liu, H. Zheng, Z. Sun, A. Han, P. Du, *ACS Catal.* **2015**, *5*, 1530.
[27] E. Skúlason, V. Tripkovic, M. E. Björketun, S. Gudmundsdóttir, G. Karlberg, J. Rossmeisl, T. Bligaard, H. Jónsson, J. K. Nørskov, *J. Phys. Chem. C* **2010**, *114*, 18182.
[28] S. E. Allen, R. R. Walvoord, R. Padilla-Salinas, M. C. Kozlowski, *Chem. Rev.* **2013**, *113*, 6234.
[29] D. Wang, D. Astruc, *Chem. Soc. Rev.* **2017**, *46*, 816.
[30] H. Wang, G. Zhan, C. Tang, D. Yang, W. Liu, D. Wang, Y. Wu, H. Wang, K. Liu, J. Li, M. Huang, K. Chen, *ACS Nano* **2023**, *17*, 4790.
[31] Y. Zhai, P. Han, Q. Yun, Y. Ge, X. Zhang, Y. Chen, H. Zhang, *eScience* **2022**, *2*, 467.
[32] C. Xiao, B-A. Lu, P. Xue, N. Tian, Z.-Y. Zhou, X. Lin, W.-F. Lin, S.-G. Sun, *Joule* **2020**, *4*, 2562.
[33] H. Luo, B. Li, J.-G. Ma, P. Cheng, *Angew. Chem., Int. Ed.* **2022**, *61*, e202116736.
[34] J. S. Elias, K. A. Stoerzinger, W. T. Hong, M. Risch, L. Giordano, A. N. Mansour, Y. Shao-Horn, *ACS Catal.* **2017**, *7*, 6843.
[35] M. Ma, K. Djanashvili, W. A. Smith, *Angew. Chem., Int. Ed.* **2016**, *55*, 6680.
[36] Z. Zhang, H. Che, Y. Wang, X. She, J. Sun, P. Gunawan, Z. Zhong, F. Su, *ACS Appl. Mater. Interfaces* **2012**, *4*, 1295.
[37] Y. Gao, Q. Wu, X. Liang, Z. Wang, Z. Zheng, P. Wang, Y. Liu, Y. Dai, M.-H. Whangbo, B. Huang, *Adv. Sci.* **2020**, *7*, 1902820.
[38] B.-H. Lee, S. Park, M. Kim, A. K. Sinha, S. C. Lee, E. Jung, W. J. Chang, K.-S. Lee, J. H. Kim, S.-P. Cho, H. Kim, K. T. Nam, T. Hyeon, *Nat. Mater.* **2019**, *18*, 620.
[39] B. Ya, Y. Xu, L. Meng, B. Zhou, J. Zhao, X. Chen, X. Zhang, *Materials* **2022**, *15*, 6488.
[40] Z. Yang, B. Chen, W. Chen, Y. Qu, F. Zhou, C. Zhao, Q. Xu, Q. Zhang, X. Duan, Y. Wu, *Nat. Commun.* **2019**, *10*, 3734.
[41] Z. Gu, H. Shen, Z. Chen, Y. Yang, C. Yang, Y. Ji, Y. Wang, C. Zhu, J. Liu, J. Li, T.-K. Sham, X. Xu, G. Zheng, *Joule* **2021**, *5*, 429.
[42] Y. Wu, C. Liu, C. Wang, Y. Yu, Y. Shi, B. Zhang, *Nat. Commun.* **2021**, *12*, 3881.
[43] S. Ma, M. Sadakiyo, M. Heima, R. Luo, R. T. Haasch, J. I. Gold, M. Yamauchi, P. J. A. Kenis, *J. Am. Chem. Soc.* **2017**, *139*, 47.
[44] Z. Ren, S. Wang, J. Yu, F. Mao, K. Wang, H. Wu, *Chem. Eng. J.* **2023**, *470*, 144107.
[45] B. Li, C. Lai, M. Zhang, G. Zeng, S. Liu, D. Huang, L. Qin, X. Liu, H. Yi, F. Xu, N. An, L. Chen, *Adv. Energy Mater.* **2020**, *10*, 2000177.
[46] A. Wang, J. Li, T. Zhang, *Nat. Rev. Chem.* **2018**, *2*, 65.
[47] Y. Chen, S. Ji, C. Chen, Q. Peng, D. Wang, Y. Li, *Joule* **2018**, *2*, 1242.
[48] R. T. Hannagan, G. Giannakakis, M. Flytzani-Stephanopoulos, E. C. H. Sykes, *Chem. Rev.* **2020**, *120*, 12044.
[49] C. Zhu, S. Fu, Q. Shi, D. Du, Y. Lin, *Angew. Chem., Int. Ed.* **2017**, *56*, 13944.
[50] W. Li, D. Wang, Y. Zhang, L. Tao, T. Wang, Y. Zou, Y. Wang, R. Chen, S. Wang, *Adv. Mater.* **2020**, *32*, 1907879.
[51] X. Yan, L. Zhuang, Z. Zhu, X. Yao, *Nanoscale* **2021**, *13*, 3327.
[52] A. Zhang, Y. Liang, H. Zhang, Z. Geng, J. Zeng, *Chem. Soc. Rev.* **2021**, *50*, 9817.
[53] C. Yang, Y. Gao, T. Ma, M. Bai, C. He, X. Ren, X. Luo, C. Wu, S. Li, C. Cheng, *Adv. Mater.* **2023**, 2301836.
[54] C. Li, Y. Liu, Z. Zhuo, H. Ju, D. Li, Y. Guo, X. Wu, H. Li, T. Zhai, *Adv. Energy Mater.* **2018**, *8*, 1801775.
[55] X. Li, Q. Liu, J. Wang, D. Meng, Y. Shu, X. Lv, B. Zhao, H. Yang, T. Cheng, Q. Gao, L. Li, H. B. Wu, *Chem* **2022**, *8*, 2148.
[56] W.-J. Sun, H.-Q. Ji, L.-X. Li, H-Y. Zhang, Z.-K. Wang, J.-H. He, J.-M. Lu, *Angew. Chem., Int. Ed.* **2021**, *60*, 22933.
[57] D. Yao, C. Tang, X. Zhi, B. Johannessen, A. Slattery, S. Chern, S.-Z. Qiao, *Adv. Mater.* **2023**, *35*, 2209386.
[58] X. Zhou, J. Shan, L. Chen, B. Y. Xia, T. Ling, J. Duan, Y. Jiao, Y. Zheng, S.-Z. Qiao, *J. Am. Chem. Soc.* **2022**, *144*, 2079.
[59] Y. Jiang, J. Shan, P. Wang, L. Huang, Y. Zheng, S.-Z. Qiao, *ACS Catal.* **2023**, *13*, 3101.
[60] A. Vasileff, X. Zhi, C. Xu, L. Ge, Y. Jiao, Y. Zheng, S.-Z. Qiao, *ACS Catal.* **2019**, *9*, 9411.
[61] H. Shen, H. Jin, H. Li, H. Wang, J. Duan, Y. Jiao, S.-Z. Qiao, *Nat. Commun.* **2023**, *14*, 2843.
[62] M. Zheng, P. Wang, X. Zhi, K. Yang, Y. Jiao, J. Duan, Y. Zheng, S.-Z. Qiao, *J. Am. Chem. Soc.* **2022**, *144*, 14936.
[63] X. Zhou, J. Dong, Y. Zhu, L. Liu, Y. Jiao, H. Li, Y. Han, K. Davey, Q. Xu, Y. Zheng, S.-Z. Qiao, *J. Am. Chem. Soc.* **2021**, *143*, 6681.
[64] P. Wang, H. Yang, C. Tang, Y. Wu, Y. Zheng, T. Cheng, K. Davey, X. Huang, S.-Z. Qiao, *Nat. Commun.* **2022**, *13*, 3754.
[65] O. S. Bushuyev, P. De Luna, C. T. Dinh, L. Tao, G. Saur, J. Van De Lagemaat, S. O. Kelley, E. H. Sargent, *Joule* **2018**, *2*, 825.
[66] H. Xie, T. Wang, J. Liang, Q. Li, S. Sun, *Nano Today* **2018**, *21*, 41.

© 2024 The Authors. Advanced Materials published by Wiley-VCH GmbH

15214095, 2024, 14, Downloaded from https://advanced.onlinelibrary.wiley.com/doi/10.1002/adma.202307913 by Cochrane Chile, Wiley Online Library on [30/09/2026]. See the Terms and Conditions (https://onlinelibrary.wiley.com/terms-and-conditions) on Wiley Online Library for rules of use; OA articles are governed by the applicable Creative Commons License

[67] A. R. Woldu, Z. Huang, P. Zhao, L. Hu, D. Astruc, *Coord. Chem. Rev.* **2022**, *454*, 214340.
[68] J. Yu, J. Wang, Y. Ma, J. Zhou, Y. Wang, P. Lu, J. Yin, R. Ye, Z. Zhu, Z. Fan, *Adv. Funct. Mater.* **2021**, *31*, 2102151.
[69] Y. Zheng, A. Vasileff, X. Zhou, Y. Jiao, M. Jaroniec, S.-Z. Qiao, *J. Am. Chem. Soc.* **2019**, *141*, 7646.
[70] Y. Wang, J. Liu, G. Zheng, *Adv. Mater.* **2021**, *33*, 2005798.
[71] D. Gao, R. M. Arán-Ais, H. S. Jeon, B. Roldan Cuenya, *Nat. Catal.* **2019**, *2*, 198.
[72] S. Popovic, M. Smiljanic, P. Jovanovic, J. Vavra, R. Buonsanti, N. Hodnik, *Angew. Chem., Int. Ed.* **2020**, *59*, 14736.
[73] H. Yu, J. Wan, M. Goodsite, H. Jin, *One Earth* **2023**, *6*, 267.
[74] C.-T. Dinh, T. Burdyny, M. G. Kibria, A. Seifitokaldani, C. M. Gabardo, F. P. García De Arquer, A. Kiani, J. P. Edwards, P. De Luna, O. S. Bushuyev, C. Zou, R. Quintero-Bermudez, Y. Pang, D. Sinton, E. H. Sargent, *Science* **2018**, *360*, 783.
[75] J. Kim, W. Choi, J. W. Park, C. Kim, M. Kim, H. Song, *J. Am. Chem. Soc.* **2019**, *141*, 6986.
[76] Y. Wang, D. Wang, C. J. Dares, S. L. Marquard, M. V. Sheridan, T. J. Meyer, *Proc. Natl. Acad. Sci. USA* **2018**, *115*, 278.
[77] X.-F. Qiu, J.-R. Huang, C. Yu, Z.-H. Zhao, H.-L. Zhu, Z. Ke, P.-Q. Liao, X.-M. Chen, *Angew. Chem., Int. Ed.* **2022**, *61*, e202206470.
[78] C. Kim, K. M. Cho, K. Park, J. Y. Kim, G.-T. Yun, F. M. Toma, I. Gereige, H.-T. Jung, *Adv. Funct. Mater.* **2021**, *31*, 2102142.
[79] C. Chen, X. Yan, S. Liu, Y. Wu, Q. Wan, X. Sun, Q. Zhu, H. Liu, J. Ma, L. Zheng, H. Wu, B. Han, *Angew. Chem., Int. Ed.* **2020**, *59*, 16459.
[80] S. Gonglach, S. Paul, M. Haas, F. Pillwein, S. S. Sreejith, S. Barman, R. De, S. Müllegger, P. Gerschel, U.-P. Apfel, H. Coskun, A. Aljabour, P. Stadler, W. Schöfberger, S. Roy, *Nat. Commun.* **2019**, *10*, 3864.
[81] F. Li, Y. C. Li, Z. Wang, J. Li, D.-H. Nam, Y. Lum, M. Luo, X. Wang, A. Ozden, S-F. Hung, B. Chen, Y. Wang, J. Wicks, Y. Xu, Y. Li, C. M. Gabardo, C.-T. Dinh, Y. Wang, T.-T. Zhuang, D. Sinton, E. H. Sargent, *Nat. Catal.* **2020**, *3*, 75.
[82] M. Luo, Z. Wang, Y. C. Li, J. Li, F. Li, Y. Lum, D.-H. Nam, B. Chen, J. Wicks, A. Xu, T. Zhuang, W. R. Leow, X. Wang, C.-T. Dinh, Y. Wang, Y. Wang, D. Sinton, E. H. Sargent, *Nat. Commun.* **2019**, *10*, 5814.
[83] X. Lv, L. Shang, S. Zhou, S. Li, Y. Wang, Z. Wang, T.-K. Sham, C. Peng, G. Zheng, *Adv. Energy Mater.* **2020**, *10*, 2001987.
[84] X. Su, Z. Jiang, J. Zhou, H. Liu, D. Zhou, H. Shang, X. Ni, Z. Peng, F. Yang, W. Chen, Z. Qi, D. Wang, Y. Wang, *Nat. Commun.* **2022**, *13*, 1322.
[85] X. Wang, Z. Wang, F. P. García De Arquer, C.-T. Dinh, A. Ozden, Y. C. Li, D.-H. Nam, J. Li, Y.-S. Liu, J. Wicks, Z. Chen, M. Chi, B. Chen, Y. Wang, J. Tam, J. Y. Howe, A. Proppe, P. Todorovic, F. Li, T.-T. Zhuang, C. M. Gabardo, A. R. Kirmani, C. Mccallum, S-F. Hung, Y. Lum, M. Luo, Y. Min, A. Xu, C. P. O'brien, B. Stephen, et al., *Nat. Energy* **2020**, *5*, 478.
[86] H. Xu, D. Rebollar, H. He, L. Chong, Y. Liu, C. Liu, C.-J. Sun, T. Li, J. V. Muntean, R. E. Winans, D.-J. Liu, T. Xu, *Nat. Energy* **2020**, *5*, 623.
[87] B. Yang, L. Chen, S. Xue, H. Sun, K. Feng, Y. Chen, X. Zhang, L. Xiao, Y. Qin, J. Zhong, Z. Deng, Y. Jiao, Y. Peng, *Nat. Commun.* **2022**, *13*, 5122.
[88] T. Zhang, B. Yuan, W. Wang, J. He, X. Xiang, *Angew. Chem., Int. Ed.* **2023**, *62*, e202302096.
[89] Y. Y. Birdja, E. Pérez-Gallent, M. C. Figueiredo, A. J. Göttle, F. Calle-Vallejo, M. T. M. Koper, *Nat. Energy* **2019**, *4*, 732.
[90] C. Peng, S. Yang, G. Luo, S. Yan, M. Shakouri, J. Zhang, Y. Chen, W. Li, Z. Wang, T.-K. Sham, G. Zheng, *Adv. Mater.* **2022**, *34*, 2204476.
[91] C. Guo, Y. Guo, Y. Shi, X. Lan, Y. Wang, Y. Yu, B. Zhang, *Angew. Chem., Int. Ed.* **2022**, *61*, e202205909.
[92] C. Peng, G. Luo, J. Zhang, M. Chen, Z. Wang, T.-K. Sham, L. Zhang, Y. Li, G. Zheng, *Nat. Commun.* **2021**, *12*, 1580.
[93] K. P. Kuhl, E. R. Cave, D. N. Abram, T. F. Jaramillo, *Energy Environ. Sci.* **2012**, *5*, 7050.
[94] K. Zhao, X. Nie, H. Wang, S. Chen, X. Quan, H. Yu, W. Choi, G. Zhang, B. Kim, J. G. Chen, *Nat. Commun.* **2020**, *11*, 2455.
[95] K. Qi, Y. Zhang, N. Onofrio, E. Petit, X. Cui, J. Ma, J. Fan, H. Wu, W. Wang, J. Li, J. Liu, Y. Zhang, Y. Wang, G. Jia, J. Wu, L. Lajaunie, C. Salameh, D. Voiry, *Nat. Catal.* **2023**, *6*, 319.
[96] J. Gao, A. Bahmanpour, O. Kröcher, S. M. Zakeeruddin, D. Ren, M. Grätzel, *Nat. Chem.* **2023**, *15*, 705.
[97] Y. Lum, J. W. Ager, *Nat. Catal.* **2019**, *2*, 86.
[98] R. M. Arán-Ais, R. Rizo, P. Grosse, G. Algara-Siller, K. Dembélé, M. Plodinec, T. Lunkenbein, S. W. Chee, B. R. Cuenya, *Nat. Commun.* **2020**, *11*, 3489.
[99] B. Zhang, J. Zhang, M. Hua, Q. Wan, Z. Su, X. Tan, L. Liu, F. Zhang, G. Chen, D. Tan, X. Cheng, B. Han, L. Zheng, G. Mo, *J. Am. Chem. Soc.* **2020**, *142*, 13606.
[100] H. Mistry, A. S. Varela, C. S. Bonifacio, I. Zegkinoglou, I. Sinev, Y.-W. Choi, K. Kisslinger, E. A. Stach, J. C. Yang, P. Strasser, B. R. Cuenya, *Nat. Commun.* **2016**, *7*, 12123.
[101] Q. Lei, H. Zhu, K. Song, N. Wei, L. Liu, D. Zhang, J. Yin, X. Dong, K. Yao, N. Wang, X. Li, B. Davaasuren, J. Wang, Y. Han, *J. Am. Chem. Soc.* **2020**, *142*, 4213.
[102] P. De Luna, R. Quintero-Bermudez, C.-T. Dinh, M. B. Ross, O. S. Bushuyev, P. Todorovic, T. Regier, S. O. Kelley, P. Yang, E. H. Sargent, *Nat. Catal.* **2018**, *1*, 103.
[103] Y. Jiang, X. Wang, D. Duan, C. He, J. Ma, W. Zhang, H. Liu, R. Long, Z. Li, T. Kong, X. J. Loh, L. Song, E. Ye, Y. Xiong, *Adv. Sci.* **2022**, *9*, 2105292.
[104] P.-P. Yang, X.-L. Zhang, F.-Y. Gao, Y.-R. Zheng, Z.-Z. Niu, X. Yu, R. Liu, Z.-Z. Wu, S. Qin, L.-P. Chi, Y. Duan, T. Ma, X.-S. Zheng, J-F. Zhu, H.-J. Wang, M.-R. Gao, S.-H. Yu, *J. Am. Chem. Soc.* **2020**, *142*, 6400.
[105] Y. Wang, Z. Wang, C.-T. Dinh, J. Li, A. Ozden, M. Golam Kibria, A. Seifitokaldani, C.-S. Tan, C. M. Gabardo, M. Luo, H. Zhou, F. Li, Y. Lum, C. Mccallum, Y. Xu, M. Liu, A. Proppe, A. Johnston, P. Todorovic, T.-T. Zhuang, D. Sinton, S. O. Kelley, E. H. Sargent, *Nat. Catal.* **2020**, *3*, 98.
[106] X. Wang, K. Klingan, M. Klingenhof, T. Möller, J. Ferreira De Araújo, I. Martens, A. Bagger, S. Jiang, J. Rossmeisl, H. Dau, P. Strasser, *Nat. Commun.* **2021**, *12*, 794.
[107] K. Jiang, R. B. Sandberg, A. J. Akey, X. Liu, D. C. Bell, J. K. Nørskov, K. Chan, H. Wang, *Nat. Catal.* **2018**, *1*, 111.
[108] J.-J. Lv, M. Jouny, W. Luc, W. Zhu, J.-J. Zhu, F. Jiao, *Adv. Mater.* **2018**, *30*, 1803111.
[109] D. Cheng, Z.-J. Zhao, G. Zhang, P. Yang, L. Li, H. Gao, S. Liu, X. Chang, S. Chen, T. Wang, G. A. Ozin, Z. Liu, J. Gong, *Nat. Commun.* **2021**, *12*, 395.
[110] Z.-Q. Liang, T.-T. Zhuang, A. Seifitokaldani, J. Li, C.-W. Huang, C.-S. Tan, Y. Li, P. De Luna, C. T. Dinh, Y. Hu, Q. Xiao, P.-L. Hsieh, Y. Wang, F. Li, R. Quintero-Bermudez, Y. Zhou, P. Chen, Y. Pang, S.-C. Lo, L.-J. Chen, H. Tan, Z. Xu, S. Zhao, D. Sinton, E. H. Sargent, *Nat. Commun.* **2018**, *9*, 3828.
[111] Y. Zhou, F. Che, M. Liu, C. Zou, Z. Liang, P. De Luna, H. Yuan, J. Li, Z. Wang, H. Xie, H. Li, P. Chen, E. Bladt, R. Quintero-Bermudez, T.-K. Sham, S. Bals, J. Hofkens, D. Sinton, G. Chen, E. H. Sargent, *Nat. Chem.* **2018**, *10*, 974.
[112] J.-Y. Kim, D. Hong, J.-C. Lee, H. G. Kim, S. Lee, S. Shin, B. Kim, H. Lee, M. Kim, J. Oh, G-D. Lee, D.-H. Nam, Y.-C. Joo, *Nat. Commun.* **2021**, *12*, 3765.
[113] H. Li, T. Liu, P. Wei, L. Lin, D. Gao, G. Wang, X. Bao, *Angew. Chem., Int. Ed.* **2021**, *60*, 14329.
[114] W. Ma, S. Xie, T. Liu, Q. Fan, J. Ye, F. Sun, Z. Jiang, Q. Zhang, J. Cheng, Y. Wang, *Nat. Catal.* **2020**, *3*, 478.
[115] T. Kim, G. T. R. Palmore, *Nat. Commun.* **2020**, *11*, 3622.
[116] Y.-F. Lu, L.-Z. Dong, J. Liu, R.-X. Yang, J.-J. Liu, Y. Zhang, L. Zhang, Y.-R. Wang, S-L. Li, Y.-Q. Lan, *Angew. Chem., Int. Ed.* **2021**, *60*, 26210.

© 2024 The Authors. Advanced Materials published by Wiley-VCH GmbH

15214095, 2024, 14, Downloaded from https://advanced.onlinelibrary.wiley.com/doi/10.1002/adma.202307913 by Cochrane Chile, Wiley Online Library on [30/09/2026]. See the Terms and Conditions (https://onlinelibrary.wiley.com/terms-and-conditions) on Wiley Online Library for rules of use; OA articles are governed by the applicable Creative Commons License

[117] Y. Xie, P. Ou, X. Wang, Z. Xu, Y. C. Li, Z. Wang, J. E. Huang, J. Wicks, C. Mccallum, N. Wang, Y. Wang, T. Chen, B. T. W. Lo, D. Sinton, J. C. Yu, Y. Wang, E. H. Sargent, *Nat. Catal.* **2022**, *5*, 564.
[118] P. Wang, H. Yang, Y. Xu, X. Huang, J. Wang, M. Zhong, T. Cheng, Q. Shao, *ACS Nano* **2021**, *15*, 1039.
[119] E. L. Clark, C. Hahn, T. F. Jaramillo, A. T. Bell, *J. Am. Chem. Soc.* **2017**, *139*, 15848.
[120] M. Zhong, K. Tran, Y. Min, C. Wang, Z. Wang, C.-T. Dinh, P. De Luna, Z. Yu, A. S. Rasouli, P. Brodersen, S. Sun, O. Voznyy, C.-S. Tan, M. Askerka, F. Che, M. Liu, A. Seifitokaldani, Y. Pang, S.-C. Lo, A. Ip, Z. Ulissi, E. H. Sargent, *Nature* **2020**, *581*, 178.
[121] Y. Chen, Z. Fan, J. Wang, C. Ling, W. Niu, Z. Huang, G. Liu, B. Chen, Z. Lai, X. Liu, B. Li, Y. Zong, L. Gu, J. Wang, X. Wang, H. Zhang, *J. Am. Chem. Soc.* **2020**, *142*, 12760.
[122] F. Hu, L. Yang, Y. Jiang, C. Duan, X. Wang, L. Zeng, X. Lv, D. Duan, Q. Liu, T. Kong, J. Jiang, R. Long, Y. Xiong, *Angew. Chem., Int. Ed.* **2021**, *60*, 26122.
[123] G. Lee, Y. C. Li, J.-Y. Kim, T. Peng, D.-H. Nam, A. Sedighian Rasouli, F. Li, M. Luo, A. H. Ip, Y.-C. Joo, E. H. Sargent, *Nat. Energy* **2021**, *6*, 46.
[124] X. Wei, Z. Yin, K. Lyu, Z. Li, J. Gong, G. Wang, L. Xiao, J. Lu, L. Zhuang, *ACS Catal.* **2020**, *10*, 4103.
[125] X. Chen, J. Chen, N. M. Alghoraibi, D. A. Henckel, R. Zhang, U. O. Nwabara, K. E. Madsen, P. J. A. Kenis, S. C. Zimmerman, A. A. Gewirth, *Nat. Catal.* **2021**, *4*, 20.
[126] G-Y. Duan, X.-Q. Li, G.-R. Ding, L.-J. Han, B.-H. Xu, S.-J. Zhang, *Angew. Chem., Int. Ed.* **2022**, *61*, e202110657.
[127] D.-H. Nam, P. De Luna, A. Rosas-Hernández, A. Thevenon, F. Li, T. Agapie, J. C. Peters, O. Shekhah, M. Eddaoudi, E. H. Sargent, *Nat. Mater.* **2020**, *19*, 266.
[128] F. Li, A. Thevenon, A. Rosas-Hernández, Z. Wang, Y. Li, C. M. Gabardo, A. Ozden, C. T. Dinh, J. Li, Y. Wang, J. P. Edwards, Y. Xu, C. Mccallum, L. Tao, Z.-Q. Liang, M. Luo, X. Wang, H. Li, C. P. O'brien, C.-S. Tan, D.-H. Nam, R. Quintero-Bermudez, T.-T. Zhuang, Y. C. Li, Z. Han, R. D. Britt, D. Sinton, T. Agapie, J. C. Peters, E. H. Sargent, *Nature* **2020**, *577*, 509.
[129] H.-L. Zhu, H.-Y. Chen, Y.-X. Han, Z.-H. Zhao, P.-Q. Liao, X.-M. Chen, *J. Am. Chem. Soc.* **2022**, *144*, 13319.
[130] Y. Jiao, Y. Zheng, P. Chen, M. Jaroniec, S.-Z. Qiao, *J. Am. Chem. Soc.* **2017**, *139*, 18093.
[131] C. F. Wen, M. Zhou, P. F. Liu, Y. Liu, X. Wu, F. Mao, S. Dai, B. Xu, X. L. Wang, Z. Jiang, P. Hu, S. Yang, H. F. Wang, H. G. Yang, *Angew. Chem., Int. Ed.* **2022**, *61*, e202111700.
[132] A. Thevenon, A. Rosas-Hernández, J. C. Peters, T. Agapie, *Angew. Chem., Int. Ed.* **2019**, *58*, 16952.
[133] D. Wakerley, S. Lamaison, F. Ozanam, N. Menguy, D. Mercier, P. Marcus, M. Fontecave, V. Mougel, *Nat. Mater.* **2019**, *18*, 1222.
[134] Q. Zhu, X. Sun, D. Yang, J. Ma, X. Kang, L. Zheng, J. Zhang, Z. Wu, B. Han, *Nat. Commun.* **2019**, *10*, 3851.
[135] J. Gao, H. Zhang, X. Guo, J. Luo, S. M. Zakeeruddin, D. Ren, M. Grätzel, *J. Am. Chem. Soc.* **2019**, *141*, 18704.
[136] A. Ozden, Y. Wang, F. Li, M. Luo, J. Sisler, A. Thevenon, A. Rosas-Hernández, T. Burdyny, Y. Lum, H. Yadegari, T. Agapie, J. C. Peters, E. H. Sargent, D. Sinton, *Joule* **2021**, *5*, 706.
[137] Y. Ji, Z. Chen, R. Wei, C. Yang, Y. Wang, J. Xu, H. Zhang, A. Guan, J. Chen, T.-K. Sham, J. Luo, Y. Yang, X. Xu, G. Zheng, *Nat. Catal.* **2022**, *5*, 251.
[138] A. Ozden, F. P. García De Arquer, J. E. Huang, J. Wicks, J. Sisler, R. K. Miao, C. P. O'brien, G. Lee, X. Wang, A. H. Ip, E. H. Sargent, D. Sinton, *Nat. Sustainability* **2022**, *5*, 563.
[139] X. Fu, J. Zhang, Y. Kang, *React. Chem. Eng.* **2021**, *6*, 612.
[140] P. B. O'mara, P. Wilde, T. M. Benedetti, C. Andronescu, S. Cheong, J. J. Gooding, R. D. Tilley, W. Schuhmann, *J. Am. Chem. Soc.* **2019**, *141*, 14093.
[141] Gurudayal, D. Perone, S. Malani, Y. Lum, S. Haussener, J. W. Ager, *ACS Appl. Energy Mater.* **2019**, *2*, 4551.
[142] C. G. Morales-Guio, E. R. Cave, S. A. Nitopi, J. T. Feaster, L. Wang, K. P. Kuhl, A. Jackson, N. C. Johnson, D. N. Abram, T. Hatsukade, C. Hahn, T. F. Jaramillo, *Nat. Catal.* **2018**, *1*, 764.
[143] J. Sisler, S. Khan, A. H. Ip, M. W. Schreiber, S. A. Jaffer, E. R. Bobicki, C.-T. Dinh, E. H. Sargent, *ACS Energy Lett.* **2021**, *6*, 997.
[144] N. S. Romero Cuellar, C. Scherer, B. Kaçkar, W. Eisenreich, C. Huber, K. Wiesner-Fleischer, M. Fleischer, O. Hinrichsen, *J. CO2 Util.* **2020**, *36*, 263.
[145] N. Theaker, J. M. Strain, B. Kumar, J. P. Brian, S. Kumari, J. M. Spurgeon, *Electrochim. Acta* **2018**, *274*, 1.
[146] D. S. Ripatti, T. R. Veltman, M. W. Kanan, *Joule* **2019**, *3*, 240.
[147] M. Jouny, G. S. Hutchings, F. Jiao, *Nat. Catal.* **2019**, *2*, 1062.
[148] Y. Pang, J. Li, Z. Wang, C.-S. Tan, P.-L. Hsieh, T.-T. Zhuang, Z.-Q. Liang, C. Zou, X. Wang, P. De Luna, J. P. Edwards, Y. Xu, F. Li, C.-T. Dinh, M. Zhong, Y. Lou, D. Wu, L.-J. Chen, E. H. Sargent, D. Sinton, *Nat. Catal.* **2019**, *2*, 251.
[149] X. Wang, Z. Wang, T.-T. Zhuang, C.-T. Dinh, J. Li, D.-H. Nam, F. Li, C.-W. Huang, C.-S. Tan, Z. Chen, M. Chi, C. M. Gabardo, A. Seifitokaldani, P. Todorovic, A. Proppe, Y. Pang, A. R. Kirmani, Y. Wang, A. H. Ip, L. J. Richter, B. Scheffel, A. Xu, S.-C. Lo, S. O. Kelley, D. Sinton, E. H. Sargent, *Nat. Commun.* **2019**, *10*, 5186.
[150] J. Lewis, US Patent 3837144, **1974**.
[151] Y. Chai, X. Han, W. Li, S. Liu, S. Yao, C. Wang, W. Shi, I. Da-Silva, P. Manuel, Y. Cheng, L. D. Daemen, A. J. Ramirez-Cuesta, C. C. Tang, L. Jiang, S. Yang, N. Guan, L. Li, *Science* **2020**, *368*, 1002.
[152] J. Li, Z. Cheng, Z. Wang, J. Dong, H. Jiang, W. Wang, X. Zou, G. Zhu, *Angew. Chem., Int. Ed.* **2023**, *62*, e202216675.
[153] X. Suo, X. Cui, L. Yang, N. Xu, Y. Huang, Y. He, S. Dai, H. Xing, *Adv. Mater.* **2020**, *32*, 1907601.
[154] H. Wang, Y. Liu, J. Li, *Adv. Mater.* **2020**, *32*, 2002603.
[155] J.-W. Wang, S.-C. Fan, H.-P. Li, X. Bu, Y.-Y. Xue, Q.-G. Zhai, *Angew. Chem., Int. Ed.* **2023**, *62*, e202217839.
[156] T. Xu, P. Zhang, F. Cui, J. Li, L. Kan, B. Tang, X. Zou, Y. Liu, G. Zhu, *Adv. Mater.* **2023**, *35*, 2204553.
[157] J. Bu, Z. Liu, W. Ma, L. Zhang, T. Wang, H. Zhang, Q. Zhang, X. Feng, J. Zhang, *Nat. Catal.* **2021**, *4*, 557.
[158] R. Shi, Z. Wang, Y. Zhao, G. I. N. Waterhouse, Z. Li, B. Zhang, Z. Sun, C. Xia, H. Wang, T. Zhang, *Nat. Catal.* **2021**, *4*, 565.
[159] S. Wang, K. Uwakwe, L. Yu, J. Ye, Y. Zhu, J. Hu, R. Chen, Z. Zhang, Z. Zhou, J. Li, Z. Xie, D. Deng, *Nat. Commun.* **2021**, *12*, 7072.
[160] W. Xue, X. Liu, C. Liu, X. Zhang, J. Li, Z. Yang, P. Cui, H.-J. Peng, Q. Jiang, H. Li, P. Xu, T. Zheng, C. Xia, J. Zeng, *Nat. Commun.* **2023**, *14*, 2137.
[161] B.-H. Zhao, F. Chen, M. Wang, C. Cheng, Y. Wu, C. Liu, Y. Yu, B. Zhang, *Nat. Sustainability* **2023**, *6*, 827.
[162] L. Zhang, Z. Chen, Z. Liu, J. Bu, W. Ma, C. Yan, R. Bai, J. Lin, Q. Zhang, J. Liu, T. Wang, J. Zhang, *Nat. Commun.* **2021**, *12*, 6574.
[163] J. Bu, S. Chang, J. Li, S. Yang, W. Ma, Z. Liu, S. An, Y. Wang, Z. Li, J. Zhang, *Nat. Commun.* **2023**, *14*, 1533.
[164] X. Xu, J. Ma, F. Wu, K. Zhu, H. Zhou, Y. Zhang, X. Li, Y. Zhou, G. Jia, D. Liu, P. Gao, W. Ye, *Inorg. Chem. Front.* **2022**, *9*, 3444.
[165] Y. Zhou, G. E. Klinger, E. L. Hegg, C. M. Saffron, J. E. Jackson, *J. Am. Chem. Soc.* **2020**, *142*, 4037.
[166] P. M. Cox, R. A. Betts, C. D. Jones, S. A. Spall, I. J. Totterdell, *Nature* **2000**, *408*, 184.
[167] A. Corma, S. Iborra, A. Velty, *Chem. Rev.* **2007**, *107*, 2411.
[168] J. Tan, M. Jiang, K. Yu, Y. Song, W. Zhang, Q. Gao, *Catal. Sci. Technol.* **2023**, *13*, 2899.
[169] A. Bohre, S. Dutta, B. Saha, M. M. Abu-Omar, *ACS Sustainable Chem. Eng.* **2015**, *3*, 1263.
[170] I. K. M. Yu, F. Deng, X. Chen, G. Cheng, Y. Liu, W. Zhang, J. A. Lercher, *Nat. Commun.* **2022**, *13*, 7154.

© 2024 The Authors. Advanced Materials published by Wiley-VCH GmbH

15214095, 2024, 14, Downloaded from https://advanced.onlinelibrary.wiley.com/doi/10.1002/adma.202307913 by Cochrane Chile, Wiley Online Library on [30/09/2026]. See the Terms and Conditions (https://onlinelibrary.wiley.com/terms-and-conditions) on Wiley Online Library for rules of use; OA articles are governed by the applicable Creative Commons License

[171] X. H. Chadderdon, D. J. Chadderdon, J. E. Matthiesen, Y. Qiu, J. M. Carraher, J.-P. Tessonnier, W. Li, *J. Am. Chem. Soc.* **2017**, *139*, 14120.
[172] P. Nilges, U. Schröder, *Energy Environ. Sci.* **2013**, *6*, 2925.
[173] S. Jung, E. J. Biddinger, *ACS Sustainable Chem. Eng.* **2016**, *4*, 6500.
[174] Y. Kwon, Y. Y. Birdja, S. Raoufmoghaddam, M. T. M. Koper, *ChemSusChem* **2015**, *8*, 1745.
[175] Z. Zhang, K. Huang, X. Qiu, W. Ge, X. Yang, Y. Zhu, C. Lian, H. Liu, H. Jiang, C. Li, *Fundam. Res.* **2022**, *3*, 763.
[176] Z. Yang, X. Chou, H. Kan, Z. Xiao, Y. Ding, *ACS Sustainable Chem. Eng.* **2022**, *10*, 7418.
[177] J. Li, N. Kornienko, *Chem. Commun.* **2021**, *57*, 5127.
[178] P. Chen, W. Zhang, J. Tan, Y. Yang, Y. Jia, Y. Tang, Q. Gao, *Catal. Sci. Technol.* **2022**, *12*, 4032.
[179] Z. Xia, Y. Li, J. Wu, Y.-C. Huang, W. Zhao, Y. Lu, Y. Pan, X. Yue, Y. Wang, C-L. Dong, S. Wang, Y. Zou, *Sci. China: Chem.* **2022**, *65*, 2588.
[180] W. Xu, C. Yu, J. Chen, Z. Liu, *Appl. Catal., B* **2022**, *305*, 121062.
[181] P. Zhou, L. Li, V. S. S. Mosali, Y. Chen, P. Luan, Q. Gu, D. R. Turner, L. Huang, J. Zhang, *Angew. Chem., Int. Ed.* **2022**, *61*, e202117809.
[182] R. J. Dixit, K. Bhattacharyya, V. K. Ramani, S. Basu, *Green Chem.* **2021**, *23*, 4201.
[183] K. Ji, M. Xu, S.-M. Xu, Y. Wang, R. Ge, X. Hu, X. Sun, H. Duan, *Angew. Chem., Int. Ed.* **2022**, *61*, e202209849.
[184] G. S. De Luna, A. Sacco, S. Hernandez, F. Ospitali, S. Albonetti, G. Fornasari, P. Benito, *ChemSusChem* **2022**, *15*, 202102504.
[185] G. Sanghez De Luna, P. H. Ho, A. Sacco, S. Hernández, J.-J. Velasco-Vélez, F. Ospitali, A. Paglianti, S. Albonetti, G. Fornasari, P. Benito, *ACS Appl. Mater. Interfaces* **2021**, *13*, 23675.
[186] Y. Zhong, R. Ren, Y. Peng, J. Wang, X. Ren, Q. Li, Y. Fan, *Mol. Catal.* **2022**, *528*, 112487.
[187] H. Li, T. Zhang, M. Peng, Q. Zhang, J. Liu, J. Zhang, Y. Fu, W. Li, *Int. J. Hydrog. Energ.* **2022**, *47*, 28904.
[188] J. J. Roylance, T. W. Kim, K.-S. Choi, *ACS Catal.* **2016**, *6*, 1840.
[189] J. Anibal, A. Malkani, B. Xu, *Catal. Sci. Technol.* **2020**, *10*, 3181.
[190] Y. Kwon, M. T. M. Koper, *ChemSusChem* **2013**, *6*, 455.
[191] N. Gruber, J. N. Galloway, *Nature* **2008**, *451*, 293.
[192] J. G. Chen, R. M. Crooks, L. C. Seefeldt, K. L. Bren, R. M. Bullock, M. Y. Darensbourg, P. L. Holland, B. Hoffman, M. J. Janik, A. K. Jones, M. G. Kanatzidis, P. King, K. M. Lancaster, S. V. Lymar, P. Pfromm, W. F. Schneider, R. R. Schrock, *Science* **2018**, *360*, eaar6611.
[193] X. Cui, C. Tang, Q. Zhang, *Adv. Energy Mater.* **2018**, *8*, 1800369.
[194] Z. Huang, M. Rafiq, A. R. Woldu, Q.-X. Tong, D. Astruc, L. Hu, *Coord. Chem. Rev.* **2023**, *478*, 214981.
[195] D. R. MacFarlane, P. V. Cherepanov, J. Choi, B. H. R. Suryanto, R. Y. Hodgetts, J. M. Bakker, F. M. Ferrero Vallana, A. N. Simonov, *Joule* **2020**, *4*, 1186.
[196] C. Guo, J. Ran, A. Vasileff, S.-Z. Qiao, *Energy Environ. Sci.* **2018**, *11*, 45.
[197] B. H. R. Suryanto, H.-L. Du, D. Wang, J. Chen, A. N. Simonov, D. R. MacFarlane, *Nat. Catal.* **2019**, *2*, 290.
[198] G. Qing, R. Ghazfar, S. T. Jackowski, F. Habibzadeh, M. M. Ashtiani, C.-P. Chen, M. R. Smith, T. W. Hamann, *Chem. Rev.* **2020**, *120*, 5437.
[199] D. Hao, Y. Liu, S. Gao, H. Arandiyan, X. Bai, Q. Kong, W. Wei, P. K. Shen, B.-J. Ni, *Mater. Today* **2021**, *46*, 212.
[200] P. Zhou, L. Jiang, F. Wang, K. Deng, K. Lv, Z. Zhang, *Sci. Adv.* **2017**, *3*, e1601945.
[201] M. A. Shipman, M. D. Symes, *Catal. Today* **2017**, *286*, 57.
[202] W. Guo, K. Zhang, Z. Liang, R. Zou, Q. Xu, *Chem. Soc. Rev.* **2019**, *48*, 5658.
[203] J. H. Montoya, C. Tsai, A. Vojvodic, J. K. Nørskov, *ChemSusChem* **2015**, *8*, 2180.
[204] J. Deng, J. A. Iñiguez, C. Liu, *Joule* **2018**, *2*, 846.
[205] D. Liu, M. Chen, X. Du, H. Ai, K. H. Lo, S. Wang, S. Chen, G. Xing, X. Wang, H. Pan, *Adv. Funct. Mater.* **2021**, *31*, 2008983.
[206] Y. Cheng, X. Li, P. Shen, Y. Guo, K. Chu, *Energy Environ. Mater.* **2023**, *6*, e12268.
[207] Y.-X. Lin, S.-N. Zhang, Z.-H. Xue, J.-J. Zhang, H. Su, T.-J. Zhao, G.-Y. Zhai, X.-H. Li, M. Antonietti, J.-S. Chen, *Nat. Commun.* **2019**, *10*, 4380.
[208] C. Li, S. Mou, X. Zhu, F. Wang, Y. Wang, Y. Qiao, X. Shi, Y. Luo, B. Zheng, Q. Li, X. Sun, *Chem. Commun.* **2019**, *55*, 14474.
[209] N. C. Kani, A. Prajapati, B. A. Collins, J. D. Goodpaster, M. R. Singh, *ACS Catal.* **2020**, *10*, 14592.
[210] C. Du, C. Qiu, Z. Fang, P. Li, Y. Gao, J. Wang, W. Chen, *Nano Energy* **2022**, *92*, 106784.
[211] H. S. Kim, J. Choi, J. Kong, H. Kim, S. J. Yoo, H. S. Park, *ACS Catal.* **2020**, *11*, 435.
[212] R. Zhao, Q. Geng, L. Chang, P. Wei, Y. Luo, X. Shi, A. M. Asiri, S. Lu, Z. Wang, X. Sun, *Chem. Commun.* **2020**, *56*, 9328.
[213] M.-M. Shi, D. Bao, S.-J. Li, B.-R. Wulan, J.-M. Yan, Q. Jiang, *Adv. Energy Mater.* **2018**, *8*, 1800124.
[214] C. Kim, J.-Y. Song, C. Choi, J. P. Ha, W. Lee, Y. T. Nam, D.-M. Lee, G. Kim, I. Gereige, W.-B. Jung, H. Lee, Y. Jung, H. Jeong, H.-T. Jung, *Adv. Mater.* **2022**, *34*, 2205270.
[215] X. Wang, S. Qiu, J. Feng, Y. Tong, F. Zhou, Q. Li, L. Song, S. Chen, K.-H. Wu, P. Su, S. Ye, F. Hou, S. X. Dou, H. K. Liu, G. Q. (Max) Lu, C. Sun, J. Liu, J. Liang, *Adv. Mater.* **2020**, *32*, 2004382.
[216] Y. Qu, T. Dai, Y. Cui, Y. Zhang, Z. Wang, Q. Jiang, *Chem. Eng. J.* **2022**, *433*, 133752.
[217] T. Wu, H. Zhao, X. Zhu, Z. Xing, Q. Liu, T. Liu, S. Gao, S. Lu, G. Chen, A. M. Asiri, Y. Zhang, X. Sun, *Adv. Mater.* **2020**, *32*, 2000299.
[218] W. Tong, B. Huang, P. Wang, L. Li, Q. Shao, X. Huang, *Angew. Chem., Int. Ed.* **2020**, *132*, 2671.
[219] L. Wen, K. Sun, X. Liu, W. Yang, L. Li, H.-L. Jiang, *Adv. Mater.* **2023**, *35*, 2210669.
[220] Z. Wang, X. Wu, J. Liu, D. Zhang, H. Zhao, X. Zhang, Y. Qin, N. Nie, D. Wang, J. Lai, L. Wang, *Nano Lett.* **2021**, *21*, 9580.
[221] F. Pang, Z. Wang, K. Zhang, J. He, W. Zhang, C. Guo, Y. Ding, *Nano Energy* **2019**, *58*, 834.
[222] W. Zang, T. Yang, H. Zou, S. Xi, H. Zhang, X. Liu, Z. Kou, Y. Du, Y. P. Feng, L. Shen, L. Duan, J. Wang, S. J. Pennycook, *ACS Catal.* **2019**, *9*, 10166.
[223] Z.-Q. Zhao, K. Li, J. Liu, J.-J. Mao, Y.-Q. Lin, *Small* **2023**, *19*, 2206626.
[224] L. Han, Z. Ren, P. Ou, H. Cheng, N. Rui, L. Lin, X. Liu, L. Zhuo, J. Song, J. Sun, J. Luo, H. L. Xin, *Angew. Chem., Int. Ed.* **2021**, *133*, 349.
[225] G.-F. Chen, Y. Yuan, H. Jiang, S-Y. Ren, L.-X. Ding, L. Ma, T. Wu, J. Lu, H. Wang, *Nat. Energy* **2020**, *5*, 605.
[226] T. Hu, C. Wang, M. Wang, C. M. Li, C. Guo, *ACS Catal.* **2021**, *11*, 14417.
[227] P. H. Van Langevelde, I. Katsounaros, M. T. M. Koper, *Joule* **2021**, *5*, 290.
[228] Z. Song, Y. Liu, Y. Zhong, Q. Guo, J. Zeng, Z. Geng, *Adv. Mater.* **2022**, *34*, 2204306.
[229] W. Wen, P. Yan, W. Sun, Y. Zhou, X.-Y. Yu, *Adv. Funct. Mater.* **2023**, *33*, 2212236.
[230] K. Wu, C. Sun, Z. Wang, Q. Song, X. Bai, X. Yu, Q. Li, Z. Wang, H. Zhang, J. Zhang, X. Tong, Y. Liang, A. Khosla, Z. Zhao, *ACS Mater. Lett.* **2022**, *4*, 650.
[231] Y. Wang, W. Zhou, R. Jia, Y. Yu, B. Zhang, *Angew. Chem., Int. Ed.* **2020**, *59*, 5350.
[232] Q. Hu, Y. Qin, X. Wang, Z. Wang, X. Huang, H. Zheng, K. Gao, H. Yang, P. Zhang, M. Shao, C. He, *Energy Environ. Sci.* **2021**, *14*, 4989.
[233] Y. Zhang, Y. Wang, L. Han, S. Wang, T. Cui, Y. Yan, M. Xu, H. Duan, Y. Kuang, X. Sun, *Angew. Chem., Int. Ed.* **2023**, *62*, e202213711.
[234] J-Y. Fang, Q.-Z. Zheng, Y.-Y. Lou, K.-M. Zhao, S.-N. Hu, G. Li, O. Akdim, X.-Y. Huang, S.-G. Sun, *Nat. Commun.* **2022**, *13*, 7899.

© 2024 The Authors. Advanced Materials published by Wiley-VCH GmbH

15214095, 2024, 14, Downloaded from https://advanced.onlinelibrary.wiley.com/doi/10.1002/adma.202307913 by Cochrane Chile, Wiley Online Library on [30/09/2026]. See the Terms and Conditions (https://onlinelibrary.wiley.com/terms-and-conditions) on Wiley Online Library for rules of use; OA articles are governed by the applicable Creative Commons License

[235] Y. Wang, A. Xu, Z. Wang, L. Huang, J. Li, F. Li, J. Wicks, M. Luo, D.-H. Nam, C.-S. Tan, Y. Ding, J. Wu, Y. Lum, C.-T. Dinh, D. Sinton, G. Zheng, E. H. Sargent, *J. Am. Chem. Soc.* **2020**, *142*, 5702.
[236] H. Yin, Z. Chen, S. Xiong, J. Chen, C. Wang, R. Wang, Y. Kuwahara, J. Luo, H. Yamashita, Y. Peng, J. Li, *Chem Catal* **2021**, *1*, 1088.
[237] W. Gao, K. Xie, J. Xie, X. Wang, H. Zhang, S. Chen, H. Wang, Z. Li, C. Li, *Adv. Mater.* **2023**, *35*, 2202952.
[238] Q. Gao, H. S. Pillai, Y. Huang, S. Liu, Q. Mu, X. Han, Z. Yan, H. Zhou, Q. He, H. Xin, H. Zhu, *Nat. Commun.* **2022**, *13*, 2338.
[239] H. Xu, J. Chen, Z. Zhang, C-T. Hung, J. Yang, W. Li, *Adv. Mater.* **2023**, *35*, 2207522.
[240] F.-Y. Chen, Z-Y. Wu, S. Gupta, D. J. Rivera, S. V. Lambeets, S. Pecaut, J. Y. T. Kim, P. Zhu, Y. Z. Finfrock, D. M. Meira, G. King, G. Gao, W. Xu, D. A. Cullen, H. Zhou, Y. Han, D. E. Perea, C. L. Muhich, H. Wang, *Nat. Nanotechnol.* **2022**, *17*, 759.
[241] H. Liu, X. Lang, C. Zhu, J. Timoshenko, M. Rüscher, L. Bai, N. Guijarro, H. Yin, Y. Peng, J. Li, Z. Liu, W. Wang, B. R. Cuenya, J. Luo, *Angew. Chem., Int. Ed.* **2022**, *134*, e202202556.
[242] X.-F. Cheng, J.-H. He, H.-Q. Ji, H-Y. Zhang, Q. Cao, W.-J. Sun, C.-L. Yan, J.-M. Lu, *Adv. Mater.* **2022**, *34*, 2205767.
[243] T. Xiang, Y. Liang, Y. Zeng, J. Deng, J. Yuan, W. Xiong, B. Song, C. Zhou, Y. Yang, *Small* **2023**, *19*, 2303732.
[244] Y. Xue, Q. Yu, Q. Ma, Y. Chen, C. Zhang, W. Teng, J. Fan, W.-X. Zhang, *Environ. Sci. Technol.* **2022**, *56*, 14797.
[245] J. Yang, H. Qi, A. Li, X. Liu, X. Yang, S. Zhang, Q. Zhao, Q. Jiang, Y. Su, L. Zhang, J.-F. Li, Z.-Q. Tian, W. Liu, A. Wang, T. Zhang, *J. Am. Chem. Soc.* **2022**, *144*, 12062.
[246] M. Jin, Y. Liu, X. Zhang, J. Wang, S. Zhang, G. Wang, Y. Zhang, H. Yin, H. Zhang, H. Zhao, *Appl. Catal., B* **2021**, *298*, 120545.
[247] Y. Gao, Q. Xue, J. Li, M. Zhang, Y. Ma, Y. Qu, *ACS Appl. Mater. Interfaces* **2022**, *14*, 14202.
[248] R. Xia, D. Tian, S. Kattel, B. Hasa, H. Shin, X. Ma, J. G. Chen, F. Jiao, *Nat. Commun.* **2021**, *12*, 1949.
[249] D. Zhang, J. Chen, Z. Hao, L. Jiao, Q. Ge, W-F. Fu, X.-J. Lv, *Chem Catal* **2021**, *1*, 393.
[250] J. Li, Y. Zhang, K. Kuruvinashetti, N. Kornienko, *Nat. Rev. Chem.* **2022**, *6*, 303.
[251] M. Jouny, J.-J. Lv, T. Cheng, B. H. Ko, J.-J. Zhu, W. A. Goddard, F. Jiao, *Nat. Chem.* **2019**, *11*, 846.
[252] C. Guo, W. Zhou, X. Lan, Y. Wang, T. Li, S. Han, Y. Yu, B. Zhang, *J. Am. Chem. Soc.* **2022**, *144*, 16006.
[253] J. Li, N. Kornienko, *Chem. Sci.* **2022**, *13*, 3957.
[254] Z. Tao, C. L. Rooney, Y. Liang, H. Wang, *J. Am. Chem. Soc.* **2021**, *143*, 19630.
[255] M. Shibata, K. Yoshida, N. Furuya, *J. Electroanal. Chem.* **1995**, *387*, 143.
[256] M. Shibata, K. Yoshida, N. Furuya, *J. Electroanal. Chem.* **1998**, *442*, 67.
[257] C. Chen, X. Zhu, X. Wen, Y. Zhou, L. Zhou, H. Li, L. Tao, Q. Li, S. Du, T. Liu, D. Yan, C. Xie, Y. Zou, Y. Wang, R. Chen, J. Huo, Y. Li, J. Cheng, H. Su, X. Zhao, W. Cheng, Q. Liu, H. Lin, J. Luo, J. Chen, M. Dong, K. Cheng, C. Li, S. Wang, *Nat. Chem.* **2020**, *12*, 717.
[258] J. Leverett, T. Tran-Phu, J. A. Yuwono, P. Kumar, C. Kim, Q. Zhai, C. Han, J. Qu, J. Cairney, A. N. Simonov, R. K. Hocking, L. Dai, R. Daiyan, R. Amal, *Adv. Energy Mater.* **2022**, *12*, 2201500.
[259] N. Cao, Y. Quan, A. Guan, C. Yang, Y. Ji, L. Zhang, G. Zheng, *J. Colloid Interface Sci.* **2020**, *577*, 109.
[260] N. Meng, X. Ma, C. Wang, Y. Wang, R. Yang, J. Shao, Y. Huang, Y. Xu, B. Zhang, Y. Yu, *ACS Nano* **2022**, *16*, 9095.
[261] S. Liu, S. Yin, Z. Wang, Y. Xu, X. Li, L. Wang, H. Wang, *Cell Rep. Phys. Sci.* **2022**, *3*, 100869.
[262] Z. Tao, Y. Wu, Z. Wu, B. Shang, C. Rooney, H. Wang, *J. Energy. Chem.* **2022**, *65*, 367.
[263] L. Chen, C. Tang, Y. Zheng, K. K. Ostrikov, Y. Jiao, *Energy Fuels* **2022**, *36*, 7213.
[264] J. E. Kim, J. H. Jang, K. M. Lee, M. Balamurugan, Y. I. Jo, M. Y. Lee, S. Choi, S. W. Im, K. T. Nam, *Angew. Chem., Int. Ed.* **2021**, *60*, 21943.
[265] Y. Wu, J. Zhao, C. Wang, T. Li, B.-H. Zhao, Z. Song, C. Liu, B. Zhang, *Nat. Commun.* **2023**, *14*, 3057.
[266] J. Li, H. Al-Mahayni, D. Chartrand, A. Seifitokaldani, N. Kornienko, *Nat Synth* **2023**, *2*, 757.
[267] J. Anibal, B. Xu, *ACS Catal.* **2020**, *10*, 11643.

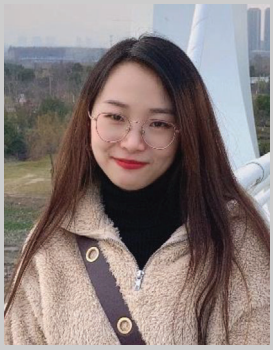

Min Zheng received her M.S. degree from Lanzhou University (China). She is currently a Ph.D. student at the School of Chemical Engineering of The University of Adelaide. Her research focuses on electrocatalyst design for the production of value-added chemicals.

© 2024 The Authors. Advanced Materials published by Wiley-VCH GmbH

15214095, 2024, 14, Downloaded from https://advanced.onlinelibrary.wiley.com/doi/10.1002/adma.202307913 by Cochrane Chile, Wiley Online Library on [30/09/2026]. See the Terms and Conditions (https://onlinelibrary.wiley.com/terms-and-conditions) on Wiley Online Library for rules of use; OA articles are governed by the applicable Creative Commons License



Yao Zheng received his Ph.D. degree in 2014 from the University of Queensland (Australia). He is currently an associate professor at The University of Adelaide. His current research focuses on fundamental studies of some key electrocatalysis processes by combining experiments and theoretical computations, and the development of advanced electrocatalysts for energy conversion processes.



Shi-Zhang Qiao received his Ph.D. degree in chemical engineering from the Hong Kong University of Science and Technology in 2000. He is currently a Chair Professor, elected Fellow of the Australian Academy of Science, ARC Industry Laureate Fellow, and ARC Australian Laureate Fellow at the School of Chemical Engineering of The University of Adelaide (Australia). His research expertise is in nanomaterials for new energy technologies (electrocatalysis, photocatalysis, batteries, and fuel cells).

© 2024 The Authors. Advanced Materials published by Wiley-VCH GmbH

15214095, 2024, 14, Downloaded from https://advanced.onlinelibrary.wiley.com/doi/10.1002/adma.202307913 by Cochrane Chile, Wiley Online Library on [30/09/2026]. See the Terms and Conditions (https://onlinelibrary.wiley.com/terms-and-conditions) on Wiley Online Library for rules of use; OA articles are governed by the applicable Creative Commons License